Dissertation zur Erlangung des Doktorgrades
der Fakultät für Chemie und Pharmazie
der Ludwig-Maximilians-Universität München

Phosphorylation of PFKL regulates glycolysis in macrophages following pattern recognition receptor activation

Meiyue Wang

aus

Linyi, Shandong, China

2023

Erklärung

Diese Dissertation wurde im Sinne von § 7 der Promotionsordnung vom 28. November 2011 von Herrn Prof. Dr. Veit Hornung betreut.

Eidesstattliche Versicherung

Diese Dissertation wurde eigenständig und ohne unerlaubte Hilfe erarbeitet.

München, 10/05/2023 Meiyue Wang

Dissertation eingereicht am 04.08.2023

1. Gutachter: Prof. Dr. Veit Hornung

2. Gutachter: Prof. Dr. Klaus Förstemann

Mündliche Prüfung am 13.07.2023

Table of Contents

1 Introduction

1.1 The immune system

The immune system is the body's frontline defense mechanism that protects an organism from a wide range of pathogens, including viruses, bacteria, fungi, and parasites, as well as harmful or allergenic chemicals. The immune system distinguishes self from non-self by identifying structural features of pathogens or toxins that mark it as distinct from host cells. This feature is central to the immune system's ability to mobilize a response to an invading pathogen, toxin, or allergen (Chaplin, 2010). Failure to distinguish between self and non-self is the cause of a broad category of autoimmune diseases. The mechanisms that enable non-self recognition can be divided into two types of immune responses: the innate immune response and the adaptive immune response. Pattern recognition receptors (PRRs) used by the innate immune response recognize molecular patterns common to microbes that are not present in host cells, enabling the host to destroy invading pathogens without causing damage to its own tissues. The innate immune response engages within minutes or hours of encountering an invading pathogen, serving as the host's first line of defense. In some cases, the innate immune response is sufficient to combat invaders. When it is not, an adaptive immune response needs to be induced to eliminate the infectious pathogens. The adaptive immune response functions through antigen-specific receptors expressed on the surface of T and B lymphocytes. Unlike the PRRs of the innate immune system, each T or B cell receptor has a distinct antigen specificity. Antigen-specific receptor genes are produced by somatic rearrangement of a few hundred germline encoded gene elements, resulting in an estimated quintillion (10^{18}) different antigen receptors in human B cells and a repertoire of approximately 10^{15} T-cell receptors (Turner et al., 2006). These novel and unique receptors enable T and B cells to recognize virtually any foreign antigen. Upon activation, B cells differentiate into plasma cells that secrete antibodies to bind pathogens or their toxic products in extracellular spaces. These antibody-antigen complexes are then recognized and cleared by phagocytes of the innate immune system. In contrast, T cells recognize foreign antigens that are processed and presented by professional antigen-presenting cells like dendritic cells (DCs). Upon activation, antigen-specific T lymphocytes proliferate and differentiate into effector T cells, including cytotoxic CD8 T cells that kill infected target cells, and different subsets of CD4 T cells that activate innate immune cells, promote allergic responses, or assist B cells in antibody production (Murphy, 2016). The differentiation of CD4 T cells into distinct subsets is regulated by cytokines produced by innate immune cells (Clark and Kupper, 2005). The adaptive immune response takes many days or weeks to develop and results in an immunological memory that allows for a faster and more potent response to reinfection with the same pathogen. Overall,

although the innate and adaptive immune responses have fundamentally different modes of action, effective protection against pathogens depend on extensive interactions between these two branches of the immune system (Chaplin, 2010).

1.2 The innate immune system

Unlike adaptive immunity, which did not evolve until the appearance of the first jawed vertebrates (fish) (Flajnik and Kasahara, 2009), the innate immune system is present in all domains of life (Krautz et al., 2014). The innate immune response is typically divided into humoral and cell-mediated responses in vertebrates, which act as rapid and non-specific defense mechanisms against invading pathogens, while also playing a critical role in maintaining homeostasis. The skin serves as the body's primary protective barrier against pathogen invasion, making it an essential component of innate immunity (Murphy, 2016). Secretory components, rich in microbicidal molecules such as antimicrobial peptides and enzymes, serve as a chemical barrier and an important innate defense mechanism by either killing the pathogen or attenuating its virulence (Akinbi et al., 2000). When a pathogen breaches the physical and chemical barriers, it encounters the complement system, which is the primary defense mechanism of the humoral component of the innate immune system. The complement system consists of soluble proteins found in blood and other body fluids. In the absence of infection, these proteins circulate in an inactive state. However, the presence of pathogens leads to their activation, which results in pathogen opsonization, followed by phagocytosis by neutrophils or macrophages. Further, activated complement factors result in the formation of a membrane-attack complex (MAC) on the surface of pathogens, which directly disrupts the cell membrane and causes cell lysis via a molecular cascade (Dunkelberger and Song, 2009).

Despite the antimicrobial properties of anatomical barriers and humoral proteins, target cells can become infected, which requires cell-mediated responses. Many microbes are recognized and engulfed by phagocytic cells that lie beyond the epithelial barriers once they invade tissues. These phagocytes include macrophages, granulocytes (neutrophils, eosinophils, and basophils), and DCs, which belong to the myeloid lineage of the innate immune system (Murphy, 2016). Upon detection of pathogens, these phagocytes produce antimicrobial chemicals such as reactive oxygen species (ROS) and nitric oxide (NO) (Fang, 2004; Lam et al., 2010; West et al., 2011). These highly reactive chemical species, combined with the action of endolysosomal proteolytic enzymes, are extraordinarily powerful in destroying pathogens. In addition, activated phagocytes can produce inflammatory mediators, primarily cytokines and chemokines, which attract new phagocytes and circulating effectors to the site of infection. Macrophages and DCs are also key players in initiating adaptive immune responses. They

degrade proteinaceous components of ingested pathogens into peptides that bind to major histocompatibility complex (MHC) proteins, which are subsequently presented on the cell surface for recognition by the appropriate T cells (Murphy, 2016). In addition to directly killing pathogens, some innate immune cells function by inducing the death of infected cells. This can occur in a cell-autonomous manner, a type of “suicide cell death”, or based on a cell-to-cell interaction between an infected cell and a killer cell. “Suicide cell death” can be induced in the form of apoptosis, pyroptosis, necroptosis, or NETosis. Apoptosis is a type of cell death that does not release cellular components with apoptotic cells being engulfed by neutrophils and macrophages (Nainu et al., 2017). Pyroptosis, necroptosis, and NETosis, however, require membrane disruption and result in the release of intracellular contents and secretion of immune mediators that further alarm and activate bystander cells, thereby amplifying inflammatory responses (Brinkmann et al., 2004; Vandenabeele et al., 2010; Yu et al., 2021). Cell-to-cell killing can be mediated by natural killer (NK) cells that belong to the lymphoid lineage of the innate system. These cells share similarities with the lymphoid cells of the adaptive immune system, but lack antigen-specific receptors (Murphy, 2016). Recognition and lysis of target cells by NK cells is regulated by activating and inhibitory receptors expressed on the surface of NK cells. Activating receptors include Fc receptors, which recognize the Fc portion of antibodies and trigger NK cell activation through a process known as antibody-dependent cell-mediated cytotoxicity (Pegram et al., 2010), whereas inhibitory receptors recognize self MHC class I molecules and prevent NK cells from attacking self cells (Raulet and Vance, 2006). However, self cells with low expression of MHC class I molecules are destroyed. This constitutes an important host defense strategy because many viruses have evolved mechanisms to reduce MHC class I molecule expression in infected cells to avoid CD8+ T cell-mediated killing (Chaplin, 2010).

1.3 Pattern recognition receptors (PRRs)

PRRs are responsible for triggering inflammatory responses when there is an infection caused by pathogens or damage inflicted on cells. These receptors do not require the gene rearrangements used by lymphocytes, but are encoded by germ-line encoded genes. This allows PRRs to rapidly recognize and respond to microbial products or inflammatory stimuli, enabling a rapid immune response without the need for genetic recombination processes to occur. PRRs recognize so called pathogen-associated molecular patterns (PAMPs), which are important structures conserved across microbial species, but absent in the host. Classical examples are lipopolysaccharide (LPS) of Gram-negative bacterial outer membranes, lipoteichoic acids of Gram-positive bacterial cell walls, or viral nucleic acids. PRRs are also responsible for recognizing damage-associated molecular patterns (DAMPs). DAMPs are self-molecules released by injured cells that result in in-advertent PRR activation. When PRRs

detect PAMPs or DAMPs, genes encoding antimicrobial proteins, proinflammatory cytokines, chemokines, and type I interferons (IFNs) are upregulated, all of which are critical in orchestrating inflammatory responses (Takeuchi and Akira, 2010). Four major distinct classes of PRRs have been identified, including Toll-like receptors (TLRs), C-type lectin receptors (CLRs), retinoic acid-inducible gene (RIG)-I-like receptors (RLRs), and nucleotide-binding and oligomerization domain (NOD)-like receptors (NLRs). TLRs and CLRs are discussed in more detail in sections 1.3.1 and 1.3.2. RLRs, which include retinoic acid-inducible gene I (RIG-I), melanoma differentiation-associated gene 5 (MDA5), and laboratory of genetics and physiology 2 (LGP2), are located in the cytosol and recognize RNA, leading to the secretion of type I IFNs and pro-inflammatory cytokines (Vabret and Blander, 2013). These receptors recognize several features of microbial RNA to distinguish non-self RNA from self RNA. For example, the RIG-I ligand has been described as an RNA molecule with a 5'-triphosphate moiety (Hornung et al., 2006; Pichlmair et al., 2006). NLRs are also cytosolic receptors that recognize intracellular ligands such as conserved microbial structures or cellular damage. Twenty-two genes encoding NLR proteins are found in the human genome (Schroder and Tschopp, 2010), which typically contain a C-terminal leucine-rich repeat (LRR) domain that is thought to function in ligand sensing, a central nucleotide binding and oligomerization (NACHT) domain that is used to form multimeric NLR complexes, and an N-terminal effector domain that allows the NLR to recruit a class of intracellular caspases that activate cell death pathways or the transcription factor NF-κB to induce pro-inflammatory responses (Chaplin, 2010). Some NLRs, including NLRP1, NLRP3, and NLRC4, are known for their ability to form so called inflammasomes (Schroder and Tschopp, 2010), which lead to the activation of inflammatory caspases. Caspase-1 plays a critical role in the processing of pro-IL-1β and pro-IL-18 to their bioactive forms, IL-1β and IL-18, and in the cleavage of gasdermin D (GSDMD). The cleaved N-terminal fragment of GSDMD oligomerizes and forms pores on the cell membrane, resulting in pyroptosis (Liu et al., 2016; Shi et al., 2015). During this process, endogenous inflammatory mediators such as IL-1β and IL-18 are preferentially released (Xia et al., 20-21), further amplifying the inflammatory cascade. This caspase-1-dependent process of pyroptosis is known as canonical inflammasome activation. Pyroptosis can also occur independently of caspase-1 through the non-canonical inflammasome pathway. In this pathway, caspase-4 or caspase-5 in human cells or caspase-11 in mouse cells are activated upon recognition of cytosolic LPS, leading to GSDMD cleavage and subsequent pyroptosis (Kayagaki et al., 2011; Man et al., 2017). In addition, the protein cyclic GMP-AMP synthase (cGAS) is also a type of PRRs that is able to detect cytosolic DNA. Upon activation, cGAS synthesizes cyclic GMP-AMP (cGAMP), a second messenger that is subsequently detected by the stimulator of interferon genes (STING). The activation of STING leads to the production of type I IFNs, which in turn induce the expression of interferon-stimulated genes (ISGs) that together

orchestrate antimicrobial defense mechanisms. Importantly, in addition to detecting microbial DNA, cGAS can also be activated by endogenous DNA, such as extranuclear chromatin from genotoxic stress and DNA released from mitochondria. Therefore, the cGAS-STING signaling pathway is important not only for antimicrobial defense, but also in the context of autoimmunity, sterile inflammatory responses, and cellular senescence (Hopfner and Hornung, 2020).

1.3.1 Toll-like receptors (TLRs)

Toll, a protein in Drosophila melanogaster, was the first molecule to prove the PRR hypothesis when it was discovered to detect fungal infection and trigger a subsequent innate response (O'Neill et al., 2013). The mammalian homologs of Drosophila Toll were thereafter named Toll-like receptors (TLRs). TLRs were the first family of proteins discovered to recognize PAMPs, shattering the notion that innate immunity was a crude and unsophisticated part of the immune system. To date, 10 TLRs (TLR1-TLR10) have been identified in humans and 12 TLRs (TLR1-9 and TLR 11-13) in mice (Figure 1.1). They are all single-pass transmembrane proteins with an extracellular domain containing LRRs, a single transmembrane domain and an intracellular Toll-interleukin 1 receptor (TIR) domain. They are synthesized in the endoplasmic reticulum (ER) and transported to either the plasma or endosomal membranes for function. TLR1, TLR2, TLR4, TLR5 and TLR6 are located on the plasma membrane and recognize microbial cell surface components. TLR4 recognizes LPS, TLR5 binds flagellin, and TLR1, 2, and 6 recognize bacterial lipoproteins. TLR3, TLR7, TLR8, TLR9 and TLR13 must be delivered to endosomes with the help of a protein chaperone known as Unc93B1 (Kim et al., 2008), where they recognize nucleic acids. TLR3 recognizes dsRNA, TLR7 and 8 detect ssRNA, TLR9 detects unmethylated CpG ssDNA, and bacterial ribosomal RNA serves as the ligand for TLR13. Interestingly, host nucleases are required for additional processing of nucleic acids prior to recognition. For example, to activate TLR8, ssRNA must be degraded by RNase T2 (Greulich et al., 2019), and DNase II-dependent DNA digestion is required for DNA recognition by TLR9 (Chan et al., 2015). Since nucleic acids are not exclusively microbial, self nucleic acids can be misidentified by PRRs leading to autoinflammatory or autoimmune diseases. Thus, endosomal localization is a key mechanism to avoid recognition of host DNA or RNA. Furthermore, unlike their plasma membrane counterparts, endosomal TLRs require cleavage for receptor dimerization and signaling (Ewald et al., 2011; Latz et al., 2007; Ohto et al., 2018; Tanji et al., 2016).

Upon recognition of PAMPs, TLRs undergo dimerization. Dimerized TIR domains are subsequently recognized by TIR domain-containing adaptor proteins, resulting in the activation of dramatic changes in cellular activities such as alterations in gene transcription,

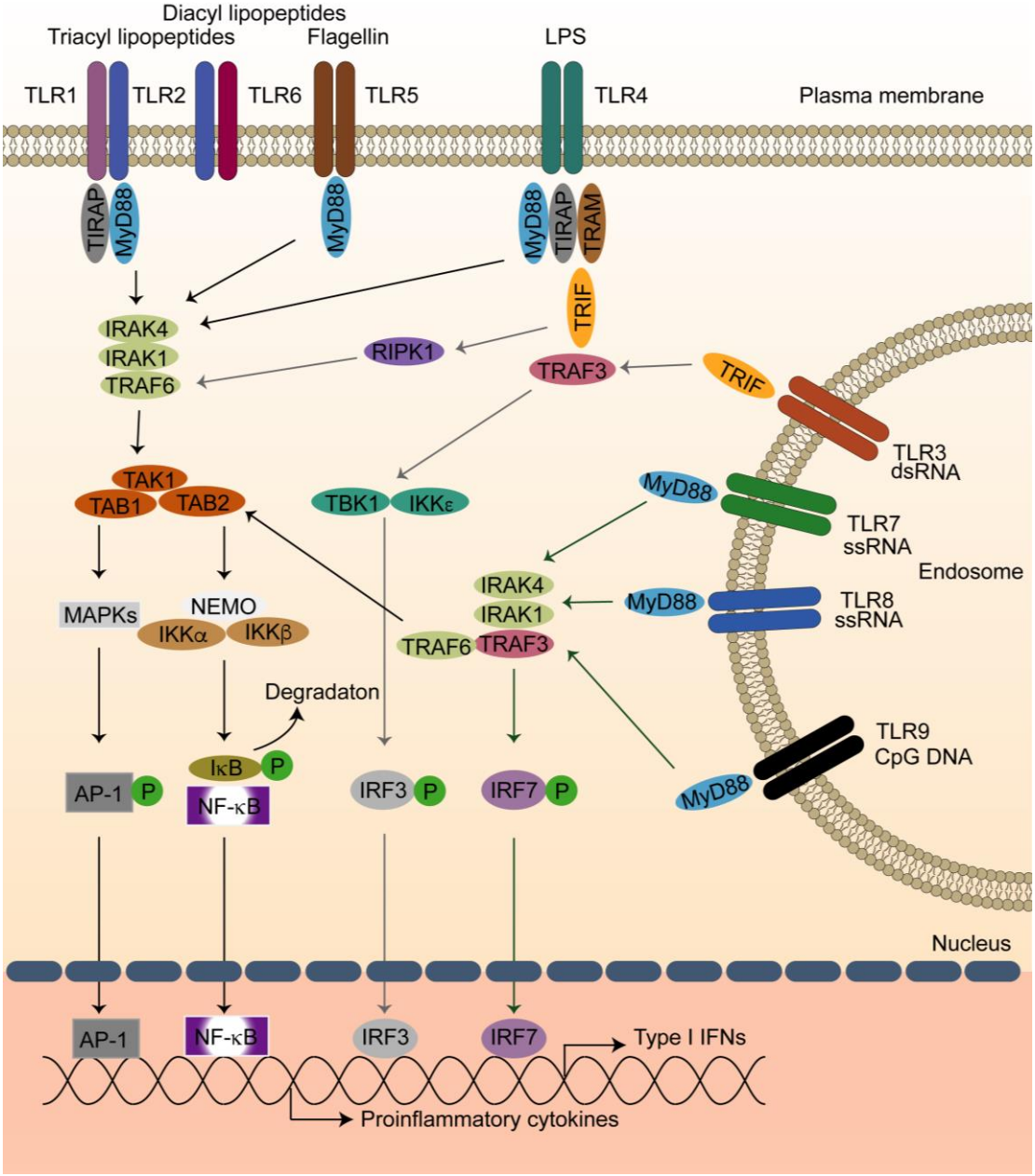

Figure 1.1 A graphical representation of the signaling pathways for each TLR receptor along with the corresponding agonists. Upon binding to a ligand, TLRs undergo dimerization, leading to the recruitment of adaptor molecules and the initiation of intracellular signaling pathways. This eventually results in the activation of transcription factors such as NF-κB, AP-1, and IRFs, which produce proinflammatory cytokines and type I IFNs.

metabolism, and autophagy (Fitzgerald and Kagan, 2020). TIR domain-containing adaptor molecules include myeloid differentiation primary response protein 88 (MyD88), TIR domain-containing adaptor protein (TIRAP) - also known as MyD88 adaptor-like protein (MAL), TIR domain-containing adaptor-inducing interferon-β (TRIF), and TRIF-related adaptor molecule (TRAM), which are recruited by various TLRs (Murphy, 2016). MyD88 is used by all TLRs

except TLR3, which only interacts with TRIF. Most TLRs, including TLR5, TLR7, TLR8, TLR9, and TLR13, interact only with MyD88, whereas some TLRs require adapter proteins in pairs such as MyD88/MAL and TRIF/TRAM. As such, signaling via TLR1/2 and TLR2/6 heterodimers requires MyD88/MAL and TLR4 signaling uses both pairs. The death domain of MyD88 recruits and activates IL-1 receptor-associated kinases (IRAKs), which serve as a signaling scaffold for the recruitment of the E3 ubiquitin ligase tumor necrosis factor receptor-associated factor 6 (TRAF6). TRAF6 stimulates transforming growth factor β (TGFβ)-activated kinase 1 (TAK1), which leads to the activation of the IkB kinase complex, consisting of IKKα and IKKβ kinases scaffolded by the regulatory subunit NEMO. This kinase complex phosphorylates IkBα, allowing it to be ubiquitinated and degraded by the proteasome, allowing NF-κB to translocate to the nucleus and induce pro-inflammatory gene expression. The NF-κB pathway can be activated by all TLRs, which is critical for altering the immune system in the presence of microorganisms (Murphy, 2016). TAK1 is a member of the mitogen-activated protein kinase kinase kinase (MAP3K) family. It also activates MAPK kinases, which in turn activate MAPKs, including extracellular signal-regulated kinases (Erks), c-Jun N-terminal kinase (JNK), and p38. These MAPKs phosphorylate and activate the transcription factor activator protein 1 (AP-1), which also promotes the transcription of pro-inflammatory genes. IRAKs recruited by MyD88 in TLR7, TLR8, and TLR9 signaling can also associate with interferon regulatory factor 7 (IRF7) and facilitate its phosphorylation, resulting in the induction of type I IFNs, which is essential for the antiviral immune response. TRIF, which is used by TLR3 and TLR4, recruits TRAF6 and receptor-interacting serine/threonine protein kinase 1 (RIPK1), leading to the activation of NF-κB as described for MyD88 signaling. On the other hand, TRIF also interacts with the E3 ubiquitin ligase TRAF3 to form a polyubiquitin platform that recruits the non-canonical kinases IKKε and TANK-binding kinases 1 (TBK1), leading to IRF3 phosphorylation and the production of type I IFNs. TRAM and TIRAP function as sorting adaptors that recruit TRIF to TLR4 and MyD88 to TLR2 and TLR4, respectively (Kawai and Akira, 2010).

1.3.2 C-type lectin receptors (CLRs)

C-type lectins are a superfamily of more than 1,000 proteins that share one or more C-type lectin-like domains (CTLDs) (Brown et al., 2018). These molecules were originally named for their ability to bind to carbohydrates in a Ca^{2+}-dependent manner. However, many C-type lectins lack the components essential for Ca^{2+}-dependent carbohydrate recognition, allowing them to recognize a wider range of ligands, including proteins, lipids, and even inorganic substances (Brown et al., 2018). C-type lectins are found as secreted molecules or transmembrane proteins in mammals, and their ability to recognize self and non-self ligands has led to their involvement in a wide range of physiological functions (Brown et al., 2018).

Soluble C-type lectins can act as growth factors, opsonins, antimicrobial proteins, and extracellular matrix (ECM) components, and they control a variety of important physiological processes such as development, respiration, coagulation, and inflammation (Brown et al., 2018). Transmembrane CLRs possess either intrinsic intracellular signaling domains or the ability to associate with signaling adaptors, allowing them to modulate intracellular signaling pathways (Brown et al., 2018). Dectin-1, for example, transduces intracellular signals using an integrated immunoreceptor tyrosine-based activation (ITAM)-like motif in its cytoplasmic tail. Conversely, receptors such as dectin-2 and Mincle rely on ITAM-bearing FcRγ adaptor molecules to transduce intracellular signals (Dambuza and Brown, 2015). Activation of these receptors is important for antifungal host defense and homeostasis.

Dectin-1 was discovered over a decade ago as the first non-Toll-like receptor capable of linking microbe detection to gene transcription (Brown and Gordon, 2001). It recognizes β-glucans, a carbohydrate found in many fungal cell walls. Dectin-1 signaling regulates numerous cellular responses including phagocytosis, respiratory burst, and production of inflammatory cytokines and chemokines (Gantner et al., 2003; Herre, 2004; Underhill et al., 2005). Upon binding of certain β-glucans, such as zymosan, dectin-1 dimerizes, leading to tyrosine phosphorylation of the ITAM-like motif by Src kinase and recruitment and activation of spleen tyrosine kinase (Syk) (Brown, 2005) (Figure 1.2). Activation of Syk induces the

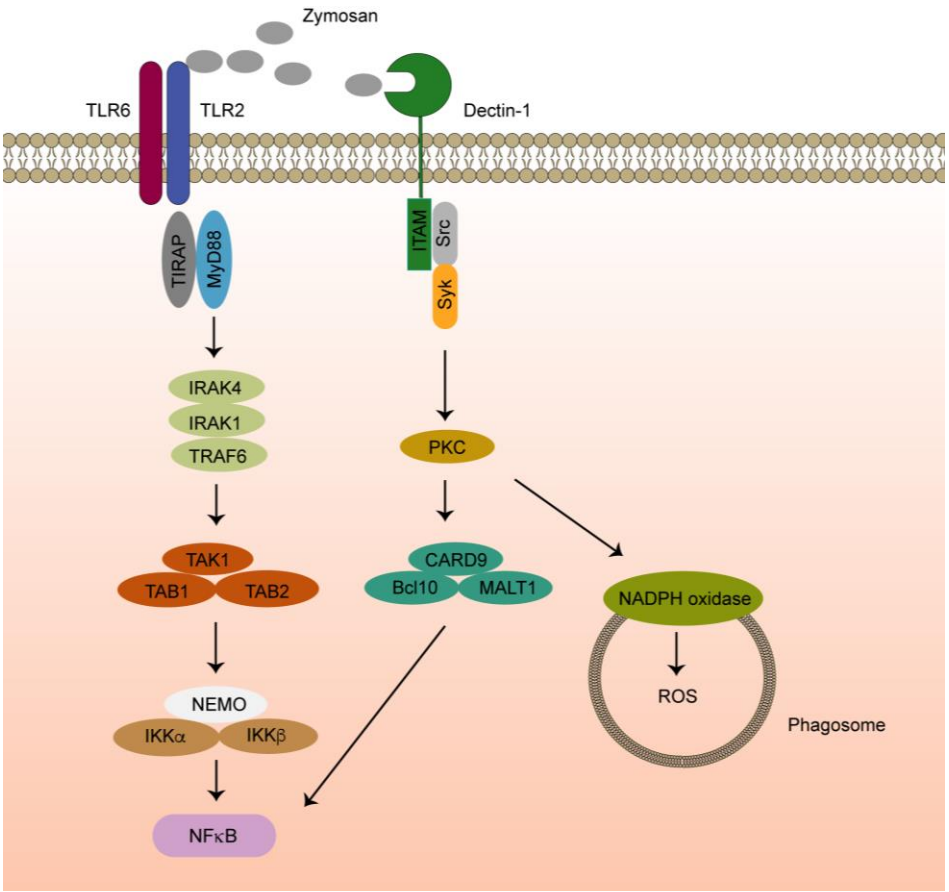

Figure 1.2 A graphic depiction of the signaling pathways for zymosan recognition by TLR2/6 and dectin-1. Zymosan is recognized by TLR2/6 and dectin-1, which activates NF-κB to produce cytokines and NADPH oxidase to produce ROS.

CARD-Bcl10-Malt1 complex, which mediates the activation of NF-κB and the production of proinflammatory cytokines (Gross et al., 2006). It can also activate protein kinase C (PKC), which then phosphorylates and activates the nicotinamide adenine dinucleotide phosphate (NADPH) oxidase complex, resulting in ROS generation (Elsori et al., 2011). Zymosan can also be sensed by TLR2/TLR6, which further promotes the generation of proinflammatory cytokines (Gantner et al., 2003; Underhill et al., 1999).

1.4 Metabolic reprogramming in immune cells

In order to respond appropriately to various internal and external stimuli, immune cells must integrate multiple signaling pathways and metabolic processes (Ganeshan and Chawla, 2014). As mentioned in Section 1.3.1, TLR signaling leads to profound changes in cellular metabolism. Cellular metabolism consists of catabolism and anabolism. The metabolic processes that break down molecules to produce ATP and intermediates for anabolic reactions and other pathways are known as catabolism, whereas anabolism is a metabolic process that requires energy to build molecules from subunits. Both catabolism and anabolism are necessary for the survival and proper functioning of cells. Hundreds of metabolic processes occur simultaneously within the cell, which can be categorized into distinct pathways involving specific enzymes and compartmentalized reactions (Judge and Dodd, 2020). Modulation of glycolysis and oxidative phosphorylation (OXPHOS) has been shown to play a critical role in immune cell function (Viola et al., 2019). Activated macrophages are typically divided into two categories, M1-like macrophages and M2-like macrophages (Yunna et al., 2020). M1 macrophages are classically activated, typically by IFNγ or LPS, and are mainly involved in pro-inflammatory responses. M2 macrophages are alternatively activated by exposure to certain cytokines such as IL-4, IL-10 or IL-13 and are mainly involved in anti-inflammatory responses. Glycolysis is mainly used by specific immune cells with pro-inflammatory functions, such as M1 macrophages or effector T cells (Kelly and O'Neill, 2015; Slack et al., 2015), as it provides a rapid energy supply. On the other hand, the more energy-efficient OXPHOS pathway is typically adopted by immune cells at rest or those with anti-inflammatory functions, such as regulatory T cells or M2 macrophages (Kelly and O'Neill, 2015; Shi and Chi, 2019).

In species that use cellular respiration, glycolysis is the first step in glucose catabolism. The glycolytic pathway involves ten consecutive enzymatic reactions that break down one molecule of glucose into two molecules of pyruvate (Figure 1.3). It occurs in most living cells

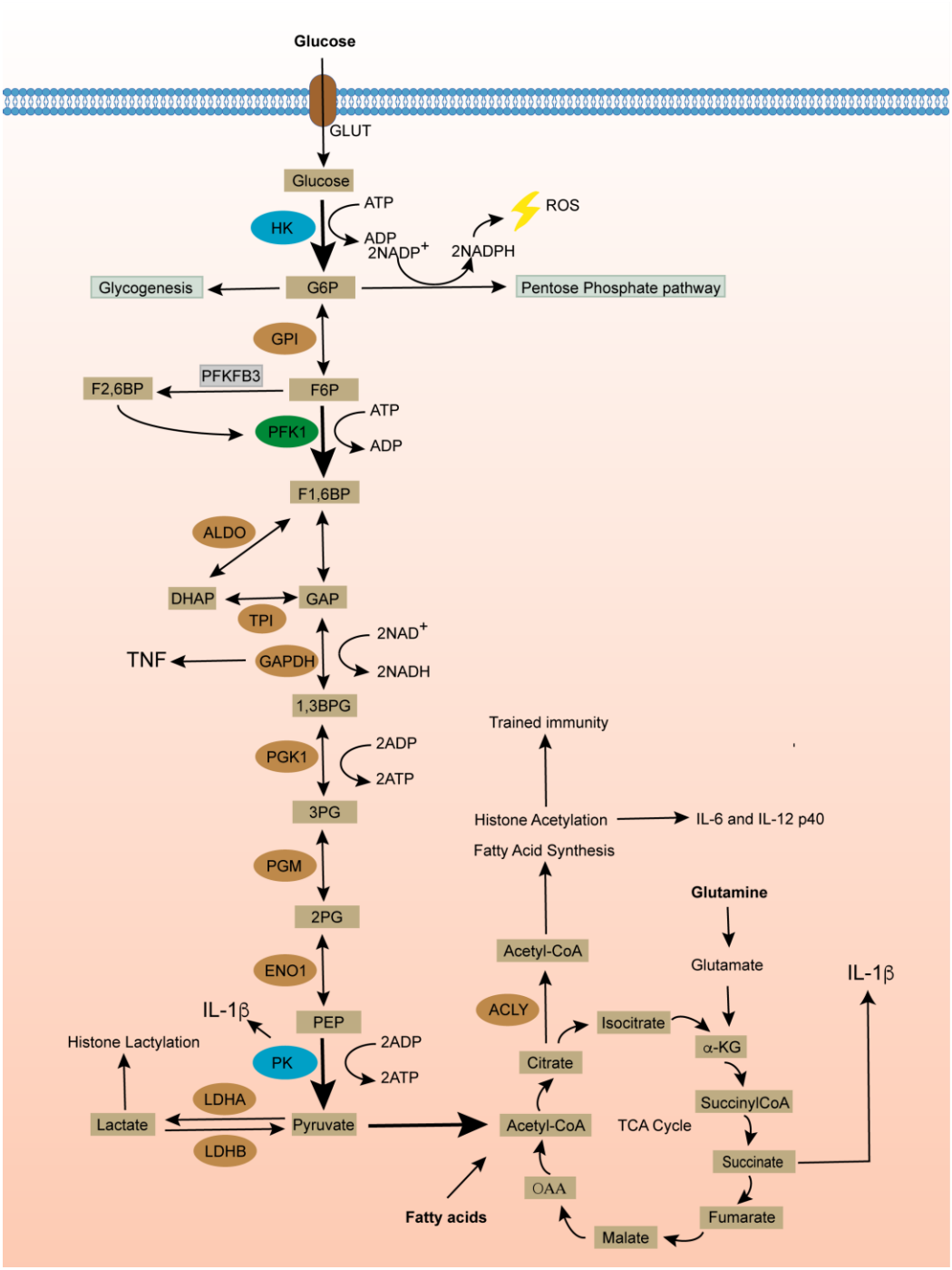

Figure 1.3 Schematic representation of the glycolytic pathway and the TCA cycle. The process of converting glucose into pyruvate is known as glycolysis, which is tightly controlled by three rate-limiting enzymes, HK, PFK1, and PK, that catalyze irreversible reactions. Under normoxia, pyruvate enters the mitochondria and is utilized by the TCA cycle, while in the absence of oxygen, it is converted to lactate. Recent studies have shown that even in the presence of abundant oxygen, TLR ligation upregulates glycolysis and suppresses OXPHOS in immune cells. Importantly, it was found that metabolites and enzymes involved in the TCA cycle and glycolytic pathway play significant roles in regulating inflammatory responses.

and can occur in the absence of oxygen. This pathway is tightly controlled by three rate-limiting enzymes that catalyze irreversible reactions: hexokinase (HK), phosphofructokinase 1 (PFK1), and pyruvate kinase (PK). To meet cellular metabolic needs under specific conditions, the activity of these enzymes is regulated by several mechanisms, such as the reversible binding of allosteric modulators and post-translational modifications. For example, to meet the metabolic demands of increased cell proliferation in response to hypoxia, cancer cells undergo a rapid and significant reprogramming of their cellular metabolism by inducing PFK1 glycosylation. Glycosylation at Ser529 of PFK1 inhibits PFK1 activity and diverts glucose from glycolysis to the pentose phosphate pathway (PPP), thereby conferring a selective growth advantage to cancer cells (Yi et al., 2012b).

Only two net molecules of ATP are produced for each unit of glucose catabolized by the glycolytic process. After glycolysis, the anaerobic or aerobic environment of the cell determines the fate of the end product. In the presence of oxygen, pyruvate enters the mitochondria where it is further metabolized by the tricarboxylic acid (TCA) cycle. The TCA cycle produces the reducing equivalents nicotinamide adenine dinucleotide (NADH) and flavin adenine dinucleotide ($FADH_2$), which donate electrons to the electron transport chain (ETC) to fuel OXPHOS, which produces 32 molecules of ATP. Cells can also metabolize other substrates, such as glutamine via glutaminolysis or fatty acids via β-oxidation, to replenish the TCA cycle and fuel OXPHOS to varying degrees. The relative availability of glucose, glutamine, and fatty acids, as well as the presence or absence of oxygen, determine if cells use OXPHOS to produce ATP (Pearce and Pearce, 2013). However, in anaerobic conditions, pyruvate is transformed to lactate in the cytosol, which regenerates NAD^+ but does not generate any additional ATP. This pathway is heavily reliant on glucose as the sole fuel source.

Although glycolysis yields only 2 net ATP, certain cells choose glycolysis over the TCA cycle as an energy source, even when sufficient oxygen is available. In the 1920s, the German scientist Otto Warburg demonstrated that tumor tissue grown in culture exhibited increased rates of glucose uptake and lactate production, even in the presence of oxygen (known as aerobic glycolysis). These three metabolic features, glucose uptake, lactate secretion, and oxygen availability, together define the Warburg effect (Koppenol et al., 2011). The basic idea of the Warburg effect is that despite the presence of sufficient oxygen for tumor samples to convert glucose to CO_2, a process favored by other tissues and much more efficient for ATP production, tumor cells still choose to convert pyruvate to lactate instead of utilizing mitochondria for greater ATP production. Recent research has shown that the release of lactate into the extracellular space by tumor cells results in an acidic extracellular microenvironment (pH 6.5-6.9) (Lee and Griffiths, 2020). The acidic tumor microenvironment (TME) is advantageous for tumor cells because it impairs the function of effector T cells. At

the same time, regulatory T cells can proliferate and maintain their suppressive function by using an alternative pathway in the TME, further promoting tumor growth (Watson et al., 2021). Experimental models have demonstrated that depriving cancer cells of glucose or obstructing glycolysis can be detrimental to their proliferation and tumorigenesis (Patra et al., 2013; Fantin et al., 2006). In the 1950s, the Warburg effect emerged in the field of innate immunity with the discovery that neutrophils rely mainly on aerobic glycolysis and have a relatively low number of mitochondria compared to other immune cells (Sbarra and Karnovsky, 1959). Subsequently, activated macrophages were observed to also exhibit increased glycolysis (Hard, 1970; Newsholme et al., 1987). In immune cells, changes in key metabolic regulatory processes can be triggered not only by nutrient and oxygen availability, as discussed above, but also by reprogramming events downstream of PRR ligation. Despite these early discoveries, the mechanisms and functions underlying these metabolic changes have only recently been elucidated. For example, glucose depletion was found to completely abolish most neutrophil effector functions, including phagocytosis, ROS production, and neutrophil extracellular trap (NET) formation (Jeon et al., 2020; Rodríguez-Espinosa et al., 2015).

Under normoxia, glucose consumption is upregulated and a metabolic switch from OXPHOS to glycolysis is induced when macrophages and DCs are activated with a variety of stimuli, including LPS, R848, poly(I:C), CpG-B, Pam_2CSK_4, and Pam_3CSK_4, in a manner similar to the Warburg effect (Everts et al., 2014; Tan and Kagan, 2019). Instead of entering mitochondria for higher ATP generation, pyruvate is catalyzed to lactate, leading to a significant increase in the extracellular acidification rate (ECAR), typically measured by Seahorse assays. This metabolic transition can be detected as early as 10 minutes after stimulation (Tan and Kagan, 2019) and is later accompanied by a reduction in mitochondrial OXPHOS, as evidenced by a decrease in oxygen consumption rate (OCR) (Lauterbach et al., 2019; Mills et al., 2016). One reason this response may have evolved is that increased glycolysis can generate ATP more quickly. Compared to the TCA cycle, glycolysis is a less efficient way to produce ATP, but it can be triggered faster and may be particularly advantageous when cellular glucose uptake capacity is high (Vazquez et al., 2010). The metabolic rewiring that occurs in macrophages during activation results in changes to their metabolic profile. This has led to increased study on the effects of altered metabolisms and has revealed a variety of mechanisms by which metabolism can shape the immune response.

Several mechanisms have been proposed to explain the process of metabolic rewiring from OXPHOS to glycolysis during macrophage activation (Figure 1.4). Extensive evidence has

shown that pro-inflammatory signaling cascades can induce the expression of key components of the glycolytic pathway. In this context, the transcription factor hypoxia-inducible

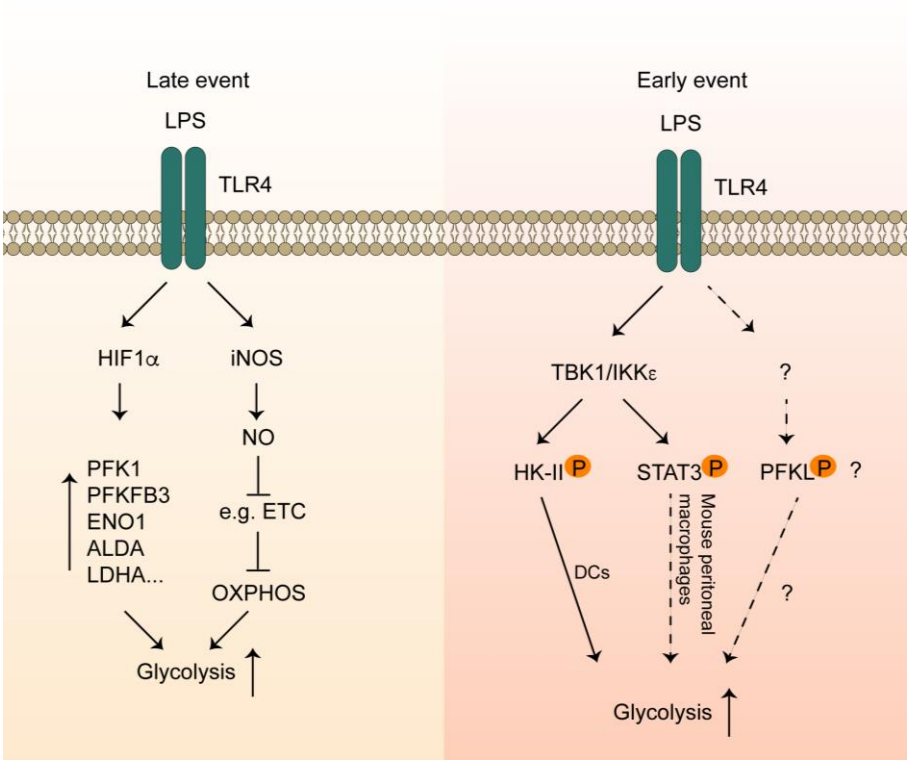

Figure 1.4 The mechanisms responsible for the early and late upregulation of glycolysis induced by LPS are described. LPS stimulation has been shown to increase glycolysis in macrophages and DCs, with late upregulation resulting from mitochondrial dysfunction and upregulation of glycolytic enzymes. For the early glycolytic burst, LPS-induced phosphorylation on HK-II and STAT3 has been implicated. Phosphoproteomic studies have also suggested that LPS induces PFKL Ser775 phosphorylation (Sjoelund et al., 2014; Weintz et al., 2010), but it is unclear if this process actually occurs and thus contributes to the onset of early glycolysis.

factor 1α (HIF1α) is considered to play a key role. The expression of HIF1α is strongly upregulated in LPS-stimulated macrophages (Blouin et al., 2004). The activity of NF-κB plays a critical role in the regulation of HIF1α accumulation. It has been shown that several subunits of NF-κB can bind directly to the promoter of HIF1α, and a decrease in NF-κB levels can lead to a decrease in basal mRNA levels of HIF1α (van Uden et al., 2008; Rius et al., 2008). Another key mechanism for HIF1α activation by LPS involves the mammalian target of rapamycin (mTOR). To meet the high metabolic demand and initiate an appropriate inflammatory response, LPS activates mTOR, a serine/threonine protein kinase (Byles et al., 2013; Weichhart et al., 2008). mTOR promotes translation of mRNAs containing the 5'-terminal oligopyrimidine (5'-TOP) signals present in HIF1α mRNA (Dodd et al., 2014; Huo et al., 2012; Land and Tee, 2007). The metabolic transition is subsequently supported by HIF1α binding to hypoxia response elements (HREs) in target genes, which initiate their transcription. Target

genes include enzymes of the glycolytic machinery such as PFK1 (Semenza GL et al., 1994), 6-phosphofructo-2-kinase/fructose-2,6-biphosphatase 3 enzyme (PFKFB3) (Obach et al., 2004), aldolase A (ALDA), enolase 1 (ENO1), and lactate dehydrogenase A (LDHA) (Semenza GL et al., 1996). Macrophages lacking HIF1α have reduced glycolytic rates and energy production, as well as reduced motility and migration (Cramer et al., 2003). In addition to HIF1α-mediated upregulation of glycolysis, impaired mitochondrial OXPHOS has been reported during the later stages of macrophage activation (Lauterbach et al., 2019; Mills et al., 2016). Mechanistically, stimulation of macrophages with LPS and IFNγ increases the expression of inducible nitric oxide synthase (iNOS or NOS2) (Lorsbach et al., 1993), a protein that generates NO, which inhibits mitochondrial respiration by nitrosylating iron-sulfur proteins in the ETC, such as complex I (Bailey et al., 2019; Clementi E et al., 1998), as well as cytochrome c oxidase (Cleeter MW et al., 1994). Furthermore, to enter the TCA cycle, pyruvate must first be converted to acetyl-coenzyme A (acetyl-CoA) by pyruvate dehydrogenase (PDH). NO inhibits PDH, thereby diverting pyruvate away from the TCA cycle (Palmieri et al., 2020). Therefore, it is thought that increased glycolysis is required to compensate for this mitochondrial dysfunction.

The above mechanisms, which depend on *de novo* gene expression, may only apply to the later switch to glycolysis. However, the upregulation of glycolysis in macrophages can be detected as early as 10-20 minutes after treatment with TLR agonists (Tan and Kagan, 2019). Indeed, HIF1α-deficient macrophages do not display any changes in metabolic flux when studied at an early to intermediate time frame (Rodríguez-Prados et al., 2010). Additionally, recent studies have revealed that mitochondrial function remains intact during the initial phases of macrophage activation triggered by LPS. Specifically, within 8 hours of LPS exposure, both basal and maximal mitochondrial respiration is increased in bone marrow-derived macrophages (BMDM) (Langston et al., 2019; Lauterbach et al., 2019). More importantly, the increase in mitochondrial respiration is attributed to increased glycolysis and pyruvate entry into the TCA cycle (Langston et al., 2019; Lauterbach et al., 2019). These findings suggest that rapid modulation of glycolysis in macrophages upon treatment with TLR ligands should concern the four flux-controlling steps of glycolysis that regulate glucose import, HK activity, PFK1 activity, and lactate export (Tanner et al., 2018). It is plausible that their activity could be enhanced by allosteric regulation, e.g., by post-translational modifications, alteration of their subcellular localization, or their stabilization. In this regard, HK-II phosphorylation was discovered to play a critical role in the early increase in glycolysis in response to TLR agonists in DCs (Everts et al., 2014). AKT phosphorylates HK-II, which promotes the association of HK-II with mitochondria through direct interactions with the voltage-dependent anion channels. This process is believed to allow HK-II greater access to

ATP, which increases the enzymatic activity of HK-II and consequently leads to an increase in glycolytic flux (Everts et al., 2014). Unexpectedly, TBK1-IKKε were identified as upstream kinases in regulating the phosphorylation and activation of AKT in response to LPS, rather than phosphoinositide 3-kinase (PI3K) or mTOR (Everts et al., 2014), since PI3K is required for the long-term commitment to aerobic glycolysis in response to stimulation via TLRs in DCs (Krawczyk et al., 2010). Consistent with these findings, both pharmacological inhibitors of TBK1-IKKε and TBK1/ IKKε deficiency dramatically impaired glycolysis in response to TLR ligands in BMDMs or immortalized BMDMs, indicating that TBK1-IKKε also play a critical role in the early glycolytic reprogramming during macrophage activation (Tan and Kagan, 2019). MyD88 is required as well for the early glycolytic responses (Tan and Kagan, 2019), which makes sense given that all TLRs (except TLR3) employ MyD88 for downstream signaling. However, TAK1-IKKα/β, the key downstream kinases of MyD88, have surprisingly not been investigated in the early glycolytic responses. More importantly, the downstream molecules that directly lead to the early glycolysis in macrophages are largely unknown. In 2020, TBK1-mediated STAT3 Ser727 phosphorylation was shown to be required for TLR4 metabolic reprogramming in mouse peritoneal macrophages (Balic et al., 2020). In addition to its canonical activity as a transcription factor in the nucleus, STAT3 is also found in mitochondria where it affects mitochondrial metabolism by augmenting the activity of the ETC in cancer cells and mouse primary tissues, and this mitochondrial STAT3 function requires S727 phosphorylation (Gough et al., 2009; Wegrzyn et al., 2009). Peritoneal macrophages carrying the STAT3 S727A mutation showed a significant defect in OCR in response to LPS when compared to WT macrophages, indicating that STAT3 S727 phosphorylation is crucial for LPS-induced increases in the TCA cycle and OCR. Even though ECAR was also decreased in macrophages expressing the STAT3 mutant upon LPS treatment, it does not appear to be critical for the induction of glycolysis, as lactate levels were found to be similar in macrophages expressing either the wild-type (WT) STAT3 or the STAT3 mutant after treatment with LPS. The decreased ECAR might be due to less carbon dioxide (CO_2) production, given that the STAT3 S727A mutant functions by disrupting mitochondrial metabolism. Further, activation of PFKFB3 downstream of LPS stimulation has been proposed as an allosteric mechanism to enhance glycolysis in macrophages. A phosphoproteomic study showed that LPS induced PFKFB3 phosphorylation at Ser461 in BMDM (Weintz et al., 2010). AMP-activated protein kinase (AMPK) was discovered to directly phosphorylate Ser461 of PFKFB3, which increases PFKFB3 activity as a kinase to produce fructose 2,6-bisphosphoate (F2,6BP) according to an in vitro kinase assay (Marsin et al., 2002). F2,6BP is the most potent allosteric activator of PFK1. However, AMPK has been shown to be inactivated upon LPS treatment in macrophages (Fan et al., 2018; Sag et al., 2008). Additionally, while PFKFB3 is the

predominant PFK2 isoenzyme expressed in macrophages, its expression is only upregulated to sufficient levels in response to pro-inflammatory signaling inputs (Ruiz-García et al., 2011). Therefore, it is unlikely that this pathway plays a significant role in the initial, transcriptionally independent metabolic rewiring of macrophages. Interestingly, PFK1, live type (PFKL) was also shown to be rapidly phosphorylated at Ser775 in macrophages in response to several TLR agonists in phosphoproteomic studies (Sjoelund et al., 2014; Weintz et al., 2010). Insulin-induced phosphorylation of PFKL at Ser775 has been shown to increase its activity, which is critical in regulating the dynamic flux in the glycolytic pathway in rat hepatoma FAO cells (Yugi et al., 2014). Therefore, if PFKL Ser775 phosphorylation does occur in response to TLR stimulation in macrophages, it is likely to be one of the key events that switches macrophages to early glycolysis. In summary, in light of the limited understanding in the current literature, the interplay between innate immune signaling and early metabolic rewiring of macrophages needs to be further investigated.

1.4.1 The roles of metabolic rewiring in innate immune response

Metabolic reprogramming is critical in regulating the innate immune response (Figure 1.3). Upregulation of glycolysis not only rapidly produces more ATP, but also feeds the PPP. The rate-limiting enzyme glucose-6-phosphate dehydrogenase (G6PD) decarboxylates glucose-6-phosphate (G6P) to form ribose-5-phosphate (R5P) in the PPP pathway, which supports inflammatory macrophage responses by producing amino acids for protein synthesis, ribose for nucleotides, and NADPH for ROS generation (Van den Bossche et al., 2017). During macrophage activation, the TCA cycle shifts from a fully catabolic ATP-generating pathway to a slightly anabolic pathway. Aerobic glycolysis allows the TCA cycle to be used for biosynthesis rather than just ATP production. After 2 hours of treatment, LPS dramatically increases mitochondrial citrate levels in macrophages (Lauterbach et al., 2019). Meanwhile, LPS increases the expression of the mitochondrial citrate carrier, solute carrier family 25 member 1 (Slc25a1), via NF-κB (Infantino et al., 2011). Citrate is then transported out of the mitochondria by this carrier in exchange for malate, resulting in cytosolic citrate accumulation. The enzyme ATP-citrate lyase (ACLY) in the cytosol converts citrate back to oxaloacetate and acetyl-CoA in the presence of ATP. Acetyl-CoA provides acetyl groups for histone acetylation (Wellen et al., 2009), which is required for the induction of late response inflammatory genes such as IL-6 and IL-12p40 in LPS-stimulated macrophages (Lauterbach et al., 2019). Interestingly, the LPS-induced metabolic switch also increases intracellular lactate over time, which drives histone lysine lactylation after 16-24 hours of stimulation (Zhang et al., 2019). Surprisingly, histone lactylation is not essential for the induction or repression of proinflammatory genes. Instead, it serves as a mechanism to initiate the expression of homeostatic genes, such as arginase 1 (Arg1), which are involved in wound healing (Lzzo and

Wellen, 2019; Zhang et al., 2019). As a result, metabolic reprogramming may also play a role in the resolution of inflammation. Acetyl-CoA can also be converted to malonyl-CoA, a metabolite used for fatty acid synthesis, by acetyl-CoA carboxylase (ACC). In LPS-activated DCs, citrate is shifted from the TCA cycle to the cytosol and used for de novo synthesis of fatty acids, which is important for membrane synthesis and further expansion of the ER and Golgi, and increased glycolysis is required to support this metabolic shift (Everts et al., 2014). In addition, macrophages activated by LPS show increased accumulation of succinate (Tannahill et al., 2013). By decreasing the activity of prolyl hydroxylase (PHD) enzymes, succinate stabilizes HIF1α, allowing it to induce inflammation by increasing IL-1β production (Tannahill et al., 2013). And succinate oxidation by succinate dehydrogenase (SDH) contributes to the generation of mitochondrial ROS via reverse electron transfer (RET), which further promotes IL-1β and inflammation (Mills et al., 2016). In addition, glycolytic enzymes themselves support proinflammatory macrophage functions. LPS induces the formation of the enzymatically inactive pyruvate kinase muscle isozyme M2 (PKM2) dimer or monomer (Hitosugi et al., 2009; Palsson-McDermott et al., 2015). Dimeric/monomeric PKM2 can translocate to the nucleus and form a complex with HIF1α, which stabilizes HIF1α and promotes IL-1β production (Palsson-McDermott et al., 2015). Glyceraldehyde-3-phosphate dehydrogenase (GAPDH), another key enzyme in the glycolytic pathway, is also regulated by macrophage metabolic status, either as a glycolytic enzyme or as a regulator of TNF mRNA translation. GAPDH dissociates from TNF mRNA and thus enhances TNF mRNA translation when glycolysis is increased (Millet et al., 2016). In addition, the metabolic changes upon stimulation also lead to epigenetic modification, resulting in increased responsiveness upon subsequent stimulation with the same or a different stimulus, a concept termed "trained immunity" (Saeed et al., 2014). For example, β-glucan was found to induce functional reprogramming of monocytes leading to enhanced cytokine production in vivo and in vitro (Quintin et al., 2012). β-glucan-trained monocytes exhibit high glucose consumption and lactate production due to increased methylation and acetylation patterns in the promoters of genes encoding enzymes involved in glycolysis and its master regulators mTOR and HIF1α (Cheng et al., 2014). Inhibition of AKT, mTOR, or HIF1α blocked the induction of trained immunity in monocytes, suggesting that AKT-mTOR-HIF1α-dependent induction of aerobic glycolysis is the metabolic basis for trained immunity in human monocytes (Cheng et al., 2014). If this is the case, trained immunity should not be limited to β-glucan stimulation, as aerobic glycolysis can be induced by a variety of stimuli. However, more work is needed to provide a clear mechanism.

In conclusion, although it is known that innate immune stimulation of macrophages induces a rapid increase in glycolysis, the underlying mechanisms and functional consequences remain unclear and require further investigation.

1.5 Phosphofructokinase 1 (PFK1)

Mammalian PFK1, which catalyzes the conversion of fructose 6-phosphate (F6P) and ATP to fructose 1,6-bisphosphate (F1,6BP) and ADP, is encoded by three genes: PFKP (platelet), PFKL (liver), and PFKM (muscle). PFKL, PFKP, and PFKM are similar in sequence (58.53% identity) and polypeptide length (780, 784, and 780 amino acids, respectively) (Bateman et al., 2021). All three isoforms are inactive as monomers and dimers and active as a tetramer (Zancan et al., 2008). The tetramer is formed by a dimer of dimers (Webb et al., 2015; Amara et al., 2021) (Figure 1.5). Human tissues express all three PFK1 isoforms, although in varying proportions, with the exception of skeletal muscle, which exclusively expresses PFKM (Dunaway et al., 1988). In liver and macrophages, PFKL is the most abundant type (Fernandes et al., 2020). PFKP, on the other hand, is found in most tissue types (Fernandes et al., 2020). Heteromeric tetramers may form in tissues expressing more than one isoform, but their biological significance is unknown (Vora et al., 1980).

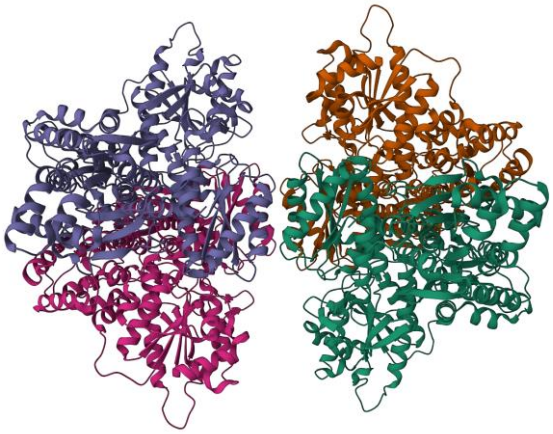

Figure 1.5 Crystal structure of human PFKL. The crystal structure of human PFKL is shown (Amara et al., 2021). It is active as a tetramer which is formed by a dimer of dimers.

Each subunit of the tetramer consists of two domains: an N-terminal catalytic domain and a C-terminal regulatory domain (Bateman et al., 2021). PFK1 is an enzyme whose activity is allosterically regulated by conformational changes between the active R and inactive T states (Schirmer and Evans, 1990). F6P binds with high affinity to the R-state enzyme, but not to the

T-state enzyme. Binding of allosteric activators or inhibitors is known to regulate PFK1 activity. In general, F2,6BP, ADP, and AMP activate all PFK1 isoforms, whereas citrate and high concentrations of ATP inhibit PFK1. However, the susceptibility to these allosteric regulators differs between isoforms. For example, PFKM is less sensitive to F2,6BP allosteric modulation and more resistant to ATP inhibition compared to PFKL and PFKP (Fernandes et al., 2020; Webb et al., 2017). The exact mechanism by which these regulations occur is unclear. It is still debated whether it is caused by direct stabilization/destabilization of the tetramer/dimer/monomer states, changes in the conformational equilibria of the tetramer between the active R-state and the inactive T-state, or a combination of both mechanisms. Lactate, the end product of glycolysis, induces the dissociation of the tetramers into dimers, which reduces the enzymatic activity of PFK1, providing negative feedback for the glycolytic rate (Costa Leite et al., 2007). In addition, PFK1 activity is enhanced by localization to actin filaments of the cytoskeleton (Park et al., 2020; Real-Hohn et al., 2010). Unlike PFKP and PFKM, PFKL itself can also assemble into filaments (Webb et al., 2017). Notably, the binding of F6P and the regulatory domain are critical for the in vitro formation of PFKL filaments. Furthermore, an exposed catalytic site is observed in the arrangement of tetramers in filaments, suggesting that the enzyme is in an active state in the assembled polymers. Thus, filament formation may provide an additional level of regulation of PFKL activity.

Depending on the cell's metabolic requirements, glucose imported into cells can be utilized by different metabolic pathways. It can either undergo catabolism through glycolysis or the PPP, or it can be utilized as a building block for glycogen in the liver and muscle (Figure 1.3). Although the glycolytic route has three rate-limiting enzymes, PFK1 is assumed to be the gatekeeper of glycolysis since it catalyzes the first irreversible step unique to glycolysis. G6P can be oxidized by the PPP or metabolized into glycogen after being synthesized from glucose by HK. As a result, the glycolytic flux and glycolysis-related cellular functions are tightly controlled by PFK1. The activity of PFK1 increases in response to proliferation signals and is associated with increased glycolysis in rapidly dividing cells. Accordingly, elevated PFK1 activity is a hallmark of cancer (Yalcin et al., 2009).

PFKP expression is dramatically increased in cancers such as glioblastoma, which has been shown to promote aerobic glycolysis, cell proliferation, and brain tumor growth (Lee et al., 2017). To survive in the nutrient-poor tumor microenvironment, cancer cells also employ a variety of tactics that target PFK1 to downregulate glycolysis. For example, MiR-135, which is significantly elevated in pancreatic ductal adenocarcinoma (PDAC) patient samples compared to adjacent healthy tissue, targets the PFK1 mRNA for degradation and inhibits aerobic glycolysis, thereby promoting pancreatic cancer cell adaptation to metabolic stress (Yang et al., 2019). Mutations in PFKM directly affect glycolysis and cause Tarui disease, which is

characterized by muscle cramps, exercise intolerance, rhabdomyolysis, and myoglobinuria (Toscano and Musumeci, 2007). PFKM-deficient mice exhibit high mortality around weaning (Horwitz et al., 2009). Muscle hypoxia and hypervascularization, impaired glycolytic and oxidative metabolism, fiber necrosis, and exercise intolerance have all been observed due to the metabolic alterations in *Pfkm*$^{-/-}$ mice, resulting in a shortened lifespan (Horwitz et al., 2009). As mentioned above, PFKL is the major isoform in the liver and immune cells (Fernandes et al., 2020). In mice, deletion of PFKL is lethal (Gerdin, 2010). During pregnancy, only a few homozygous mutant embryos were found, but none survived to weaning (Gerdin, 2010), suggesting that PFKL cannot be replaced by the other two isoforms during development. Heterozygous mutant adult mice with a hair follicle degeneration phenotype have been observed (Gerdin, 2010). The mechanism is unknown, but is most likely related to dysregulation of glycolysis.

In macrophages, a functional knockdown screen identified PFKL as a negative regulator of ROS production (Graham et al., 2015). PFKL knockdown switches glucose metabolism from glycolysis to PPP, resulting in increased NADPH synthesis and ROS production, thereby enhancing bacterial killing efficiency (Graham et al., 2015). The compound NA11, which suppresses ROS production and NETosis in neutrophils, was found to function by activating PFKL (Amara et al., 2021). However, how PFKL expression is controlled in immune cells in response to a stimulus is unclear. Analysis of monocyte-derived macrophages revealed that PFKL transcript levels are nearly unchanged after LPS treatment (Fernandes et al., 2020). Interestingly, according to published phosphoproteomic data, PFKL is phosphorylated at Ser775 in macrophages treated with TLR agonists (Sjoelund et al., 2014; Weintz et al., 2010). It will be interesting to see if this phosphorylation is indeed in response to TLR ligands and thus controls PFKL activity in immune cells to regulate glycolysis and their functions.

2 Aim of this work

When macrophages are activated by pro-inflammatory stimuli, their metabolism shifts from OXPHOS to glycolysis. Increased glycolysis has been described as beneficial for inflammatory responses through a variety of mechanisms (Section 1.4). Mitochondrial dysfunction and upregulation of the transcription factor HIF1α play an essential role in the upregulation of glycolysis during the late phases of stimulation (Section 1.4). However, glycolysis is induced in macrophages as early as 10 minutes after stimulation, and the underlying mechanism is unknown. Conceptually, rapid modulation of glycolysis should involve changes in the rate-limiting enzymes of glycolysis. For example, in DCs, TBK1-mediated HK-II phosphorylation promotes its association with mitochondria, thereby upregulating its activity and contributing to the early glycolytic burst (Everts et al., 2014). Based on the hypothesis that PRR pathways may rapidly influence the activity of rate-limiting enzymes of glycolysis through allosteric mechanisms in macrophages, we focused our efforts on exploring potential post-translational modifications affecting these enzymes. Interestingly, our analysis of published phosphoproteomic data revealed that PFKL was among the top 10 proteins with increased phosphorylation, specifically at Ser775, in macrophages after 30 minutes of LPS treatment (Sjoelund et al., 2014). Furthermore, PFKL Ser775 phosphorylation is also strongly induced by N-formylmethionyl-leucyl-phenylalanine (fMLP) in neutrophils (Muschter et al., 2015), which rely on glycolysis for their effector functions. As discussed in Section 1.5, PFKL catalyzes the first reaction of glucose binding to the glycolytic pathway, making it critical in determining glycolytic flux. Therefore, if phosphorylation of PFKL at Ser775 does indeed occur in macrophages upon stimulation, it is highly likely that it contributes to the induction of the early glycolytic burst. Therefore, in this work we aim to:

1. Generate an anti-PFKL Ser775 phosphospecific antibody to study PFKL phosphorylation at Ser775 in macrophages after treatment with TLR agonists.

2. To study the signaling pathway upstream of PFKL Ser775 phosphorylation.

3. To study whether PFKL Ser775 phosphorylation regulates its activity.

4. Generate a mouse model in which PFKL cannot be phosphorylated at Ser775 to study the role of PFKL Ser775 phosphorylation in the induction of early glycolysis and innate immune response.

3 Materials and Methods

3.1 Materials

3.1.1 Mouse bone marrow-derived macrophages (mBMDM)

mBMDM were derived from bone marrow (BM) of C57BL/6J mice.

3.1.2 Human monocyte derived macrophages (hMDM)

hMDM were derived from healthy donors.

3.1.3 Neutrophils

Neutrophils were isolated from BM of 8-12 weeks old C57BL/6J mice.

3.1.4 Cell lines

Cell lines	**Information**
HEK293T	Human embryonal kidney cells stably expressing SV 40 large T antigen
L929 fibroblast	Mouse fibroblast cell line used to generate L929 sup

3.1.5 Bacterial strains

Strain	**Source**
E.coli DH5α	DH5α were generated according to the protocol described in the Promega brochure “Subcloning Notebooks” (Promega).

3.1.6 Cell culture materials

Name	**Supplier**
RPMI 1640	Thermo Fisher Scientific
DMEM	Thermo Fisher Scientific
Fetal Bovine Serum (FBS)	Thermo Fisher Scientific
Penicillin-Streptomycin	Thermo Fisher Scientific
Sodium pyruvate	Thermo Fisher Scientific
Doxycycline hyclate	Sigma-Aldrich
Puromycin	InvivoGen
OptiMEM	Thermo Fisher Scientific

Trypsin-EDTA (0.05%)	Thermo Fisher Scientific
Seahorse XF DMEM medium, pH7.4	Agilent Technologies
Seahorse XF RPMI medium, pH7.4	Agilent Technologies
DMEM, no glucose	Thermo Fisher Scientific
HEPES	Sigma-Aldrich
D-Glucose-^{13}C6	Sigma-Aldrich
Fetal Bovine Serum dialyzed	Thermo Fisher Scientific
Seahorse XF 200 mM glutamine solution	Agilent Technologies
Seahorse XF 1.0 M glucose solution	Agilent Technologies
Seahorse XF 100 mM pyruvate solution	Agilent Technologies
M-CSF	Max Plank protein facility
Mouse IFNγ	ImmunoTools
Gentamicin	Thermo Fisher Scientific

3.1.7 Plasmids

Plasmids	**Usage**
pLI_Strep_PFKL^{WT}_Puro	Generation of stable human PFKL expressing HEK293T
pLI_Strep_PFKL^{S775A}_Puro	Generation of stable human PFKL S775A expressing
pLK0.1-gRNA-CMV-GFP	KO generation
pRZ-CMV-mCherry-Cas9	KO generation
pMDLg/pRRE	Lentivirus generation
pRSV-Rev	Lentivirus generation
pCMV-VSVg	Lentivirus generation
pcDNA3.1_IKKβ	Transfection
pCMV_HA_PKCδ	Transfection

3.1.8 Primers

Primers	**Sequence**	**Application**
PFKL.fwd.Nhe.strep	ATTAGCTAGCATGTGGAGCCACCCCCAGTTC GAGAAGAGCGCCGCCGCGGTGGACCTG	Cloning

Ser-ala.PFKL.rev.Bcl1	ATTATGATCATCAGAAGCCCTTGTCCATGGCC AGGGTGCGG	Cloning
PFKL.rev.Bcl1	ATTATGATCATCAGAAGCCCTTGTCCATGCTC	Cloning
EF-TREfwdseq	GTATGTCGAGGTAGGCGTGTACG	Sequencing
PFKL-M-Fwd	GACTGAACATCATCATCATCGCTG	Sequencing
EF-PGKrevseq	GCAAACCCAGGGCTGCCTTG	Sequencing
Fwd-PFKL	ACACTCTTTCCCTACACGACGCTCTTCCGATC TTGGCAGGAGAGGGGTCTC	Miseq
Rev-PFKL	TGACTGGAGTTCAGACGTGTGCTCTTCCGATC TCACTCACCTCTGGGCAGTG	Miseq
mutagenic single-stranded oligodeoxynucleotide	GGTGAGAGTCCGGGAACGCAGGAACAGTAGT GACAGTAAGCTCAGAAACCCTTGTCTATGgcC AAGGTGCGGCGTGTGACGTGCTCCAGCTCCC CAGACACATAGTCTGCCATGCTGATGCG	*Pfkl*$^{S775A/S775A}$ mouse generation
Pfkl-Ex22-GT-for	CAGACTCAGCCTGTGTGATCG	Mouse genotyping
Pfkl-Ex22-GT-rev	CTCTGGTCATGTTGTCCCAGT	Mouse genotyping
mIL1B_qPCR_Fwd	ACGGACCCCAAAAGATGAAG	RT-qPCR
mIL1B_qPCR_Rev	TTCTCCACAGCCACAATGAG	RT-qPCR
mHIF1a_qPCR_Fwd	GAACATCAAGTCAGCAACGTG	RT-qPCR
mHIF1a_qPCR_Rev	TTTGACGGATGAGGAATGGG	RT-qPCR
qPCR_mBeta actin_F	TGGATCGGTGGCTCCATCCTGG	RT-qPCR
qPCR_mBeta actin_R	GCAGCTCAGTAACAGTCCGCCTAGA	RT-qPCR
mIL6_qPCR_Fwd	CAAAGCCAGAGTCCTTCAGAG	RT-qPCR
mIL6_qPCR_Rev	GTCCTTAGCCACTCCTTCTG	RT-qPCR
mTNF_qPCR_Fwd	CTTCTGTCTACTGAACTTCGGG	RT-qPCR
mTNF_qPCR_Rev	CAGGCTTGTCACTCGAATTTTG	RT-qPCR
mNOS2_qPCR_Fwd	GCAAACATCACATTCAGATCCC	RT-qPCR
mNOS2_qPCR_Rev	TCAGCCTCATGGTAAACACG	RT-qPCR

3.1.9 sgRNA

Target Gene	Target Site and PAM
PFKL	CGCGATGTTCAGGTGCGAGT**AGG**

3.1.10 Antibodies

Antibody	Application	Supplier	Dilution
β-actin-HRP	WB	Santa Cruz	1:5000
HIF1α (D1S7W) XP® Rabbit mAb	WB	Cell Signaling	1:1000
Mouse IL-1 beta /IL-1F2 Antibody	WB	R&D system	1:1000
IgG (H+L) Donkey anti-Goat, HRP	WB	Invitrogen	1:3000
Anti-rabbit IgG-HRP	WB	Cell Signaling	1:3000
Phospho-NF-κB p65 (Ser536) (93H1) Rabbit mAb	WB	Cell Signaling	1:1000
HA Tag (6E2) Mouse mAb (HRP Conjugate)	WB	Cell Signaling	1:1000
HRP-Goat Anti-Mouse IgG, Fcγ secondary antibody	WB	Jackson ImmunoResearch	1:3000
Ikkβ (D30C6) Rabbit mAb	WB	Cell Signaling	1:1000
Phospho-Akt (Thr308) (C31E5E)	WB	Cell Signaling	1:500
Phospho-Akt (Ser473) (D9E) XP® Rabbit mAb	WB	Cell Signaling	1:1000
Akt (pan) (C67E7) Rabbit mAb	WB	Cell Signaling	1:1000
PFKL (4B2)	WB	This study	1:250
pSer775-PFKL (6C12)	WB; IP	This study	1:100; 100 µl
APC/Cyanine7 anti-mouse CD3ε Antibody (145-2C11)	FACS	BioLegend	1:50
PE/Dazzle 594 anti-mouse CD4 Antibody (GK1.5)	FACS	BioLegend	1:100

PerCP/Cyanine5.5 anti-mouse CD8b.2 Antibody (53-5.8)	FACS	BioLegend	1:100
PE/Cyanine7 anti-mouse CD19 Antibody (6D5)	FACS	BioLegend	1:200
Brilliant Violet 421™ anti-mouse CD335 (NKp46) Antibody (29A1.4)	FACS	BioLegend	1:50
Alexa Fluor 488 anti-mouse/human CD11b Antibody (M1/70)	FACS	BioLegend	1:200
Brilliant Violet 605 anti-mouse Ly-6G Antibody (1A8)	FACS	BioLegend	1:200
Brilliant Violet 785 anti-mouse F4/80 Antibody (BM8)	FACS	BioLegend	1:500
Alexa Fluor 700 anti-mouse CD11c Antibody (N418)	FACS	BioLegend	1:200
APC anti-mouse I-A^b Antibody (AF6-120.1)	FACS	BioLegend	1:50

3.1.11 Chemicals and reagents

Chemicals and Reagents	**Supplier**
GeneJuice® Transfection Reagent	Merck Chemicals GmbH
cOmplete™, EDTA-free Protease inhibitor-Cocktail	Roche
DNase I (1 U / µL)	Thermo Fisher Scientific
RevertAid Reverse Transcriptase (200 U / µL)	Thermo Fisher Scientific
RiboLock Rnase Inhibitor (40 U / µL)	Thermo Fisher Scientific
dNTP	Genaxxon
Phusion High-Fidelity DNA Polymerase	Thermo Fisher Scientific
ROTI GelStain	Roth
PhosSTOP	Sigma-Aldrich
D-Fructose-6-phosphate Dinatriumsalz Hydrat	Sigma-Aldrich
D-Fructose 1,6-bisphosphate trisodium salt hydrate	Sigma-Aldrich
Adenosine 5′-triphosphate (ATP) disodium salt hydrate	Sigma-Aldrich

Biotin	Sigma-Aldrich
Go 6983	Selleck Chemicals
Methanol, Optima ™ LC / MS Grade	Fisher Scientific
Trypan Blue	Sigma-Aldrich
β-mercaptoethanol	Sigma-Aldrich
FcR Blocking Reagent, mouse	Miltenyi Biotec
Pierce ™ Water, LC-MS Grade	Thermo Fisher Scientific
D-(+)-Maltose Monohydrat	Sigma-Aldrich
Diphenyleneiodonium chloride	Sigma-Aldrich
Antimycin A aus Streptomyces sp	Sigma-Aldrich
Rotenone	Sigma-Aldrich
Carbonyl cyanide-p-trifluoromethoxyphenylhydrazone (FCCP)	Sigma-Aldrich
Oligomycin A	Sigma-Aldrich
2-Deoxy-D-glucose (2-DG)	Sigma-Aldrich
Proteinase K	Roth
SYTOX ™ Green Nucleic Acid Stain	Invitrogen
Zymosan A from Saccharomyces cerevisiae	Sigma-Aldrich
RBC Lysis Buffer (10X)	BioLegend
Strep-Tactin ™ XT Superflow ™ 50% suspension	IBA Lifesciences
Pierce Protein A Agarose	Thermo Fisher Scientific
Wortmannin	Selleck Chemicals
MK2206 2HCl	Selleck Chemicals
Takinib	Selleck Chemicals
Trifluoroacetic acid	Sigma-Aldrich
Phorbol 12-myristate 13-acetate (PMA)	Enzo Life Sciences
TPCA-1	R&D Systems
UltraPure 0.5M EDTA, pH 8.0	Thermo Fisher Scientific
nitrocellulose membrane (0.45µm)	GE Healthcare
Bovine Serum Albumin (BSA)	Sigma-Aldrich
L-glutamine	Cambridge Isotope
L-arginine	Cambridge Isotope

Hoechst 33342 Solution	Thermo Fisher Scientific
LPS	InvivoGen
R848	InvivoGen
Pam_3CSK_4	InvivoGen
poly(I:C)	InvivoGen
Octyl-α-KG	Sigma-Aldrich
DMOG	Sigma-Aldrich

3.1.12 Commercial kits

Name	**Supplier**
Live/dead™ Fixable Aqua Dead Cell Stain Kit	Invitrogen
EasySep™ Mouse Neutrophil Enrichment Kit	STEMCELL Technologies
Anti-Rat and Anti-Hamster Ig κ /Negative Control	BD Biosciences
Anti-Mouse Ig, κ/Negative Control Compensation Particles Set	BD Biosciences
Seahorse XFe96 FluxPak	Agilent Technologies
ArC ™ Amine Reactive Compensation Bead Kit	Invitrogen
Seahorse XF Glycolysis Stress Test Kit	Agilent Technologies
Pierce BCA Protein Assay Kit	Thermo Fisher Scientific
QIAquick PCR Purification Kit	Qiagen
Total RNA Purification Mini Spin Kit	Genaxxon
Mouse IL-6 ELISA Set	BD Bioscience
Mouse TNF ELISA Set	BD Bioscience
LEGENDplex™ Mouse Inflammation Panel (13-plex) with V-bottom Plate	BioLegend

3.1.13 Media and buffers

Buffer	**Components**
HEK293T and L929 fibroblast culture medium	DMEM 10% FBS

	Sodium pyruvate (1 mM) 100 U/ml Penicillin-Streptomycin
mBMDM differentiation medium	DMEM 10% FBS Sodium pyruvate (1 mM) 100 U/ml Penicillin-Streptomycin 30% L929 sup
hMDM differentiation medium	RPMI 1640 10% FBS Sodium pyruvate (1 mM) 100 U/ml Penicillin-Streptomycin 200 ng/ml M-CSF
Neutrophil culture medium	RPMI 1640 HEPES (10 mM)
Neutrophil isolation buffer	PBS 2% FBS 1 mM EDTA
Isotopic tracing assay medium	DMEM, no glucose D-Glucose-$^{13}C_6$ (10 mM) 10% FBS, dialyzed Sodium pyruvate (1 mM) 100 U/ml Penicillin-Streptomycin
DISC cell lysis buffer	30 mM Tris-HCl pH 7.5 150 mM NaCl 10% Glycerol (v/v) 1% Triton-X-100 (v/v)
Direct lysis buffer	0.2 mg/ml Proteinase K 1 mM $CaCl_2$ 3 mM $MgCl_2$ 1 mM EDTA 1% Triton X-100 10 mM Tris pH 7.5
LB agar	20 g LB

	15 g Agar 1 L H2O Autoclave before usage
LB medium	20 g LB 1 L H2O Autoclave before usage
Miniprep buffer N3	4.2 M Guanidinhydrochlorid 0.9 M Kaliumacetat pH 4.8
Miniprep buffer P1	50 mM Tris pH 8 10 mM EDTA 100 µg/ml RNase A
Miniprep buffer P2	200 mM NaOH 1% SDS
Miniprep buffer PE	10 mM Tris pH 7.5 80% ethanol
HBS buffer	50 mM HEPES pH 7 280 mM NaCl 1.5 mM Na_2HPO_4 sterile filtered
TAE buffer	40 mM Tris pH 8.0 20 mM acetic acid 1 mM EDTA
TBS buffer (10x)	1.5 M NaCl 100 mM Tris pH 8
6x Lämmli buffer	450 mM Tris-HCl pH 6.8 600 mM DTT 12% SDS (w/v) 60% glycerol (v/v) 0.06% bromophenol blue (w/v)
10 x Tris-Glycine buffer	290 g Tris 1440 g Glycine

	add water to volume 10 L
Western Blot transfer buffer	200 ml 10 x Tris-Glycine buffer 400 ml ethanol 1400 ml water
Enzymatic reaction buffer	50 mM Tris-HCl pH 7.4 100 mM KCl 10 mM $MgCl_2$ 1 mM DTT 2 mM F6P 2 mM ATP
Elution buffer for strep tag protein purification	50 mM Tris-HCl pH 7.8 100 mM KCl 1 mM DTT 50 mM biotin
Sample dilution buffer for in vitro enzymatic assay	10% acetonitrile (v/v) 90% 20 mM ammonium formate (v/v) pH 3.0
FACS buffer	PBS 2% FBS
Metabolite extraction buffer	LC/MS grade MeOH (80%, v/v) LC/MS grade H_2O (20%, v/v) Maltose (10 µM) L-Arginine (10 µM) L-Glutamine (10 µM)
HPLC buffer A	95% (v/v) water 5% (v/v) acetonitrile 20 mM ammonium hydroxide 20 mM ammonium acetate pH 9.0
HPLC buffer B	100% acetonitrile
ELISA coating buffer	0.1 M sodium carbonate/NaOH pH 9.5 7.13 g/l $NaHCO_3$ 1.59 g/l Na_2CO_3

ELISA dilution buffer	10% (v/v) FCS in PBS

3.1.14 Laboratory equipment

Device	**Supplier**
PCR cycler	Bio-Rad
Mini Gel Tank	ThermoFisher Scientific
Mini Trans-Blot	Bio-Rad
Absorbance reader	TECAN/Epoch
Fusion Fx device	Vilber
Nanodrop	Peqlab
Centrifuge	Eppendorf
Sony sorter SH800Z	Sony
Chemidoc imaging system	Bio-Rad
BD LSR Fortessa	BD Biosciences
Seahorse XFe96 Analyzer	Agilent Technologies
Cytation 5 Imaging Reader	BioTek
Thermoshaker	Eppendorf
Amicon Ultra-15, 10kDa	Merck
QTRAP ® 5500 LC-MS/MS System	SCIEX
Savant SpeedVac concentrator	Thermo Fisher Scientific
XBridge Amide HPLC column	Waters
CFX96 Touch Real-Time PCR Detection System	Bio-Rad
TripleTOF 5600 mass spectrometer	SCIEX
Ultimate 3000 chromatography system	Thermo Fisher Scientific
Newcrom B HPLC column	SIELC Technologies Wheeling
NEPA21 electroporator	NEPAGENE
TC-20 Automated Cell Counter	Bio-Rad

3.1.15 Bioinformatic tools

Name	**Supplier**

FlowJo v10	Becton, Dickinson, and Company
ImageJ	(Schindelin et al., 2012)
GraphPad Prism 9	GraphPad
Outknocker	(Schmid-Burgk et al., 2014)
Illustrator	Adobe Creative Cloud
SnapGene	GSL Biotech LLC
Primer3plus	(Untergasser et al., 2007)
Image Lab	Bio-Rad
PeakView V2.2 software	SCIEX
Analyst software	ABSciex

3.2 Molecular biology methods

3.2.1 Restriction enzyme cloning

To get the DNA plasmids, insert genes were amplified from the cDNA of mammalian cells by polymerase chain reaction (PCR). The required restriction sites and strep tag were added by primers. The PFKL^{S775A} mutation was generated using a primer carrying Ser-Ala mutation. The insert and the vector were digested with the same restriction enzymes at 37°C for 1 h. The digested fragments were purified by agarose gel purification and ligated with T4 ligase. The ligation mixture was transformed into *E.coli* DH5α.

3.2.2 Ligation independent cloning (LIC)

sgRNA targeting the early coding exon of human PFKL was designed using the web-based tool CHOPCHOP (http://chopchop.cbu.uib.no/). The oligonucleotide used for ligation independent cloning is composed of 5'-GGAAAGGACGAAACACCG-3' overhang followed by the target sequence without the first nucleotide and PAM, followed by 5'-GTTTTAGAGCTAGAAATAGCAAGTTAAAATAAGG-3' overhang.

The expression plasmid was digested with the FastDigest enzymes ApaI and SpeI followed by agarose gel purification. The overhangs were generated by the 3'-5' exonuclease activity of T4 DNA polymerase in the presence of dTTP as stop nucleotide:

10 µl	10x NEB2 buffer
10 µl	Vector 70 ng/µl
1 µl	BSA 10 mg/ml

1 µl	dTTP 100 mM
3.33 µl	T4 DNA polymerase 3 U/µl
74.66 µl	H_2O

The reaction was incubated at 27°C for 5 min and heat inactivated at 75°C for 20 min. The mixture was mixed with the universal reverse binding oligonucleotide LICsgRNA_rev (PAGE purified, 100 µM, IDT):

20 µl	10x NEB2 buffer
69.5 µl	H_2O
0.5 µl	LICsgRNA_rev 100 µM
10 µl	Vector mixture

2.5 µl the above master mixture was mixed with 2.5 µl of sgRNA oligonucleotide (0.25 µM) and annealed according to the following program:

70°C	1 min
65°C	1 min
60°C	30 s (29 cycles; -1°C/cycle)
55°C	2.5 min
25°C	∞

The mixture was transformed into *E. coli* DH5α.

3.2.3 *E. coli* transformation

Chemically competent *E. coli* DH5α were thawed on ice and the plasmid DNA of interest was added, mixed, and incubated for 30 min on ice. Then the bacteria were heat-shocked at 42°C for 1 min, immediately put on ice for 2 min, and then cultured in 500 µl LB medium for 45 min at 37°C with vigorous shaking. Afterward, bacteria were pelleted by centrifugation (2,000 rpm, 2 min), suspended in 50 µl LB medium, plated on LB agar plates with the appropriate antibiotic, and incubated at 37°C overnight.

3.2.4 Isolation of plasmids

A small scale of plasmid DNA from *E. coli* DH5α was isolated using self-made buffers according to the protocol of the QIAprep Spin Miniprep Kit. For higher yield, the plasmid was isolated using the PureLink HiPure Plasmid Maxiprep Kit according to the manufacturer's instructions.

3.2.5 RNA extraction and purification

RNA from mammalian cells was extracted and purified using Total RNA Purification Mini Spin Kit according to the supplier's protocols, followed by DNase I treatment:

0.5 µl	10 x DNase Buffer I with $MgCl_2$
0.5 µl	DNase I (1 U/µl)
4 µl	RNA

The mixture was incubated for 30 min at 37°C followed by the addition of 0.5 µl EDTA and incubation at 70°C for 10 min. RNA can be stored at -80°C or directly used for cDNA synthesis.

3.2.6 cDNA synthesis

A master mix was prepared for each reaction as follows:

2 µl	5 x RT buffer
0.5 µl	Oligo dT
1 µl	dNTPs
0.5 µl	revertAid reverse transcriptase (200 U/µl)
0.5 µl	RiboLock Rnase inhibitor (40 U/µl)

4.5 µl the above master mix was mixed with 5.5 µl purified RNA and annealed according to the following program:

42°C	1 h
70°C	10 min
-20°C	storage

cDNA was diluted by adding 30 µl of dH_2O and stored at – 20°C.

3.2.7 Quantitative PCR (qPCR)

The reaction was prepared as follows:

SYBR green	5 µl
Fwd Primer	0.5 µl
Rev Primer	0.5 µl
cDNA	4 µl

qPCR was performed using a CFX96 Touch Real-Time PCR detection system according to the following annealing program:

95°C	3 min	
95°C	15 s	45 cycles
58°C	20 s	
72°C	15 s	
65°C	5 s	
95°C	5 s	

The cycle threshold (Ct) was used to quantify the expression of target genes, which was then normalized to the expression of β-actin (ΔCt). To determine the relative gene expression using the ΔCt method, the following equation was employed:

$$\text{Relative gene expression} = 2^{(-(Ct(\text{target gene}) - Ct(\beta\text{-actin})))}$$

3.2.8 PCR

To amplify a specific DNA sequence, a Phusion High-Fidelity PCR Kit was applied according to the manufacturer's instructions.

3.2.9 DNA gel electrophoresis

DNA fragments generated by PCR or digested plasmids were analyzed by agarose gel electrophoresis. Agarose powder was dissolved in 1 x TAE buffer and heated until fully dissolved. 0.005% (v/v) ROTI GelStain was added to the gel before pouring it into the electrophoresis chamber. Samples were mixed with DNA loading buffer and loaded on the agarose gels. Gels were run in 1× TAE buffer at 120 V for 30-40 min and visualized under UV light.

3.2.10 Sanger sequencing

Sanger sequencing was performed by Eurofins (TubeSeq service).

3.3 Cell culture methods

3.3.1 Cell lines

HEK293T and L929 fibroblast cells were maintained in DMEM medium supplemented with 10% fetal bovine serum (FBS), 1 mM sodium pyruvate, 100 U/ml Penicillin-Streptomycin at 37°C in 5% CO_2 incubator.

L929 fibroblast cells were cultured for 2-3 weeks, and the supernatant was harvested every 3 days before passage. All supernatant was pooled together, passed through a 0.22 µM filter, aliquoted, and stored at -80°C.

3.3.2 mBMDM culture

Bone marrow cells were rinsed from the femur and tibia of C57BL/6J mice into Ca^{2+}- and Mg^{2+}-free PBS using a syringe. Clumps and debris in the cell suspensions were removed by passing the cell suspension through a 100 µm cell sieve. Cells were spun down at 400 g for 10 min and the cell pellet was resuspended in 2 ml of 1x RBC lysis buffer for 2 min at room temperature to remove red blood cells. After centrifugation, the cells were differentiated in DMEM medium supplemented with 10% FCS, 100 U/ml penicillin-streptomycin, 1 mM sodium pyruvate, and 30% L929-conditioned medium (obtained from the supernatant of L929 fibroblast cells) in low-adhesion dishes for 6 days. On the 6^{th} day of differentiation, mBMDM were detached with PBS containing 2 mM EDTA and replated into 12-well plates for Western blot (10^6 cells per well). To check AKT and PFKL phosphorylation by Western blot, detached mBMDM were seeded overnight in DMEM medium supplemented with 0.5% FCS. For other experiments, mBMDM were plated in normal DMEM medium supplemented with 10% FCS.

3.3.3 hMDM culture

Human peripheral blood mononuclear cells (PBMCs) were isolated from healthy donors by density gradient centrifugation. Human monocytes were then purified from PBMCs using CD14 microbeads and differentiated into monocytes-derived macrophages in RPMI 1640 supplemented with 10% FCS, 100 U/ml Penicillin-Streptomycin, 1 mM sodium pyruvate, and 200 ng/ml M-CSF for 6 days. Freshly M-CSF was added on day 3 and day 5. To check AKT and PFKL Ser775 phosphorylation by western blot, the medium was changed into RPMI 1640 medium supplemented with 0.5% FCS on day 5. Human monocytes were differentiated in seahorse 96-well cell culture plates for seahorse assays (7×10^4 cells per well), and 12-well plates for western blot (10^6 cells per well).

3.3.4 Neutrophil isolation and culture

BM cells derived from 8-12 weeks old C57BL/6J mice were flushed from the femur and tibia into PBS which is free of Ca^{2+} and Mg^{2+} using a syringe. Clumps and debris in cell suspensions were removed by passing the cell suspension through a 100 µm cell strainer. Cells were spun down at 300 g for 10 min and the cell pellet was resuspended in 2 ml 1x RBC lysis buffer for 2 min at room temperature to get rid of red blood cells. After centrifugation, cells were resuspended into PBS containing 2% FCS and 1 mM EDTA. Neutrophil isolation was performed using the EasySep mouse neutrophil enrichment kit according to the

manufacturer's protocol. Neutrophils were maintained in RPMI 1640 medium containing 10 mM HEPES.

3.3.5 Cell stimulation

In order to investigate the activation of PFKL at Ser775, mBMDM or hMDM were stimulated with LPS (200 ng/ml), R848 (1 µg/ml), poly(I:C) (20 µg/ml), or Pam_3CSK_4 (500 ng/ml) for appropriate time periods. To assess whether zymosan induces phosphorylation of PFKL at Ser775, mBMDM were first primed with 20 ng/ml mouse IFNγ overnight and then stimulated with zymosan (100 ng/ml) for indicated time periods. To determine which upstream kinases are responsible for the phosphorylation of PFKL Ser775, cells were pretreated with DMSO, Takinib, TPCA-1, MK2206 2HCl, Wortmannin, or Go 6983 for 1 h followed by stimulation with TLR agonists for 30 min or 1 h.

3.4 Generation of knockout cell line

Gene-deficient HEK293T cells were generated using the CRISPR/Cas9 system. gRNA targeting the early coding exon of PFKL was designed and cloned into the plasmid pLKO.1-gRNA-CMV-GFP using LIC.

3.4.1 Transfection of HEK293T cells

HEK293T cells were seeded at a density of 1.5 x 10^5 cells per well in 24-well plates. The next day, 500 ng DNA was transfected using GeneJuice according to the manufacturer's instructions. mCherry-Cas9 and gRNA constructs were transfected in a ratio of 3:1.

3.4.2 FACS sorting of HEK293T cells

24 h after transfection, HEK293T cells were trypsinized, spun down for 5 min at 500 g, resuspended in 500 µl DMEM medium, and passed through a 40 µm cell strainer. mCherry positive cells were sorted using SONY SH800Z and subjected to limiting dilution cloning.

3.4.3 Serial dilution

To get monoclones, mCherry positive cells were serially diluted. Three plates of each 4, 2, and 1 cell per well were plated. After 2-3 weeks, monoclones were identified, replated, and grown for genotyping by deep sequencing (Illumina's Miseq-platform).

3.4.4 Deep sequencing

Monoclones were lysed using direct lysis buffer for 10 min at 65°C, followed by a heat inactivation step at 95°C for 15 min. A two-step PCR was then used. The first PCR uses primers carrying overhanging adapter sequences which not only amplifies the gene of interest but also form the binding site for the second PCR primers. The first PCR usually generates an

approximately 250 bp long amplicon and the target region should not be within the first or last 50 bp of the amplicon. The PCR reaction was prepared as follows:

HF or GC buffer	1.2 µl
dNTPs (10 mM)	0.12 µl
Fwd primer (50 µM)	0.06 µl
Rev primer (50 µM)	0.06 µl
Phusion polymerase	0.06 µl
H_2O	3.5 µl
Lysate	1 µl

The PCR reaction was then incubated as follows:

95°C	3 min	
95°C	30 s	18 cycles
62°C	30 s	
72°C	30 s	
72°C	3 min	
12°C	storage	

The second PCR is used to add a unique set of barcodes carrying the Illumine sequencing adapters to the first-PCR product. 16 diverse forward and 24 diverse reverse barcode primers were mixed to obtain 384 unique primer combinations. The PCR reactions were prepared as follows:

HF or GC buffer	1.2 µl
dNTPs (10 mM)	0.12 µl
primer mix (2.5 µM)	1.2 µl
Phusion polymerase	0.06 µl
H_2O	3.92 µl
Lysate	1 µl

The same program used for PCR1 was run. All PCR products were then pooled, subjected to agarose gel purification and precipitation, and sequenced using an Illumina Miseq instrument (MiSeq Reagent Kit v2, 300 cycles, #MS-102-2002). FastQ files were generated and analyzed using the published web-based tool "Outknocker" (Schmid-Burgk et al., 2014). Monoclones with both allelic out-of-frame indels were selected and used for further experiments.

3.5 Cell biology methods

3.5.1 Virus production and transduction of target cells

To generate HEK293T cells expressing the target gene in an inducible manner, the third generation lentiviral vector system was used. This system uses 4 plasmids: pLI_Gene Of Interest_puro (transfer plasmid), pMDLg/pRRE, pRSV-rev (packaging plasmids), and pCMV-VSV-G (envelope plasmid). To generate lentiviruses, 3 x 10^6 HEK293T cells were plated in a 10 cm dish. The next day, the DNA (8 µg transfer plasmid, 12 µg pMDLg/pRRE, 4 µg pRSV-rev and 8 µg pCMV-VSV-G in 500 µl water) was mixed with 500 µl 2 x HBS buffer and 50 µl 2.5 M $CaCl_2$ was added. After shaking briefly, the mixture was incubated at room temperature for 20 min and then dispensed into the dish. 8 h after transfection, the culture medium was changed to DMEM containing 15% FCS. 72 h after transfection, the supernatant was collected, centrifuged at 1000 g for 10 min, and filtered (0.45 µm). Virus was used fresh or stored at -80°C until use.

To infect HEK293T *PFKL*$^{-/-}$ cells, cells were seeded at a density of 3 x 10^5 cells per well in 6-well plates overnight and then infected with different amounts of virus. At 48 h post infection, medium containing 2.5 µg/ml puromycin was added to each well and cells were kept under selection for 48 - 72 h. When control cells without infection died, surviving cells were analyzed for expression of the gene of interest. The polyclonal cell population was used for further experiments.

3.5.2 Isotopic tracing assay

mBMDM were primed with 20 ng/ml mouse IFNγ overnight in normal culture medium and stimulated with 100 µg/ml zymosan in glucose-free DMEM medium supplemented with 10% dialyzed FCS, 10 mM uniformly labeled U-^{13}C-glucose, 100 U/ml Penicillin-Streptomycin, and 1 mM sodium pyruvate the following day. After stimulation, the medium was removed and 1 ml ice-cold 80% methanol: water solution (v/v), including maltose as an internal standard was added to each well. After 20 min incubation at −80°C, cells were scraped and the cell suspension was centrifuged at 13,000 × g at 4°C for 10 min, and then the supernatants were dried in a SpeedVac concentrator. Lyophilized samples were reconstituted in 40 µl of LCMS-grade water, vortexed, and centrifuged again for 10 min at 13,000 × g at 4°C. Samples were analyzed by liquid chromatography-mass spectrometry (LC-MS).

3.5.3 Bacterial killing assay

mBMDM were plated in antibiotic-free DMEM medium containing 20 ng/ml mouse IFNγ in 24-well plates at a density of 5 x 10^5 per well. On the next day, *E. coli* was subcultured to reach OD 0.5-0.6 and added to cells at a multiplicity of infection (MOI) of 10. mBMDM were then

incubated for 30 min at 37°C to allow internalization. After 30 min, cells were washed 3 times with PBS, and DMEM medium containing 200 µg/ml gentamicin was added to kill extracellular bacteria. 1 h later, the medium was replaced with the fresh DMEM medium containing 50 µg/ml gentamicin to block the division of extracellular bacteria. At indicated time points (time after internalization), cells were washed once with PBS and lysed with 500 µl 0.05% triton-X 100 in sterile water for 10 min at room temperature. Lysates were serially diluted in PBS and plated on antibiotic-free agar plates and colonies were counted after overnight incubation at 37°C. The protocol is similar for neutrophils, with the exception that *E. coli* was opsonized with 10% mouse serum before infection.

3.6 LC-MS

3.6.1 LC-MS analysis of cellular metabolites

Samples were analyzed using an Agilent 1200 series HPLC system coupled to an ABSciex 5500 hybrid triple quadrupole/linear ion trap mass spectrometer equipped with an electrospray ionization source operating in positive or negative mode. The Q1 (precursor ion) and Q3 (fragment ion) transitions, metabolite identifier, retention times, and collision energies for both positive and negative ion modes were used according to published methods with additional transitions for our internal standards (Yuan et al., 2012; Yuan et al., 2019). Five microliters of sample were injected into an XBridge Amide HPLC column (3.5 µm; 4.6 mm × 100 mm). The mobile phases were run at 400 µL min-1 and consisted of HPLC buffer A and HPLC buffer B. The HPLC settings were as follows: from 0 to 0.1 min, the mobile phase was maintained at 85% buffer B; from 0.1 to 3 min, the percentage of buffer B was decreased from 85% to 30%; from 3 to 12 min, the percentage of buffer B was decreased from 30% to 2% and maintained at 2% for an additional 3 min. At minute 15, the percentage of buffer B was increased to 85% and the column was flushed with 85% buffer B for an additional 8 min. Data analysis was performed using Analyst software (ABSciex). Metabolite peaks were normalized to cell number and internal standards prior to statistical analysis. Retention times for all metabolites were verified using individual purified standards from Sigma: (Glycolysis/Gluconeogenesis Metabolite Library (ML0013-1KT), Pentose Phosphate Metabolite Library (ML0012), TCA Cycle Metabolite Library (ML0010)), L-glutathione reduced (G4251), L-glutathione oxidized (G6654), L-serine (S4500), and α-D-glucose 1-phosphate (G6750) using the same chromatographic method. Metabolites were quantified by integrating the chromatographic peak area of the precursor ion.

3.6.2 LC-MS analysis of F1,6BP

Samples were diluted in the mobile phase consisting of 10% acetonitrile and 90% 20 mM ammonium formate buffer (pH 3.0). 15 µl of the samples were transferred to an Ultimate 3000

chromatography system (Thermo Fisher Scientific) and separated on a Newcrom B HPLC column (0.5 mm x 100 mm, 5 µm, 100A, SIELC Technologies Wheeling, IL USA). Separation was performed at an isocratic flow rate of 75 µl/min for 15 min. A TripleTOF 5600 mass spectrometer (SCIEX, Toronto, Canada) was used for detection. The instrument was operated in negative ion mode with the following scan parameters: Scan type TOF-MS; mass range 200-400 Da; accumulation time 1 s; declustering potential -50. Chromatographic peaks were quantified using PeakView V2.2 software (SCIEX) at 259.0 m/z for F6P and 338.9 m/z for F1,6BP.

3.7 Biochemical methods

3.7.1 Protein purification

Transduced HEK293T cells were plated in 15 cm dishes (1 x 10^7 cells per dish) overnight and treated with 2 µg/ml doxycycline overnight for protein induction. Cells were then washed with cold PBS once and lysed in dishes with 1 ml DISC buffer supplemented with phosphatase inhibitor and protease inhibitor for 10 min on ice. The lysate was collected into 2 ml tubes and centrifuged at 16,000 g for 10 min at 4°C. The supernatant was transferred to 15 ml falcons and incubated with pre-washed Strep-Tactin XT beads overnight at 4°C. Proteins were eluted by incubating beads with elution buffer containing 50 mM biotin, 100 mM KCl, 1 mM DTT, and 50 mM Tris-HCl (pH 7.8). The eluents were further purified and concentrated using a 10 kDa MWCO Amicon Ultra Centrifugal Filter according to the manufacturer's instructions. Concentrations of purified proteins were determined by doing BCA Assay and purities were determined by Coomassie staining. Purified proteins were stored at -80°C.

3.7.2 In vitro enzymatic reaction

Enzymatic reactions were performed in reaction buffer containing 50 mM Tris-HCl (pH 7.4), 100 mM KCl, 10 mM $MgCl_2$, 1 mM DTT, 2 mM F6P, 2 mM ATP and 50 ng/µl $PFKL^{WT}$ or $PFKL^{S775A}$ protein at 37°C for 2, 4, 6, 8, and 10 min and stopped by the addition of 20 µl of trifluoroacetic acid (pH 2.0). F1,6BP production was quantified by LC-MS. Because the PFKL kinase reaction rate was linear for the first 2 min, the amount of F1,6BP formed per min during the first 2 min was used as the initial velocity.

3.7.3 Immunoprecipitation

HEK293T cells expressing inducible $PFKL^{WT}$ were plated in 15 cm dishes (1 x 10^7 cells per dish) overnight and then treated with 2 µg/ml doxycycline for 24 h. Cells were washed once with cold PBS and lysed in DISC buffer supplemented with phosphatase inhibitor and protease inhibitor for 10 min on ice. The cell lysate was collected after centrifugation and incubated with 100 µl of pSer775-PFKL antibody or 1 µg of the isotype control overnight at 4°C. The protein

A beads were prepared by 3 times washing with the lysis buffer. 100 µl of protein A resin slurry per sample was added to the antigen-antibody complex. After 2 h of incubation at room temperature, the supernatant was collected as flow-through samples. Beads were washed 5 times with PBS, resuspended in 50 µl of 2 x Laemmli buffer, boiled for 5 min at 95°C, and centrifuged. The supernatant was taken as immunoprecipitated samples.

3.7.4 Immunoblotting

All cells mentioned above were washed with cold PBS and then lysed directly on plates in DISC buffer supplemented with phosphatase inhibitor and protease inhibitor on ice for 10 min. The lysate was collected into 1.5 ml tubes and centrifuged at 16,000 g for 10 min at 4°C. Protein concentration in the supernatant was quantified by BCA assay according to the manual instruction. Proteins were mixed with 6 x Lämmli buffer and heated at 95°C for 5 min and loaded on an SDS-PAGE gel. Afterward, proteins were transferred on nitrocellulose membranes at 100 voltages for 1 h at 4°C, blocked in 5% BSA for 30-60 min at room temperature, and incubated with the primary antibodies overnight at 4°C. The next day, membranes were washed with TBS-T 3 times and incubated for another 1 h in the appropriate secondary antibodies at room temperature. After 3-time washing, chemiluminescent signals were detected by a CCD camera.

3.7.5 Flow cytometry

Single bone marrow cells were obtained as described in 3.3.2. Single splenocyte suspension was obtained by mincing the spleen thoroughly using a scissor, followed by passage through a 100 µm cell strainer. Red blood cells were depleted by incubating splenic cells with 5 ml RBC lysis buffer for 2 min at room temperature. Cells were then centrifuged and resuspended with FACS buffer (2% FCS in PBS) and blocked using FcR blocking reagent for 20 min at 4°C to avoid unspecific binding of antibodies. For cell surface staining, cells were stained with 100 µl of appropriate antibodies against surface antigens on ice for 30 min in the dark. After washing twice with PBS, the aqua fluorescent reactive dye was used according to the introduction from the manufacturer to exclude dead cells. Fluorescence minus one (FMO) controls were used to distinguish positively from negatively staining cell populations. Flow cytometry was performed on BD LSR Fortessa flow cytometer and data was acquired using BD FACSDiva Software. Data were analyzed using FlowJo software.

3.7.6 Enzyme-linked immunosorbent assay (ELISA)

Mouse IL6 and TNF ELISA kits were used according to the supplier’s protocols. In short, capture antibodies were applied onto high binding plates with ELISA coating buffer overnight at 4°C. The following day, plates were washed with PBST and blocked with 10% FCS in PBS

for 1 h at room temperature. Samples or standards were added to the plates, and if necessary, were diluted in PBS containing 10% FCS to ensure they did not exceed the highest point of the standard. After incubating for 2 h at room temperature, the plates were washed 5 times and a mix of detection antibody and streptavidin-HRP was added and incubated for 1 h in the dark. Then, the plates were washed 5 more times, and TMB solution was added. The reaction was stopped using 2N sulfuric acid, and the absorbance was read at 450 nm and 570 nm by a Gen5-Epoch microplate reader from BioTek.

3.8 Bioenergetic methods

3.8.1 Glycolytic stress text

HEK293T cells were seeded at a density of 2.5 x 10^4 per well in seahorse 96-well cell culture plates coated with poly-L-ornithine and treated with 1 µg/ml doxycycline for 24 h. For mBMDM, 7 x 10^4 per well were plated and stimulated with 200 ng/ml LPS for indicated time periods. Cells were then washed with the seahorse assay medium (Seahorse XF DMEM medium supplemented with 10 mM glucose and 2 mM glutamine) 3 times and cultured in this medium at 37°C for 60 min in a CO_2-free incubator. Real-time glycolytic rates were then measured in response to sequential injections (10 mM glucose, 1.5 µM oligomycin, and 50 mM 2DG) by Seahorse XFe96 Analyzer.

3.8.2 Mitochondrial stress test

mBMDM were seeded in seahorse 96-well cell culture plates (7 x 10^4 per well) overnight. The following day, cells were stimulated with 200 ng/ml LPS for indicated time periods. Cells were then washed with the seahorse assay medium (Seahorse XF DMEM medium supplemented with 10 mM glucose and 2 mM glutamine) 3 times and cultured in this medium at 37°C for 60 min in a CO_2-free incubator. Real-time respiratory rates were then measured in response to sequential injections (1.5 µM oligomycin, 1 µM FCCP, and 0.5 µM rotenone and antimycin A) by Seahorse XFe96 Analyzer.

3.8.3 Detection of respiratory burst by Seahorse assay

Seahorse 96-well cell culture plates were coated with poly-L-ornithine one day before the experiment. Freshly isolated neutrophils were washed with seahorse assay medium (Seahorse XF DMEM medium supplemented with 10 mM glucose, 2 mM glutamine, and 2 mM pyruvate) twice and seeded at a density of 7 x 10^4 per well. mBMDM (7 x 10^4 per well) were seeded in seahorse 96-well cell culture plates and primed with 20 ng/ml mouse INFγ one day before the experiment. The next day, mBMDM were washed with seahorse assay medium 3 times and cultured in this medium at 37°C for 60 min in a CO_2-free incubator. Real-time

respiratory rates were then measured in response to sequential injections (0.5 µM rotenone and antimycin A, 100 µg/ml zymosan or 100 ng/ml PMA) by Seahorse XFe96 Analyzer.

3.9 Animal study

3.9.1 Generation of *Pfkl*$^{S775A/S775A}$ mice

Pfkl$^{S775A/S775A}$ mice were generated using CRISPR/Cas9-mediated gene editing in zygotes, as previously outlined (Wefers et al., 2017). In brief, pronuclear stage zygotes were obtained by mating C57BL/6J male mice with superovulated C57BL/6J female mice. Embryos were then electroporated using the NEPA21 electroporator and a 1 mm electrode with a Pfkl-specific CRISPR/Cas9 ribonucleoprotein (RNP) solution consisting of 200 ng/µl S.p. Cas9 HiFi protein (IDT), 6 µM crRNA (protospacer GAAACCCTTGTCTATGCTCA; IDT), 6 µM tracrRNA (IDT), and 300 ng/µl mutagenic single-stranded oligodeoxynucleotide (ssODN) (5'-GGTGAGAGTCCGGGAACGCAGGAACAGTAGTGACAGTAAGCTCAGAAACCCTTGTCTATGgcCAAGGTGCGGCGTGTGACGTGCTCCAGCTCCCCAGACACATAGTCTGCCATGCTGATGCG-3'), comprising the S775A substitution (AGC>GCC). Post-electroporation, zygotes were implanted into pseudopregnant CD-1 surrogate animals.

Potential off-target sites for the Pfkl-specific crRNA were predicted using the CRISPR online tool (Concordet and Haeussler, 2018) to eliminate any unwanted modifications. Genomic DNA from the F1 generation was PCR-amplified and confirmed through Sanger sequencing, revealing no additional sequence variations.

All animal experiments were approved by the Bavarian government under license number ROB-55.2Vet-2532.Vet_02-16-121. All mice were treated in compliance with the institutional guidelines approved by the animal welfare and use committee of the government of Upper Bavaria. They were housed in standard cages in a specific pathogen-free facility, maintained on a 12-hour light/dark cycle, and given unrestricted access to food and water.

3.9.2 *Pfkl*$^{S775A/S775A}$ mouse genotyping

Mouse ear biopsy was lysed using 250 µl of direct lysis buffer at 55°C, 800 rpm overnight. Following this, the lysate was centrifuged at 16000 g for 10 min. To precipitate DNA, 250 µl of isopropanol was added to the supernatant, and the tubes were inverted 10 times. After centrifugation, the supernatant was discarded and the DNA pellet was washed with 175 µl of 70% ethanol. The DNA pellet was then spun down, dried for 10 min, and resuspended in 50 µl of TE buffer at 55°C, 800rpm overnight. The PCR reaction was then prepared as described below:

DNA	1 µl

5 X HF buffer	4 µl
Pfkl-Ex22-GT-for (10 µM)	1 µl
Pfkl-Ex22-GT-rev (10 µM)	1 µl
dNTPs	0.4 µl
Phusion	0.4 µl
water	12.2 µl

The program was as follows:

98°C	2 min	
98°C	20 s	30 cycles
55°C	20 s	
72°C	45 s	
72°C	5 min	
12°C	storage	

PCR products were then gel purified and sequenced. Since the S775A mutation gives rise to a cutting site for StyI, PCR products were digested with StyI for 3 h at 37°C and analyzed by agarose gel electrophoresis.

3.9.3 Measurement of serum cytokines

Serum cytokines were measured according to the manufacturer's instructions. Briefly, diluted serum and standards were incubated with capture beads which were coated with antibodies for 2 h at room temperature. The beads were washed once and incubated with detection antibodies for another hour at room temperature. SA-PE was then directly added to each well. After 30 min of incubation at room temperature, beads were washed once, resuspended in wash buffer, and analyzed by flow cytometry.

3.10 Statistical analysis

All statistical analysis was performed using GraphPad Prism 9. The exact number of replicates and statistical tests are indicated in figure legends. Unless otherwise indicated in the figure legends, *n* represents the number of biological replicates using cells from different mice or independent cultures.

4 Results

4.1 Primary macrophages undergo metabolic reprogramming upon activation

To characterize the metabolic changes during the early phase of macrophage activation, we performed seahorse assays on both mBMDM and hMDM using TLR agonists as stimuli. In both cell types, we found that the ECAR, an indicator of glycolysis, increased in response to all tested TLR ligands, including R848 (for TLR7/8), LPS (for TLR4), poly(I:C) (for TLR3), and Pam_3CSK_4 (for TLR1/2), but with different kinetics (Figure 4.1a and 4.1b). Specifically, R848 caused an early induction of glycolysis in both cell types as early as 10 min, whereas LPS-induced glycolysis reached maximal levels approximately 1 h after its addition to the cells (Figure 4.1a and 4.1b). To further characterize mitochondrial metabolism during the early phase of macrophage activation, mBMDM were stimulated with LPS for 1 or 2 h and then subjected to a mitochondrial stress test. We observed that both the basal and maximal mitochondrial respiration were upregulated in activated mBMDM compared to unstimulated mBMDM (Figure 4.1c), which is consistent with previously reported data (Langston et al., 2019; Lauterbach et al., 2019). Furthermore, the early increase in oxidative metabolism was shown to be driven by glucose oxidation (Langston et al., 2019), suggesting that glycolysis is a key driver of the early metabolic reprogramming induced by TLR stimulation. Collectively, these experiments demonstrate that TLR stimulation results in early metabolic reprogramming in primary macrophages, which is characterized by an increase in both glycolysis and oxidative metabolism.

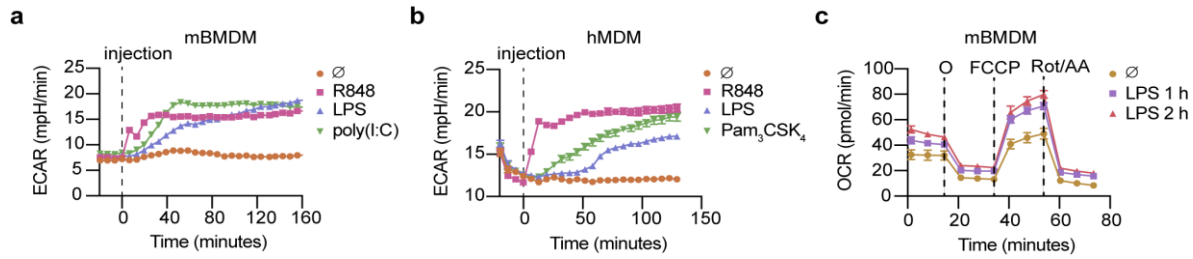

Figure 4.1 TLR stimulation increases both glycolysis and oxidative metabolism in primary macrophages during the early phase of activation. **a** and **b**, ECAR was measured over time in response to indicated TLR agonists in mBMDM (**a**) and hMDM (**b**). **c**, OCR in mBMDM after LPS stimulation for 1 and 2 h was measured over time in response to indicated compounds. O, oligomycin; FCCP, carbonyl cyanide-p-trifluoromethoxyphenylhydrazone; Rot/AA, rotenone and antimycin A. R848 (1 µg/ml), LPS (200 ng/ml), Pam_3CSK_4 (500 ng/ml), and poly(I:C) (20 µg/ml). Measurement of one representative experiment is shown (**a**, **b**, and **c**). Data are presented as mean ± SEM (**a**, *n* = 7; **b**, *n* = 6; **c**, ∅, *n* = 5, LPS, *n* = 6 technical replicates). **a**-**c** are representative of two independent experiments.

4.2 TAK1 and the IKK complex are required for R848-induced glycolysis in primary macrophages

One of the apical events of TLR signaling is the activation of the TAK1 and IKK kinase complexes, which are activated sequentially by the protein kinases TAK1 and IKKβ. TAK1 and AKT have been shown to play a role in the early glycolytic burst in response to TLR agonists in DCs (Everts et al., 2014). However, the function of TAK1 and IKKβ in this process remains unknown. To investigate this, we pretreated mBMDM and hMDM with TAK1 or IKKβ inhibitors: Takinib and TPCA-1, respectively. R848 was used as a stimulus because it is the most potent for early glycolytic induction. Testing these inhibitors, we found that R848-induced glycolysis was significantly reduced in both cell types pretreated with either inhibitor compared to control cells pretreated with DMSO (Figure 4.2a-4.2d), suggesting that TAK1 and the IKK complex are essential for the early glycolytic response induced by TLR stimulation. To investigate the function of AKT in TLR-triggered early glycolysis in primary macrophages, MK2206 2HCl, a highly selective AKT inhibitor, was administered to mBMDM and hMDM 1 h before R848 injection. In both cell types, it showed only a marginal reduction of R848-induced glycolysis (Figure 4.2e and 4.2f). PI3K has been shown to be essential for the long-term commitment to aerobic glycolysis in response to stimulation via TLRs in DCs (Krawczyk et al., 2010). However, in macrophages, wortmannin, a PI3K inhibitor, attenuated glycolysis only in the initial phase after R848 injection in both mBMDM and hMDM, and glycolysis levels returned to those of untreated cells at a later stage (Figure 4.2g and 4.2h). Taken together, these results suggest that TAK1 and the IKK complex are essential components in the TLR-triggered early glycolytic burst, whereas AKT and PI3K do not appear to play a significant role in TLR-induced glycolysis in primary macrophages.

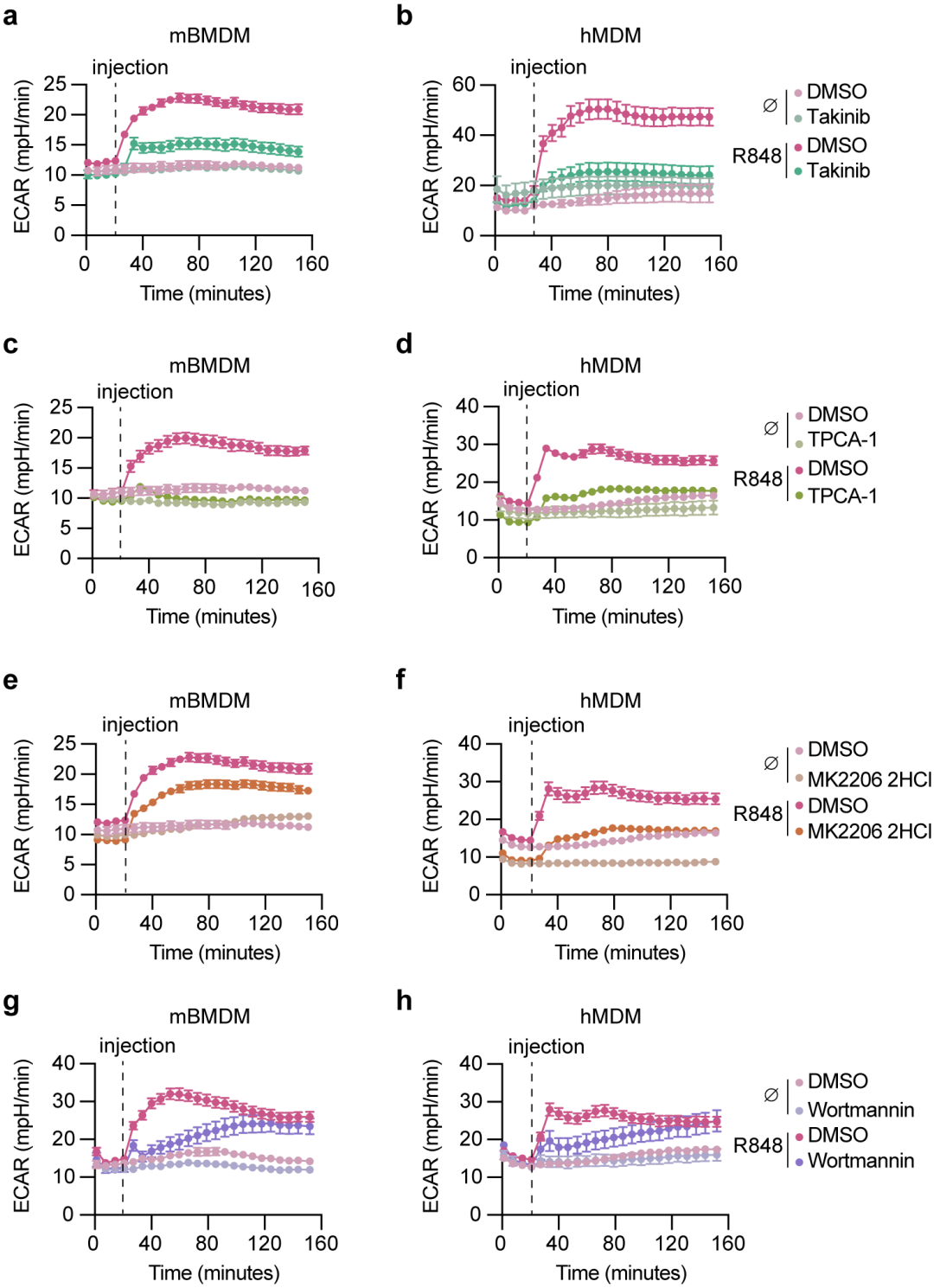

Figure 4.2 TAK1 and the IKK complex are essential for TLR-induced early glycolysis in primary macrophages. **a** and **b**, mBMDM (**a**) and hMDM (**b**) were pretreated with DMSO or Takinib (50 µM) for 1 h, and ECAR was measured over time in response to R848 (1µg/ml). **c** and **d**, mBMDM (**c**) and hMDM (**d**) were pretreated with DMSO or TPCA-1 (10 µM) for 1 h, and ECAR was measured

time in response to R848. **e** and **f**, mBMDM (**e**) and hMDM (**f**) were pretreated with DMSO or MK2206 2HCl (10 μM) for 1 h, and ECAR was measured over time in response to R848. **g** and **h**, mBMDM (**g**) and hMDM (**h**) were pretreated with DMSO or Wortmannin (10 μM) for 1 h, and ECAR was measured over time in response to R848. Measurement of one representative experiment is shown (**a**-**h**). Data are presented as mean ± SEM (**a**, DMSO, *n* = 5, Takinib, *n* = 6; **b**, *n* = 3; **c**, DMSO, *n* = 5, TPCA-1, *n* = 6; **d**, *n* = 3; **e**, DMSO, *n* = 5, MK2206 2HCl; **f**, *n* = 3; **g**, *n* = 4; **h**, *n* = 3 technical replicates). **b** and **h** are representative of two independent experiments. The rest are representative of three independent experiments.

4.3 TLR activation induces PFKL Ser775 phosphorylation in primary macrophages

Given that glycolysis can be upregulated as early as 10 min in response to TLR agonists in primary macrophages (Figure 4.1a and 4.1b), and that this process requires the protein kinases TAK1 and the IKK complex (Figure 4.2a-4.2d), we hypothesized that a post-translational modification acting as an allosteric switch might be added by TLR signaling to one of the rate-limiting enzymes of the glycolytic pathway. To explore this hypothesis, we analyzed a previously published phosphoproteomic dataset of LPS-stimulated mBMDM and found that PFK1, liver type (PFKL) was among the top 10 proteins with increased phosphorylation compared to unstimulated cells (Sjoelund et al., 2014). In particular, serine residue 775 at the C-terminal tail of PFKL was robustly phosphorylated in macrophages after 30 min of LPS treatment (Figure 4.3a). As discussed in Section 1.5, PFKL is part of the PFK1 enzyme complex responsible for the first committed step of the glycolytic pathway. Interestingly, the Ser775 residue within PFKL is highly conserved among vertebrates (Figure 4.3b). In mammals, PFK1 functions as a homo- or heterotetramer composed of three distinct isoforms encoded at separate gene loci: PFKP (platelet), PFKL (liver), and PFKM (muscle). While these three isoforms share a high degree of sequence identity, they differ in their C-terminal extensions, which in turn have been implicated in the allosteric regulation of their activity (Fernandes et al., 2020; Webb et al., 2017; Yugi et al., 2014). Furthermore, PFKL is most abundantly expressed in macrophages (Figure 4.3c), suggesting that PFKL may be critical for regulating glycolysis in macrophages in the context of immune responses.

To investigate whether macrophage activation indeed triggers phosphorylation of PFKL at Ser775, we generated antibodies against a C-terminal PFKL peptide specifically containing phosphorylated Ser775 or its unphosphorylated counterpart. The monoclonal antibodies generated a specific signal for either Ser775 phosphorylated PFKL or total PFKL in immunoblots (Figure 4.6a and 4.6c). Examination of the level of PFKL Ser775 phosphorylation by immunoblots revealed a rather weak signal in resting mBMDM (Figure 4.3d). However,

upon treatment of mBMDM with various TLR ligands such as LPS, R848, Pam_3CSK_4, and poly(I:C), PFKL Ser775 phosphorylation increased significantly, whereas total PFKL levels did not change (Figure 4.3d). Similar results were observed in hMDM. Resting hMDM showed little to no phosphorylated PFKL signal, whereas stimulation with R848, LPS, or Pam_3CSK_4 resulted in a dramatic increase in PFKL Ser775 phosphorylation (Figure 4.3e). In addition, zymosan, which activates both TLR2 and dectin-1, also resulted in a significant increase in PFKL Ser775 phosphorylation in mBMDM (Figure 4.3f). Taken together, these results demonstrate that TLR activation induces PFKL phosphorylation at Ser775 in primary macrophages, which may be a critical mechanism for the TLR-induced early glycolytic burst.

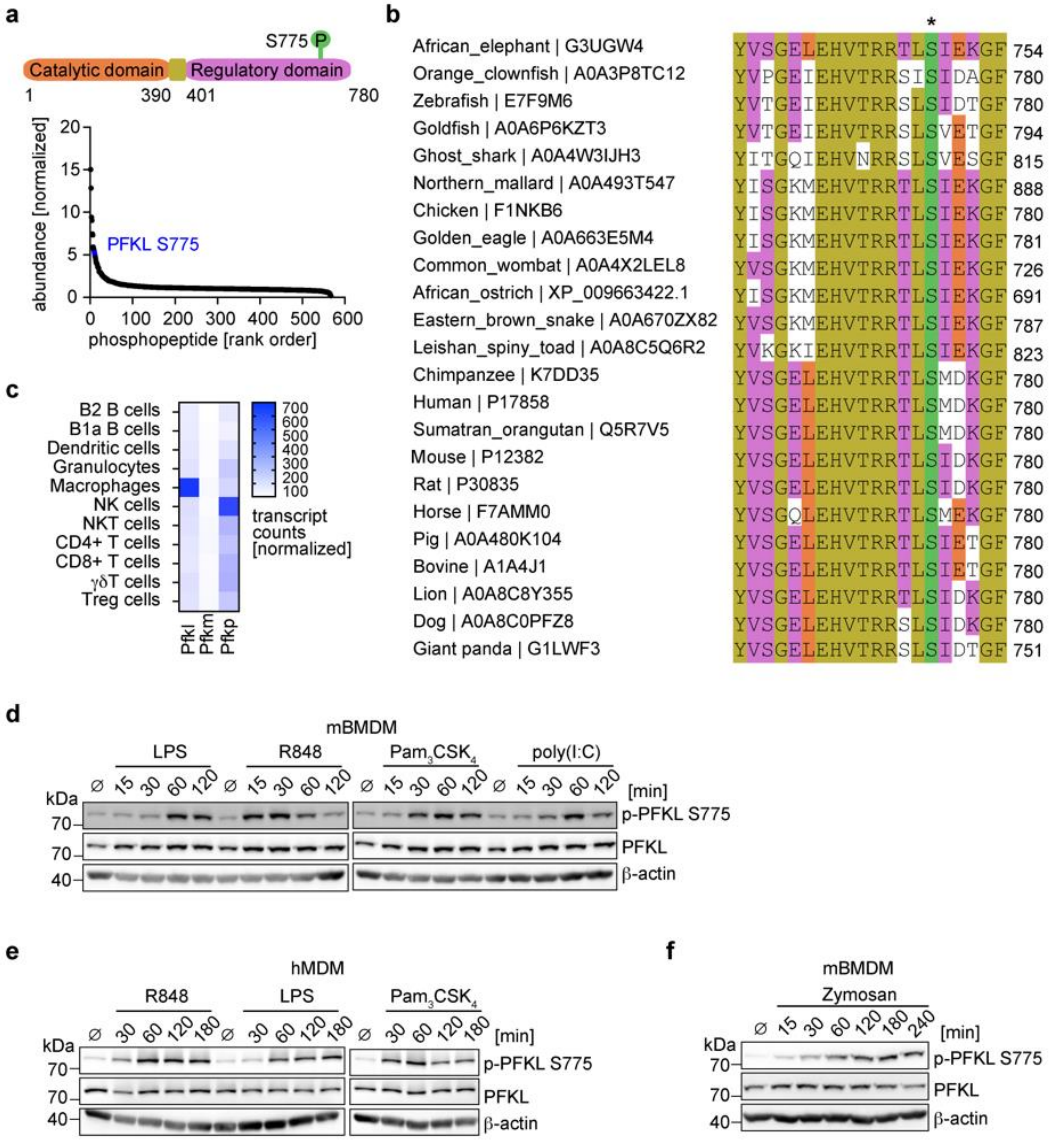

Figure 4.3 Innate immune stimulation induces PFKL phosphorylation at Ser775 in primary macrophages. **a**, Structural domains of PFKL (top). PFKL was shown as one of top 10 genes with increased phosphorylation in immortalized mBMDM after 30 min of LPS treatment (Sjoelund et al., 2014) (bottom). **b**, Multiple sequence alignment of PFKL from different species. Only residues from 761 to 780 (human numbering) are shown. Ser775 (human numbering) is highlighted in green and annotated with an asterisk. **c**, Normalized transcript counts of PFK1 isoforms in immune cells. **d** and **e**, mBMDM (**d**) and hMDM (**e**) were stimulated with indicated TLR agonists for indicated time periods. **f**, mBMDM were primed with 20 ng/ml mouse IFNγ overnight and then stimulated with zymosan (100 μg/ml) for indicated time periods. PFKL Ser775 phosphorylation and PFKL were analyzed by western blot. β-actin was used as a loading control. R848 (1 μg/ml), LPS (200 ng/ml), Pam_3CSK_4 (500 ng/ml), and poly(I:C) (20 μg/ml). **d** and **f** are representative of three independent experiments. **e** is representative of two independent experiments.

4.4 The IKK complex and PKC are upstream kinases for PFKL Ser775 phosphorylation

TLR activation leads to the activation of TAK1 and its downstream kinases, the IKK complex, which we found to be necessary for TLR-induced early glycolysis in primary macrophages (Figure 4.2a-4.2d). To investigate whether TAK1 and the IKK complex are responsible for TLR-induced PFKL Ser775 phosphorylation, phosphorylation levels at Ser775 of PFKL were assessed in R848-activated macrophages pretreated with Takinib or TPCA-1. To test the activity and specificity of these inhibitors, we also examined the phosphorylation of p65 downstream of the IKK complex. This revealed that R848-induced PFKL Ser775 phosphorylation was significantly impaired when TAK1 and the IKK complex were inhibited, while the reduction in PFKL Ser775 phosphorylation was paralleled by a comparable reduction in p65 phosphorylation in mBMDM (Figure 4.4a and 4.4b). Similar results were observed when human macrophages were examined. Thus, increasing doses of Takinib and TPCA-1 completely abolished PFKL Ser775 phosphorylation (Figure 4.4c and 4.4d). AKT has been proposed to play a critical role in the activation of the glycolytic response in DCs (Everts et al., 2014; Krawczyk et al., 2010). Therefore, we also studied AKT phosphorylation at residues T308 and S473, which are required for maximal activation of AKT (Manning and Toker, 2017). The results showed that R848 treatment induced AKT phosphorylation at both residues (Figure 4.4a-4.4d). More importantly, treatment with Takinib or TPCA-1 significantly reduced AKT phosphorylation at both sites in response to R848 in both mBMDM and hMDM (Figure 4.4a-4.4d). Zymosan activates both TLR2 and dectin-1. Consistent with this notion, inhibition of TAK1 and the IKK complex also suppressed zymosan-mediated PFKL Ser775 phosphorylation, but to a lesser extent compared to the inhibition of p65 phosphorylation (Figure 4.4e). To further investigate the specific role of dectin-1 signaling, we also used Go 6983 to block PKC, which is the critical signaling component downstream of the dectin-1

pathway. Treatment with Go 6983 reduced zymosan-induced PFKL Ser775 phosphorylation to a similar extent as IKK inhibition, while it slightly increased p65 phosphorylation (Figure 4.4f), indicating that the IKK complex and PKC are redundant for zymosan-induced PFKL Ser775 phosphorylation. However, when PKC was inhibited, there may be a feedback mechanism for increased p65 phosphorylation. Furthermore, Go 6983 had no effect on PFKL Ser775 phosphorylation induced by other TLR agonists (Figure 4.4g). To verify the involvement of IKKβ and PKC in the phosphorylation of PFKL Ser775, we examined the phosphorylation of PFKL Ser775 in HEK293T cells overexpressing either IKKβ or PKCδ. PKCδ was selected for this study because of its critical function in the zymosan-induced activation of neutrophils, primary monocytes, and mBMDM (Bey et al., 2004; Elsori et al., 2011; Li et al., 2016). Overexpression of these constructs in HEK293T showed that IKKβ induced PFKL Ser775 phosphorylation in a dose-dependent manner (Figure 4.4h). The induction was independent of PKC, as Go 6983 did not affect this process (Figure 4.4i). While PKCδ overexpression alone caused only a slight increase in PFKL Ser775 phosphorylation (Figure 4.4h and 4.4j), the addition of PMA, a PKC activator, significantly enhanced PKCδ-induced PFKL Ser775 phosphorylation (Figure 4.4j), suggesting that transiently expressed PKCδ is in an autoinhibitory state and requires upstream signals to be activated (Steinberg, 2008). Furthermore, the effect was only reduced by Go 6983 and not by TPCA-1 (Figure 4.4j), indicating that PKCδ-induced PFKL Ser775 phosphorylation relies on a distinct pathway from IKKβ. In summary, these results suggest that TLR-induced phosphorylation of PFKL Ser775 and AKT proceeds downstream of the IKK complex. PKC activation could also induce PFKL phosphorylation in an IKKβ-independent manner.

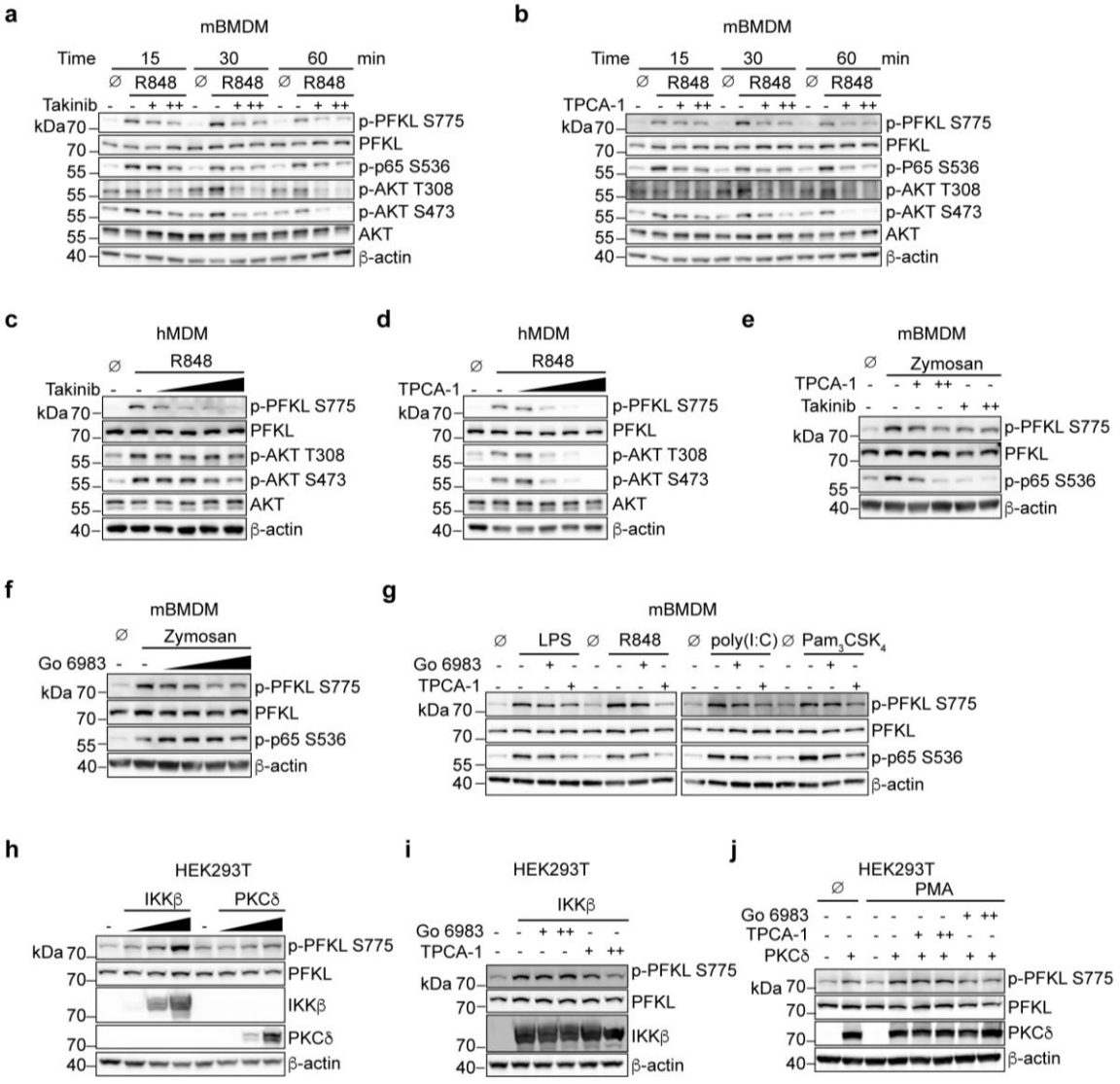

Figure 4.4 The IKK complex and PKC function in PFKL Ser775 phosphorylation. Immunoblot analysis of indicated genes. **a** and **b**, mBMDM were pretreated with DMSO, Takinib (+, 50 μM; ++, 100 μM) (**a**) or TPCA-1 (+, 5 μM; ++, 10 μM) (**b**) for 1 h and then stimulated with R848 (1 μg/ml) for indicated time periods. **c** and **d**, hMDM were pretreated with DMSO, Takinib (1, 5, 10 and 20 μM) (**c**) or TPCA-1 (1, 5, 10 and 20 μM) (**d**) for 1 h and stimulated with R848 for 1 h. **e** and **f**, mBMDM, primed with 20 ng/ml mouse IFNγ overnight, were pretreated with DMSO, TPCA-1 (+, 1 μM; ++, 5 μM) or Takinib (+, 1 μM; ++, 5 μM) (**e**) or Go 6983 (0.1, 1, 5 and 10 μM) (**f**) for 1 h and then stimulated with zymosan (100 μg/ml) for 1 h. **g**, mBMDM were pretreated with DMSO, TPCA-1 (5 μM) or Go 6983 (5 μM) for 1 h and then stimulated with indicated TLR agonists for 1 h (LPS, poly(I:C) and Pam_3CSK_4) or for 30 min (R848). **h**, HEK293T cells were transfected with IKKβ or PKCδ (0, 0.25, 0.5 and 1 μg) for 24 h. **i**, HEK293T cells were transfected with IKKβ (1 μg). 16 h post transfection, indicated inhibitors (+, 1 μM; ++, 5 μM) were added for 6 h. **j**, HEK293T cells were transfected with PKCδ (1 μg). 16 h post transfection, cells were treated with indicated inhibitors (+, 1 μM; ++, 5 μM) for 5 h, followed by PMA (10 ng/ml) stimulation for 1 h. β-actin was used as a loading control. **a**-**j** are representative of three independent experiments.

4.5 PI3K and AKT are indispensable for TLR-induced PFKL Ser775 phosphorylation

AKT was found to be involved in TLR-induced glycolytic burst by phosphorylating and activating HK-II in DCs (Everts et al., 2014). In both hMDM and mBMDM, AKT activation, evidenced by phosphorylation at T308 and S473, was induced by R848 and inhibited by Takinib and TPCA-1 (Figure 4.4a-4.4d), indicating that AKT is downstream of TAK1 and the IKK complex. We then investigated whether the PI3K-AKT axis was involved in R848-induced PFKL Ser775 phosphorylation in macrophages by pretreating the cells with either PI3K inhibitor (Wortmannin) or AKT inhibitor (MK2206 2HCl) prior to R848 stimulation. In mBMDM, R848-induced AKT phosphorylation was almost blocked by both Wortmannin and MK2206 2HCl, whereas PFKL Ser775 phosphorylation was not affected at all by these two inhibitors (Figure 4.5a and 4.5b). Wortmannin completely blunted R848-induced AKT phosphorylation in hMDM, but again showed no inhibitory effect on PFKL Ser775 phosphorylation (Figure 4.5c). Overall, these results suggest that TLR-induced PFKL phosphorylation at Ser775 in primary macrophages is independent of PI3K-AKT.

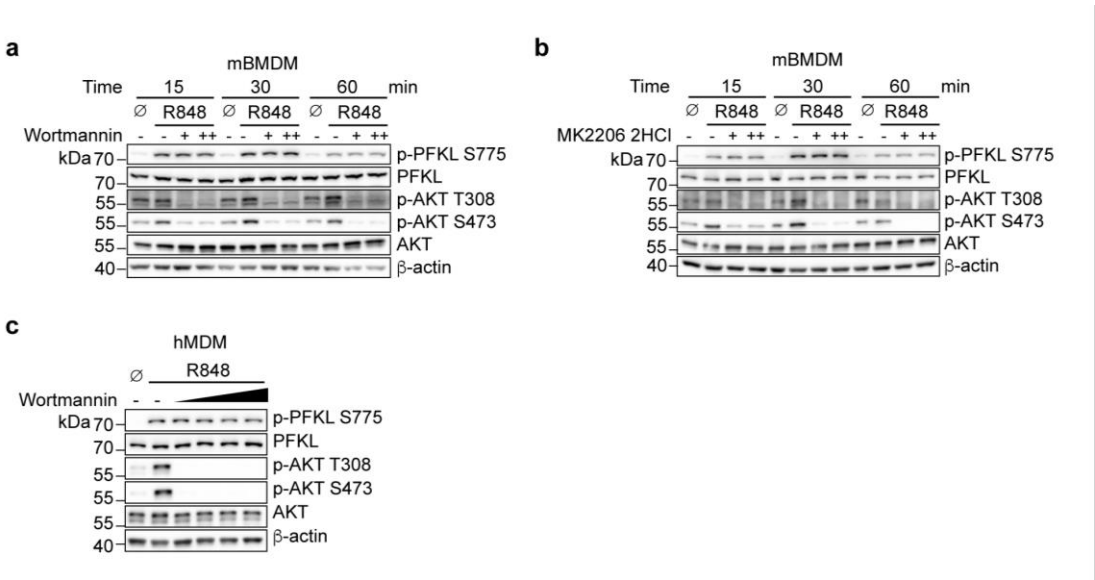

Figure 4.5 TLR-induced PFKL phosphorylation at Ser775 is not dependent on PI3K-AKT in primary macrophages. Immunoblot analysis of indicated genes. **a** and **b**, mBMDM were pretreated with DMSO, Wortmannin (+, 10 μM; ++, 20 μM) (**a**) or MK2206 2HCl (+, 10 μM; ++, 20 μM) (**b**) for 1 h and then stimulated with R848 (1 μg/ml) for indicated time periods. **c**, hMDM were pretreated with DMSO or Wortmannin (1, 5, 10 and 20 μM) for 1 h and stimulated with R848 for 1 h. β-actin was used as a loading control. **a**-**c** are representative of three independent experiments.

4.6 PFKL Ser775 phosphorylation upregulates its catalytic activity

Since the regulatory domain of PFK1 is known to regulate its kinase activity by binding to allosteric modulators (Fernandes et al., 2020), we hypothesized that phosphorylation of Ser775, which is located within the regulatory domain, affects the activity of PFKL. To test this hypothesis, we sought to determine how glycolytic activity is affected by a non-phosphorylatable PFKL mutant. We first deleted PFKL in HEK293T cells (*PFKL*$^{-/-}$, Figure 4.6a) and subjected them to a glycolysis stress test. Despite having a normal basal ECAR, *PFKL*$^{-/-}$ cells exhibited a significantly reduced glycolytic rate after glucose injection compared to WT cells (Figure 4.6b). Inhibition of mitochondrial ATP production with oligomycin did not further increase ECAR under these circumstances, but rather showed a similar deficiency in glycolytic rate for *PFKL*$^{-/-}$ cells (Figure 4.6b). In *PFKL*$^{-/-}$ cells, we then reintroduced either WT PFKL (PFKL^{WT}) or a PFKL point mutant in which Ser775 is exchanged for alanine (PFKL^{S775A}) using a doxycycline-inducible system. Immunoblot analysis confirmed that PFKL^{WT} was phosphorylated at Ser775 to a similar extent as PFKL in WT cells and that PFKL^{S775A} was unable to be phosphorylated at Ser775 (Figure 4.6c). Interestingly, although both PFKL^{WT} and PFKL^{S775A} were expressed at comparable levels (Figure 4.6c), *PFKL*$^{-/-}$ cells expressing PFKL^{S775A} exhibited significantly lower glycolytic activity compared to cells expressing PFKL^{WT} (Figure 4.6d and 4.6e). These results suggest that phosphorylation of Ser775 plays a critical role in enhancing PFKL activity, which ultimately leads to an increase in glycolysis. To confirm our results, we further investigated the enzymatic activity of PFKL^{WT} and PFKL^{S775A} in vitro. We expressed these N-terminal strep-tagged enzymes in HEK293T cells and then purified them. The purified enzymes were identified by both Coomassie staining (Figure 4.6f) and Western blotting (Figure 4.6g). To evaluate their catalytic activity, we measured the production of F1,6BP over time using LC-MS (Figure 4.6h). Their kinase activity was represented by the initial rate. Since the reaction rate of PFKL kinase was linear for the first 2 min (Figure 4.6h), the amount of F1,6BP formed per minute during the first 2 min was used as the initial rate. The result showed that the enzyme activity of the PFKLS^{775A} mutant was approximately half that of its WT counterpart (Figure 4.6i). To estimate the amount of phosphorylated PFKL^{WT} enzyme under these heterologous expression conditions, we performed immunoprecipitation experiments using the phosphorus-specific Ser775 PFKL antibody or isotype control. We then determined the amount of total PFKL that was not bound by the p-Ser775 PFKL antibody or the isotype control (Figure 4.6j). We found that approximately 30% of the PFKL^{WT} enzyme was phosphorylated at Ser775 (Figure 4.6k). In summary, our results indicate that phosphorylation

of Ser775 enhances PFKL kinase activity, providing a mechanistic basis for regulating PFKL activity following innate immune stimulation.

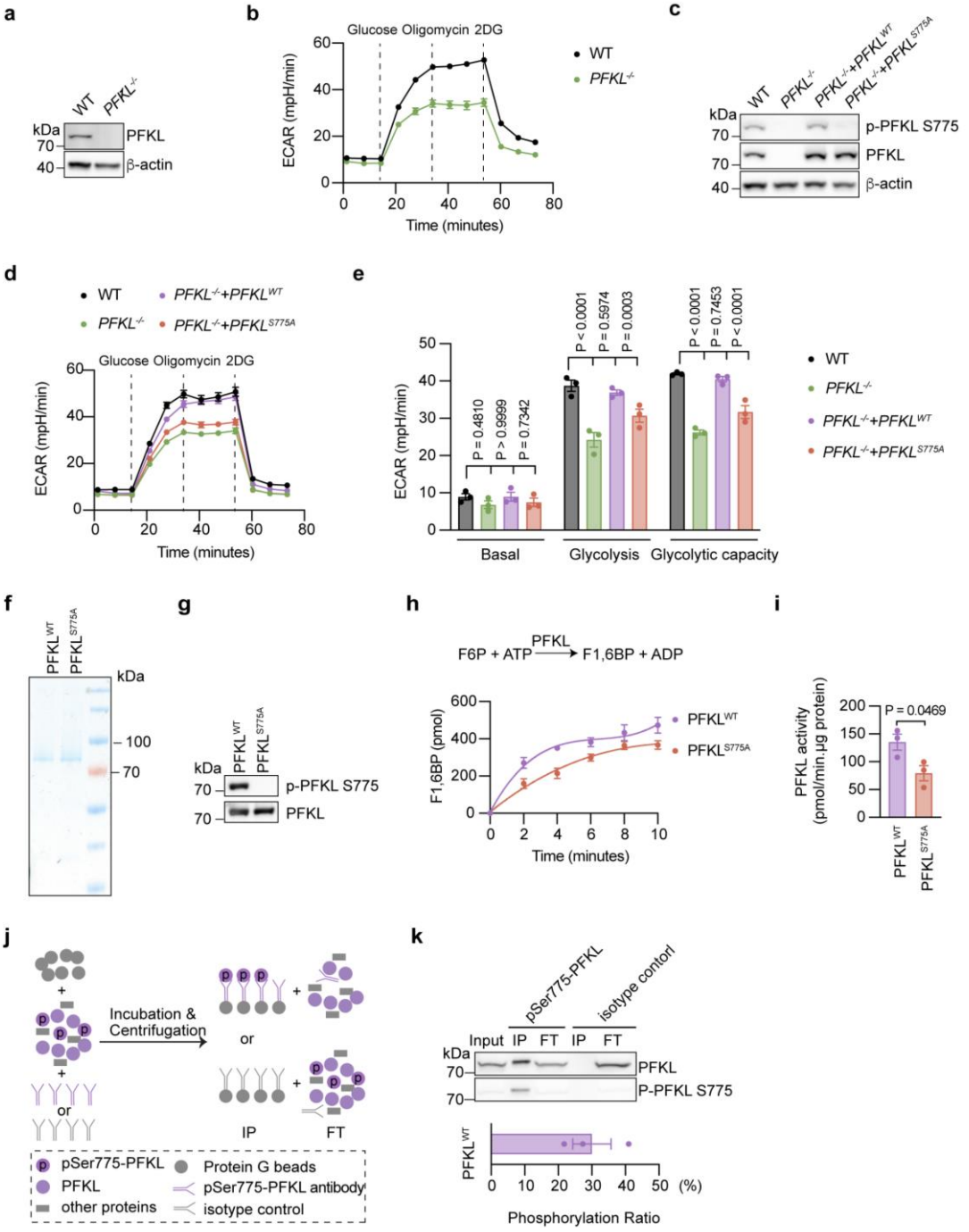

Figure 4.6 PFKL Ser775 phosphorylation enhances its catalytic activity. **a**, PFKL knockout in HEK293T cells was analyzed by western blot. β-actin was used as a loading control. **b**, ECAR in indicated HEK293T cells was measured over time in response to indicated compounds. 2DG, 2-Deoxy-D-glucose. Measurement of one representative experiment is shown. Data are presented as mean ± SEM (WT, *n* = 5; *PFKL*$^{-/-}$, *n* = 6 technical replicates). **c**, PFKL knockout reconstituted with

either PFKL^{WT} or PFKL^{S775A} was analyzed by western blot. β-actin was used as a loading control. **d**, ECAR in indicated HEK293T cells was measured over time in response to indicated compounds. Measurement of one representative experiment is shown. Data are presented as mean ± SEM (WT, *n* = 6; other genotypes, *n* = 8 technical replicates). **e**, ECAR in different stages of the measurement from **d** are presented as mean ± SEM (*n* = 3), statistics indicate two-way ANOVA with Dunnett's correction for multiple testing. **f**, Purified PFKL^{WT} and PFKL^{S775A} were analyzed by Coomassie staining. **g**, Purified PFKL^{WT} and PFKL^{S775A} were analyzed by western blot. **h**, Formation of F1,6BP over time from in vitro enzymatic assays using purified PFKL^{WT} or PFKL^{S775A} was measured by LC-MS. Data are presented as mean ± SEM (*n* = 3). **i**, The enzymatic activity of purified PFKL^{WT} and PFKL^{S775A} was represented by the initial velocity. Data are presented as mean ± SEM (*n* = 3), statistics indicate unpaired two-tailed student's *t*-test. **j**, Workflow for analyzing the Ser775 phosphorylation ratio of PFKL^{WT} was illustrated. IP, immunoprecipitated samples. FT, flow through samples. **k**, PFKL from the indicated fractions was analyzed by immunoblot (top panel), and the phosphorylation ratio at Ser775 of PFKL^{WT} was statistically analyzed by measuring PFKL band intensities in FT using ImageJ software (bottom panel). Data are presented as mean ± SEM (*n* = 3). Immunoblot results in **a**, **c**, **g**, and **k** are representative of three independent experiments.

4.7 Generation of *Pfkl*$^{S775A/S775A}$ mice

To investigate the impact of PFKL Ser775 phosphorylation in primary macrophages and in vivo, we created a mouse model in which PFKL can no longer undergo phosphorylation at Ser775. This was achieved by using CRISPR/Cas9 technology to mutate *Pfkl* Ser775 to Ala775 in murine blastocysts. The resulting mice were bred to obtain bi-allelic mutations of the Ser775Ala *Pfkl* (*Pfkl*$^{S775A/S775A}$) (Figure 4.7a). This mutation also gives rise to an additional cutting site for StyI, which is further employed for genotyping (Figure 4.7b). Upon digestion of *Pfkl* PCR products by StyI, homozygotes produced two fragments (527 bp + 356 bp), while WT mice only yielded a single fragment of 883 bp (Figure 4.7c). Moreover, mBMDM isolated from *Pfkl*$^{S775A/S775A}$ mice did not exhibit detectable phosphorylation at Ser775 following R848 stimulation, although the total levels of PFKL remained unaffected compared to mBMDM isolated from WT mice (Figure 4.7d). This observation provides further evidence that this mouse model can be employed to investigate the function of PFKL Ser775 phosphorylation specifically.

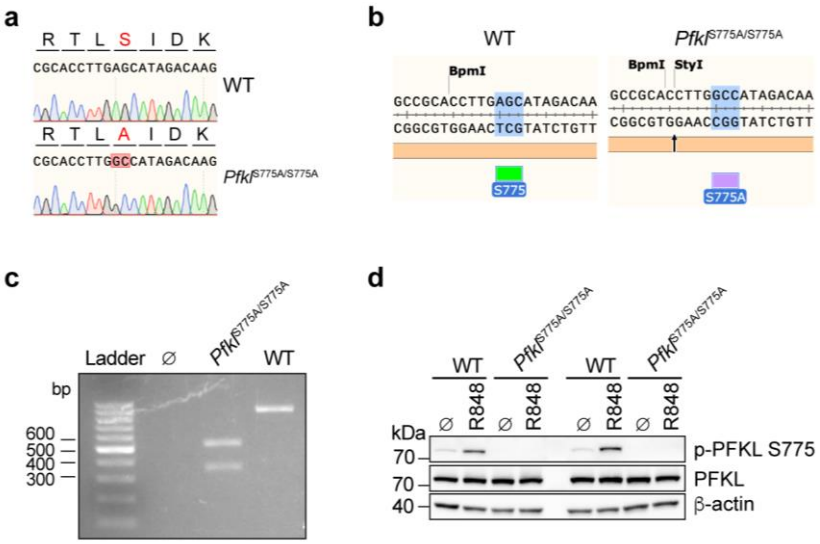

Figure 4.7 Genotyping of *Pfkl*$^{S775A/S775A}$ mice. **a**, The S775A mutation in *Pfkl*$^{S775A/S775A}$ mice was confirmed by Sanger sequencing. **b**, S775A mutation in *Pfkl*$^{S775A/S775A}$ mice creates a cutting site for StyI. **c**, *Pfkl* PCR products from WT and *Pfkl*$^{S775A/S775A}$ mice were digested with StyI and then analyzed by agarose gel electrophoreses. **d**, mBMDM isolated from WT and *Pfkl*$^{S775A/S775A}$ mice were stimulated with R848 (1 µg/ml) for 30 min. PFKL Ser775 phosphorylation and total PFKL were analyzed by western blot. β-actin was used as a loading control.

4.8 Characterization of *Pfkl*$^{S775A/S775A}$ mice

Considering that PFKL plays a crucial role as the rate-limiting enzyme in the glycolytic pathway, we proceeded to investigate whether *Pfkl*$^{S775A/S775A}$ mice exhibit any developmental issues compared to their WT counterparts. Our results showed that there were no differences in body weight (Figure 4.8a), spleen weight (Figure 4.8b), and the ratio of spleen weight to body weight (Figure 4.8c) between the two groups.

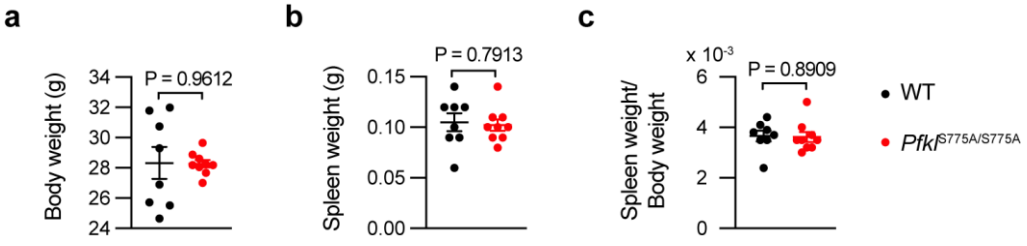

Figure 4.8 Characterization of *Pfkl*$^{S775A/S775A}$ mice. **a**-**c**, Body weight (**a**), spleen weight (**b**), and the ratio of spleen weight to body weight (**c**) of 10-week old WT and *Pfkl*$^{S775A/S775A}$ mice. Data are presented as mean ± SEM (WT mice, *n* = 8; *Pfkl*$^{S775A/S775A}$ mice, *n* = 9), statistics indicate unpaired two-tailed student's *t*-test.

To further investigate whether the systemic immune response was affected in *Pfkl*$^{S775A/S775A}$ mice, we created a FACS panel to analyze immune cell proportions in the spleen and bone marrow of both WT and *Pfkl*$^{S775A/S775A}$ mice by flow cytometry. Our results revealed a significant decrease in the percentages of CD4$^+$ T cells (Figure 4.9a), NKp46$^+$ NK cells (Figure 4.9b), and CD11c$^+$MHCII$^+$ DCs (Figure 4.9c) in the bone marrow of *Pfkl*$^{S775A/S775A}$ mice compared to that of WT mice. In addition, the proportion of CD19$^+$ B cells was also decreased in *Pfkl*$^{S775A/S775A}$ mice, although the difference was not statistically significant (Figure 4.9d). Notably, the percentages of CD11b$^+$Ly-6G$^+$ neutrophils were significantly higher in the bone marrow of *Pfkl*$^{S775A/S775A}$ mice (Figure 4.9e). However, there was no significant change in the percentages of CD8$^+$ T cells (Figure 4.9f) and CD11b$^+$F4/80$^+$ macrophages (Figure 4.9g).

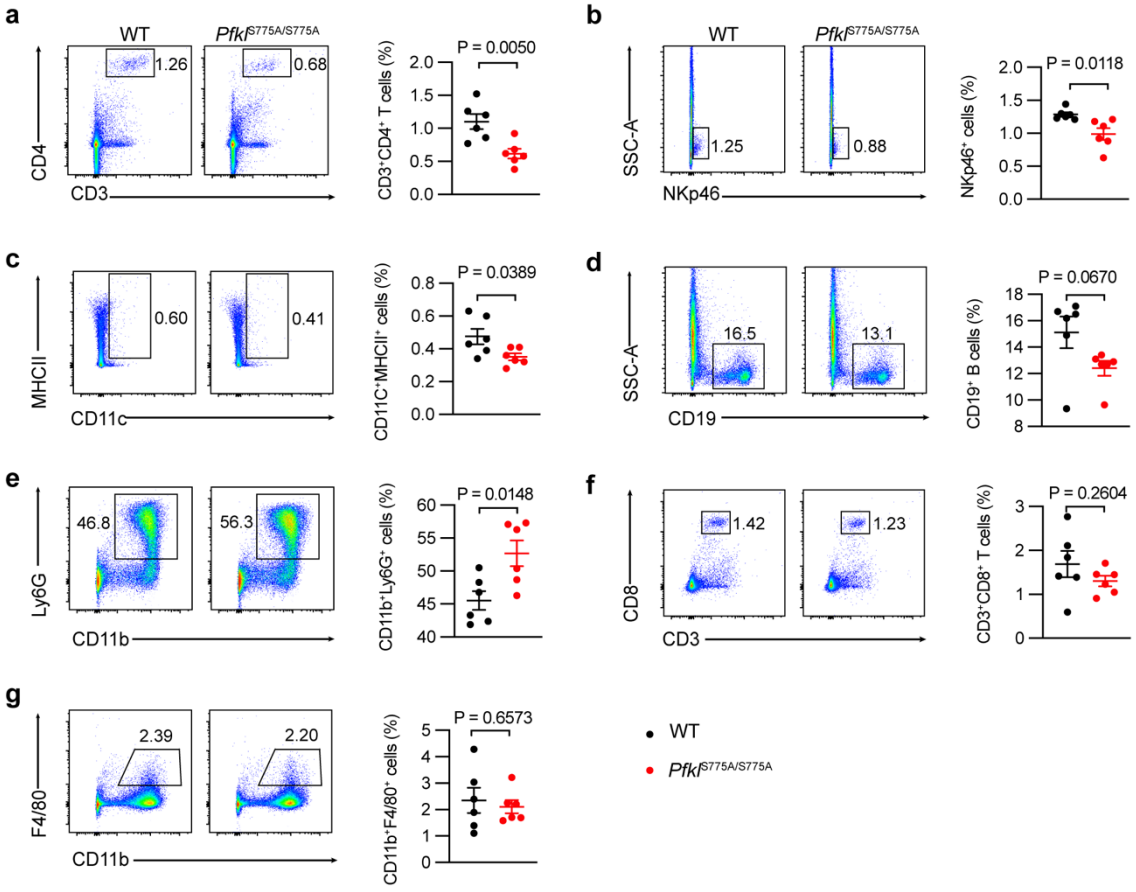

Figure 4.9 Flow cytometry analysis of immune cells in the bone marrow of WT and *Pfkl*$^{S775A/S775A}$ mice. **a**-**g**, Bone marrow cells were isolated from WT and *Pfkl*$^{S775A/S775A}$ mice and analyzed by flow cytometry for the indicated cell surface markers. Gating strategies for each immune cell type are shown, and the numbers next to the outlined areas indicate the percentage of each immune cell type among living cells (left panel). The percentages of indicated immune cells among living cells were summarized and statistically analyzed (right panel). Data are presented as mean ± SEM (n = 6), statistics indicate unpaired two-tailed student's t-test.

In the spleen of *Pfkl*$^{S775A/S775A}$ mice, we observed significantly higher proportions of NKp46^{+} NK cells (Figure 4.10a), CD11b^{+}F4/80^{+} macrophages (Figure 4.10b), and CD11b^{+}Ly-6G^{+} neutrophils (Figure 4.10c) in comparison to WT mice. CD11c^{+}MHCII^{+} DCs were also increased in *Pfkl*$^{S775A/S775A}$ mice (Figure 4.10d). No significant differences were observed in CD4^{+} T cells (Figure 4.10e), CD8 T^{+} cells (Figure 4.10f), and CD19^{+} B cells (Figure 4.10g).

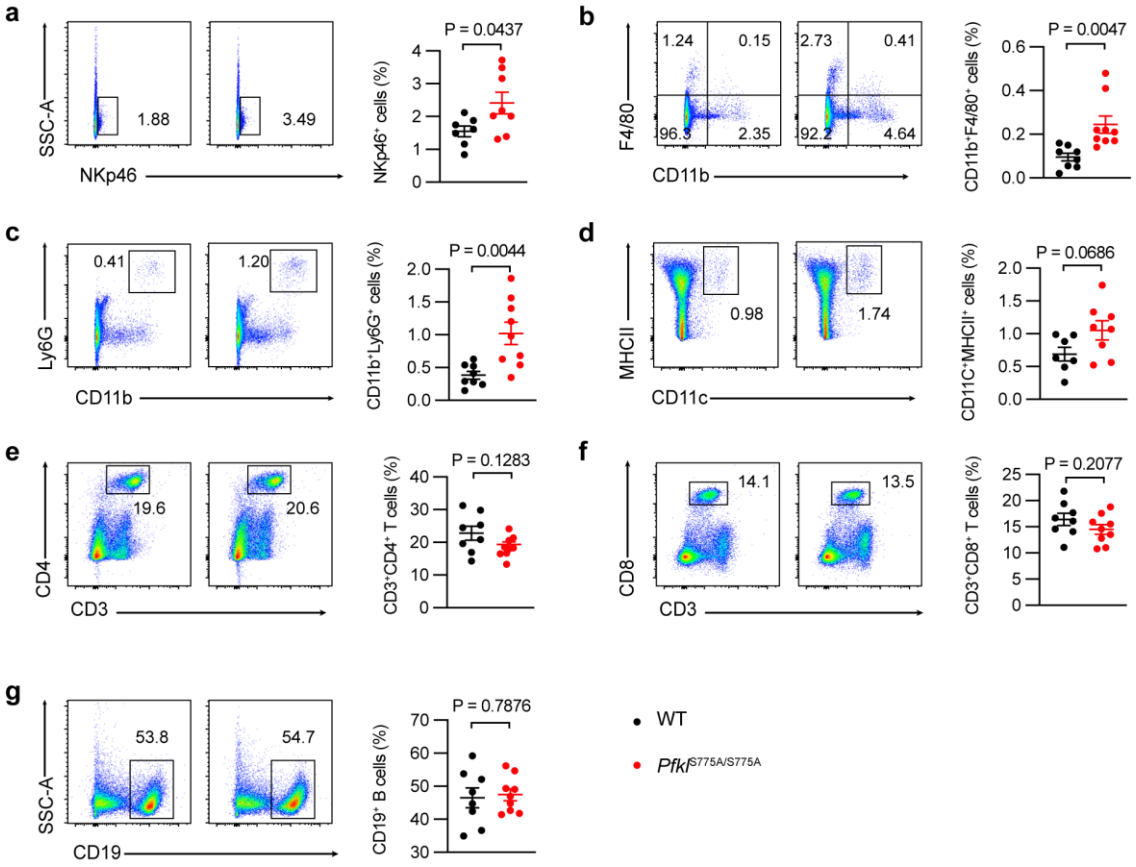

Figure 4.10 Flow cytometry analysis of immune cells in the spleen of WT and *Pfkl*$^{S775A/S775A}$ mice. **a**-**g**, Splenocytes were isolated from WT and *Pfkl*$^{S775A/S775A}$ mice and analyzed by flow cytometry for the indicated cell surface markers. Gating strategies for each immune cell type were shown, and the numbers next to the outlined areas indicate the percentage of each immune cell type among living cells (left panel). The percentages of indicated immune cells among living cells were summarized and statistically analyzed (right panel). Data are presented as mean ± SEM (*n* = 7-9 as indicated), statistics indicate unpaired two-tailed student's *t*-test.

The higher levels of neutrophils found in both the spleen and bone marrow of *Pfkl*$^{S775A/S775A}$ mice suggest the possibility of ongoing inflammation in these mice. To investigate this further, we examined the levels of various cytokines such as IL-1α, IL-1β, IL-6, IL-27, IFNβ, IFNγ, and IL-10 in the serum of both WT and *Pfkl*$^{S775A/S775A}$ mice. However, we did not observe any significant differences in the levels of these cytokines between the two groups (Figure 4.11a-4.11g). Taken together, these findings suggest that inhibiting phosphorylation-induced PFKL activity does not result in significant disruptions to the immune system, at least not under the

steady-state conditions investigated in this study. However, there was a slight but consistent rise in the number of neutrophils in both the bone marrow and spleen of *Pfkl*$^{S775A/S775A}$ mice, suggesting a possible increase in granulopoiesis in these mice.

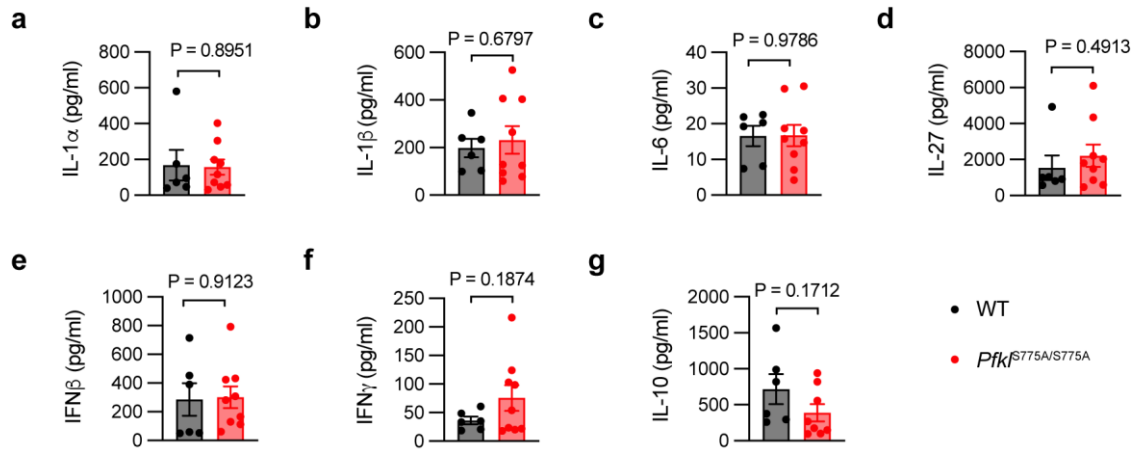

Figure 4.11 Flow cytometry analysis of serum cytokines in WT and *Pfkl*$^{S775A/S775A}$ mice. **a**-**g**, IL-1α (**a**), IL-1β (**b**), IL-6 (**c**), IL-27 (**d**), IFNβ (**e**), IFNγ (**f**), and IL-10 (**g**) in the serum from WT and *Pfkl*$^{S775A/S775A}$ mice were measured by flow cytometry. Data are presented as mean ± SEM (WT mice; *n* = 6; *Pfkl*$^{S775A/S775A}$ mice, *n* = 9), statistics indicate unpaired two-tailed student's *t*-test.

4.9 PFKL Ser775 phosphorylation plays a crucial role in TLR-induced early glycolysis in primary macrophages

To investigate whether the Ser775 phosphorylation of PFKL contributes to the increase in glycolysis during innate immune stimulation in primary macrophages, we conducted glycolytic stress tests using mBMDM isolated from both WT and *Pfkl*$^{S775A/S775A}$ mice. There was no difference in glycolysis between WT and *Pfkl*$^{S775A/S775A}$ macrophages in the resting state (Figure 4.12a). However, after 1 h of LPS treatment, the glycolysis and glycolytic capacity in *Pfkl*$^{S775A/S775A}$ macrophages decreased by approximately one-third compared to WT cells. (Figure 4.12a and 4.12b). In addition, we found that after 24 h of LPS treatment, glycolysis and glycolytic capacity in *Pfkl*$^{S775A/S775A}$ macrophages were still reduced to around 80% of the levels observed in WT cells (Figure 4.12c and 4.12d). To gain a deeper understanding of how PFKL Ser775 phosphorylation impacts metabolism, we conducted metabolic flux assays using a stable isotope tracer. In this experiment, we treated mBMDM from both WT and *Pfkl*$^{S775A/S775A}$ mice with zymosan in a medium containing U-^{13}C-glucose and then quantified the cellular metabolites using mass spectrometry. Following zymosan stimulation, we observed a significant increase in glycolysis in both cell types, as evidenced by the marked increase in total levels of F6P m+6, F1,6BP m+6, dihydroxyacetone phosphate (DHAP) m+3, and

glyceraldehyde 3-phosphate (GA3P) m+3 derived from U-^{13}C-glucose (Figure 4.12e-4.12h). Importantly, it is worth noting that the levels of these metabolites were higher in WT cells than in *Pfkl*$^{S775A/S775A}$ cells (Figure 4.12e-4.12h), suggesting a higher glycolytic rate in WT cells. Interestingly, we also observed that *Pfkl*$^{S775A/S775A}$ cells had slightly higher levels of m+5-labeled UTP, dGDP, and dGTP than WT cells after 30 min of zymosan stimulation (Figure 4.12i-4.12k), implying that more glucose was shuttled through the PPP towards purine/pyrimidine synthesis in *Pfkl*$^{S775A/S775A}$ mBMDM cells. Our previous research has already shown that phosphorylation of PFKL at Ser775 increased its activity (Figure 4.6). Consistent with our previous findings, phosphorylation of PFKL at Ser775 induced by the activation of the innate immune system was essential for the enhancement of glycolysis in primary macrophages.

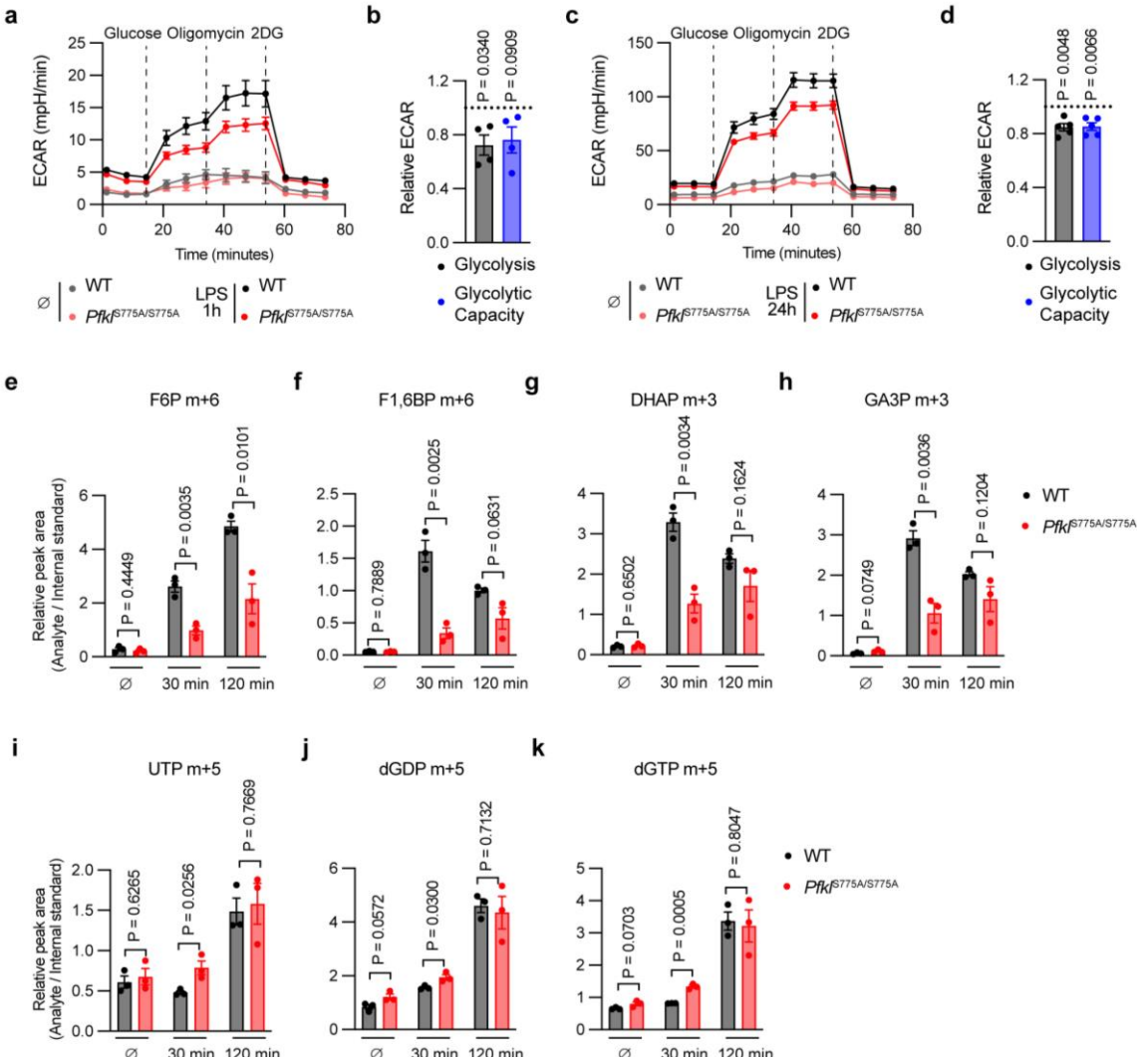

Figure 4.12 PFKL Ser775 phosphorylation is critical for the increase in early glycolysis in activated primary macrophages. **a**, mBMDM from WT and *Pfkl*$^{S775A/S775A}$ mice were stimulated with LPS (200 ng/ml) for 1 h and ECAR was then measured over time in response to the indicated compounds. Measurement of one representative experiment is shown. Data are presented as mean ± SEM (∅, *n* = 5; LPS, *n* = 6 technical replicates). **b**, ECAR values of *Pfkl*$^{S775A/S775A}$ relative to WT mBMDM at different stages of the measurement from **a** are presented as mean ± SEM (*n* = 4), statistics indicate one sample *t* and Wilcoxon test. **c**, mBMDM from WT and *Pfkl*$^{S775A/S775A}$ mice were stimulated with LPS (200 ng/ml) for 24 h and ECAR was then measured over time in response to the indicated compounds. Measurement of one representative experiment is shown. Data are presented as mean ± SEM (∅, *n* = 5; LPS, *n* = 6 technical replicates). **d**, ECAR values of *Pfkl*$^{S775A/S775A}$ relative to WT mBMDM at different stages of the measurement from **c** are presented as mean ± SEM (*n* = 5), statistics indicate one sample *t* and Wilcoxon test. **e**-**k**, mBMDM from WT and *Pfkl*$^{S775A/S775A}$ mice were primed overnight with 20 ng/ml mouse IFNγ and then stimulated with 100 µg/ml zymosan for the indicated time periods in medium containing U-^{13}C-glucose. Relative abundances of F6P m+6 (**e**), F1,6BP m+6 (**f**), DHAP m+3 (**g**), GA3P m+3 (**h**), UTP m+5 (**i**), dGDP m+5 (**j**), and dGTP m+5 (**k**) are shown. Data are presented as mean ± SEM (*n* = 3), statistics indicate unpaired two-tailed student's *t*-test.

4.10 PFKL Ser775 phosphorylation regulates ROS production in primary macrophages and neutrophils

The flux analysis had suggested that ablation of PFKL Ser775 phosphorylation might increase flux through the PPP. Recent studies have shown that PFKL activity serves as a crucial regulator of ROS formation in macrophages (Graham et al., 2015) and neutrophils (Amara et al., 2021). By increasing glycolysis through allosteric activation of PFKL, the flux through the PPP is concurrently reduced, leading to decreased NADPH production. This limits the capacity of the phagosomal NADPH oxidase NOX2 to generate ROS. We found that zymosan, a potent inducer of ROS, was able to trigger the phosphorylation of PFKL at Ser775 (Figure 4.3f), which enhances its catalytic activity (Figure 4.6). To test whether PFKL Ser775 phosphorylation regulates ROS generation in macrophages, a seahorse assay was performed on WT and *Pfkl*$^{S775A/S775A}$ mBMDM. In this assay, all oxygen consumption from mitochondrial respiration was ruled out by injecting the mitochondrial inhibitors rotenone and antimycin A prior to macrophage activation. Following zymosan injection, the measurement of OCR in real-time was used as a biomarker of ROS production. The result showed that OCR dropped after the injection of the mitochondrial inhibitors and then increased only in response to zymosan and not to the medium control (Figure 4.13a). Interestingly, *Pfkl*$^{S775A/S775A}$ macrophages produced significantly more ROS than WT cells (Figure 4.13a and 4.13b), which is consistent with prior research showing that PFKL activity is negatively correlated with ROS formation (Amara et al., 2021; Graham et al., 2015). To address the functional relevance of the change in ROS production, mBMDM from WT and *Pfkl*$^{S775A/S775A}$ mice were infected with *E. coli* at an MOI of 10 for specific time periods. Surviving bacteria at each time point were counted after overnight incubation. After 1 and 2 h of bacterial internalization, similar numbers of bacteria were

counted in both WT and *Pfkl*$^{S775A/S775A}$ cells (Figure 4.13c), indicating that phagocytosis was not compromised in *Pfkl*$^{S775A/S775A}$ cells. However, after 4 and 6 h of internalization, fewer bacteria were counted in *Pfkl*$^{S775A/S775A}$ cells than in WT cells (Figure 4.13c), suggesting that *Pfkl*$^{S775A/S775A}$ cells were more effective at killing bacteria than WT cells. After 24 h, WT cells were able to kill the same number of bacteria as *Pfkl*$^{S775A/S775A}$ cells (Figure 4.13c).

We also investigated the impact of PFKL Ser775 phosphorylation on ROS production in neutrophils, as these cells have fewer mitochondria and rely on glycolysis for their effector functions (Jeon et al., 2020; Rodríguez-Espinosa et al., 2015). To assess this, we first confirmed that PMA, a potent activator of neutrophil activation, induced PFKL Ser775 phosphorylation within 15 min in neutrophils isolated from WT mice (Figure 4.13d). Seahorse assays showed that neutrophils isolated from *Pfkl*$^{S775A/S775A}$ mice produced significantly more ROS than WT cells in response to PMA (Figure 4.13e and 4.13f). The increased ROS production in *Pfkl*$^{S775A/S775A}$ neutrophils corresponded with the enhanced bacterial killing ability (Figure 4.13g). It is worth noting that neutrophils cannot be cultured for long periods and usually die within hours after isolation. More bacteria were counted over time in both WT and *Pfkl*$^{S775A/S775A}$ neutrophils, which could be due to cell death leading to more bacteria being released into the medium.

In summary, these findings suggest that the induction of PFKL Ser775 phosphorylation in response to infection, by increasing glycolytic flux, is a mechanism by which macrophages and neutrophils thwart ROS production.

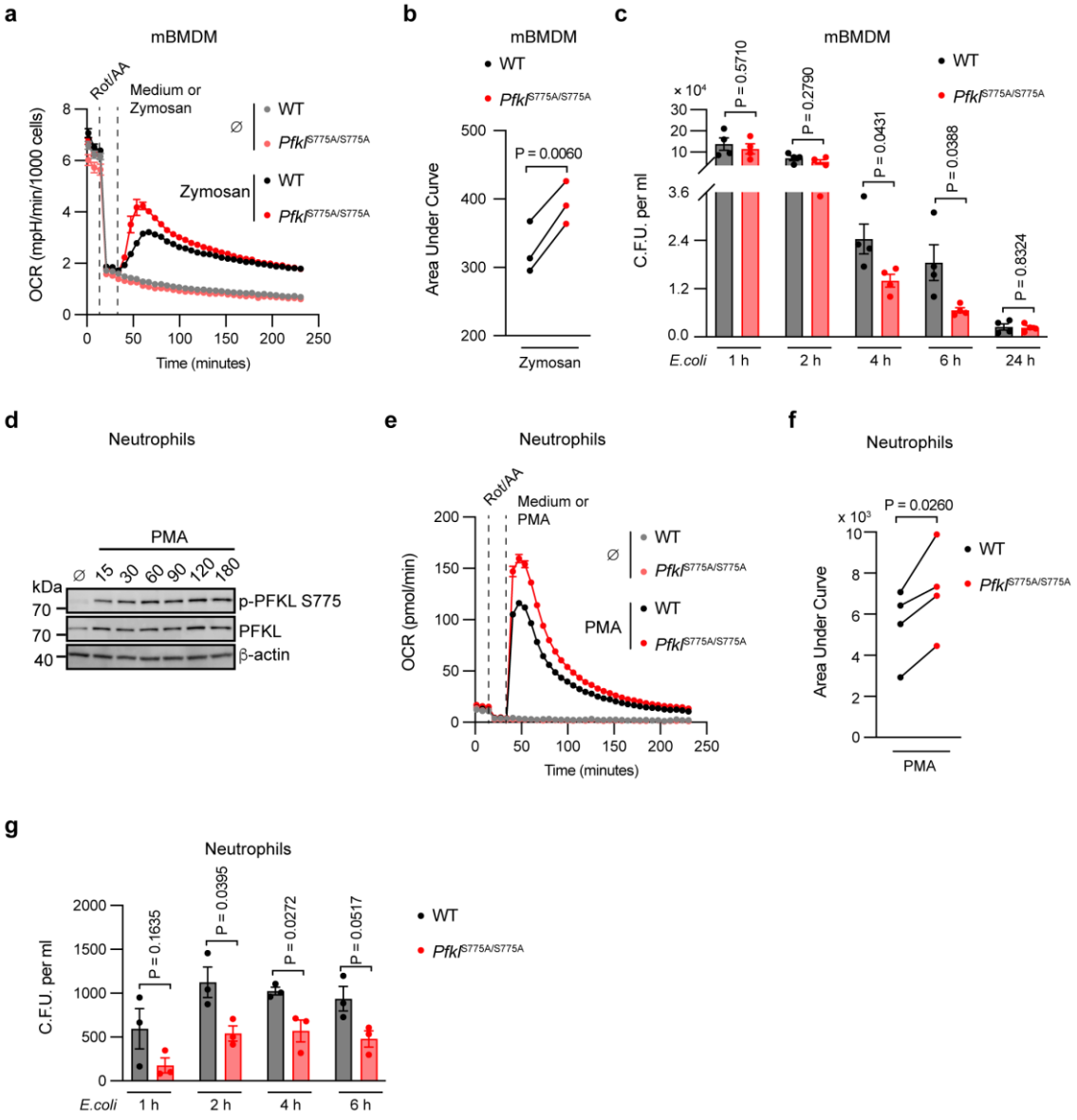

Figure 4.13 *Pfkl*$^{S775A/S775A}$ macrophages and neutrophils generate more ROS and display higher bactericidal activity. mBMDM were primed with 20 ng/ml mouse IFNγ overnight before stimulation or infection. **a**, OCR was measured over time in response to the indicated compounds and zymosan (100 µg/ml) in WT and *Pfkl*$^{S775A/S775A}$ mBMDM. Rot/AA, rotenone and antimycin A (0.5 µM). Measurement of one representative experiment is shown. Data are presented as mean ± SEM (∅, *n* = 5; zymosan, *n* = 6 technical replicates). **b**, Oxygen consumption after zymosan injection from **a** was represented by calculating the area under the curve of the complete kinetic range between activation and return to basal rates. Data are presented as mean ± SEM (*n* = 3), statistics indicate paired two-tailed student's *t*-test. **c**, WT and *Pfkl*$^{S775A/S775A}$ mBMDM were infected with *E. coli* at a MOI of 10 and colony-forming units (C.F.U.) recovered after bacterial phagocytosis for the indicated time periods were quantified and are presented as mean ± SEM (*n* = 4), statistics indicate unpaired two-tailed student's *t*-test. **d**, Neutrophils were isolated from WT mice and then stimulated with PMA (100 ng/ml) for indicated time periods. PFKL Ser775 phosphorylation and PFKL levels were analyzed by western blot. β-actin was used as a loading control. **e**, OCR was measured over time in response to the indicated compounds and PMA (100 ng/ml) in WT and *Pfkl*$^{S775A/S775A}$ neutrophils.

Measurement of one representative experiment is shown. Data are presented as mean ± SEM (∅, *n* = 5; PMA, *n* = 6 technical replicates). **f**, Oxygen consumption after PMA injection from **e** was represented by calculating the area under the curve of the complete kinetic range between activation and return to basal rates. Data are presented as mean ± SEM (*n* = 4), statistics indicate paired two-tailed student's *t*-test. **g**, WT and *Pfkl*$^{S775A/S775A}$ neutrophils were infected with *E. coli* at a MOI of 1 and C.F.U. recovered after bacterial phagocytosis for the indicated time periods were quantified and are presented as mean ± SEM (*n* = 3), statistics indicate unpaired two-tailed student's *t*-test. **d** is representative of three independent experiments.

4.11 PFKL Ser775 phosphorylation is required for LPS-induced HIF1α and IL-1β production

Studies have demonstrated that glycolysis can enhance the pro-inflammatory functions of macrophages by contributing to the accumulation of metabolites such as succinate (Tannahill et al., 2013) and citrate (Lauterbach et al., 2019). Succinate has been found to stabilize HIF1α, which plays a critical role in the synthesis of IL-1β, but not other pro-inflammatory cytokines (Tannahill et al., 2013). Supporting this concept, immunoblot analysis showed that in response to LPS treatment, WT mBMDM, which showed higher glycolytic activity (Figure 4.12), had considerably higher levels of HIF1α compared to *Pfkl*$^{S775A/S775A}$ mBMDM (Figure 4.14a). Analysis of *Hif1a* mRNA levels did not show any difference between WT and *Pfkl*$^{S775A/S775A}$ mBMDM in response to LPS (Figure 4.14b). We then investigated the expression of *Il1b*, *Tnf*, and *Il6* in both WT and *Pfkl*$^{S775A/S775A}$ mBMDM. We observed that *Il1b* mRNA levels were significantly lower in *Pfkl*$^{S775A/S775A}$ mBMDM than in WT mBMDM upon LPS treatment (Figure 4.14c). However, no difference was observed in the expression of *Il6* and *Tnf* between the two groups (Figure 4.14d and 4.14e). These findings were supported by our protein-level analysis, which revealed a significant reduction in pro-IL-1β levels in *Pfkl*$^{S775A/S775A}$ mBMDM (Figure 4.14f), while the levels of secreted TNF and IL-6 remained unchanged (Figure 4.14g and 4.14h). Furthermore, we examined the expression of *Nos2*, another well-known HIF1α-target gene (Melillo et al., 1995; Peyssonnaux et al., 2005), and found that its mRNA levels were significantly decreased in *Pfkl*$^{S775A/S775A}$ mBMDM compared to WT mBMDM after 24 h of LPS stimulation (Figure 4.14i).

Succinate stabilizes HIF1α through a product inhibition mechanism because PHDs hydrolyze HIF1α for degradation while using α-KG as a substrate and producing succinate (Selak et al., 2005). To confirm that the observed differences in HIF1α levels between LPS-stimulated WT

and *Pfkl*$^{S775A/S775A}$ mBMDM were due to differential succinate levels, cells were pretreated with

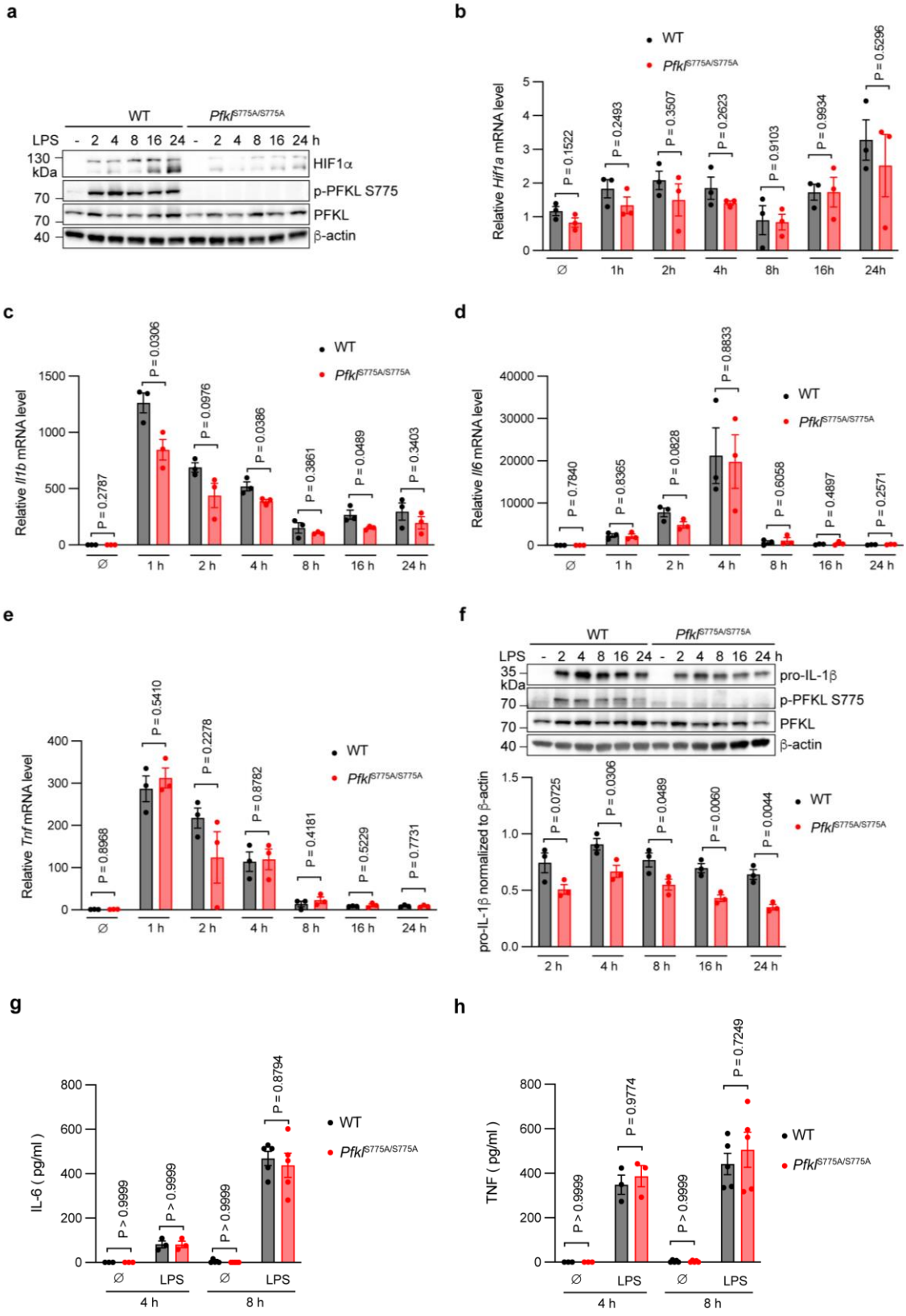

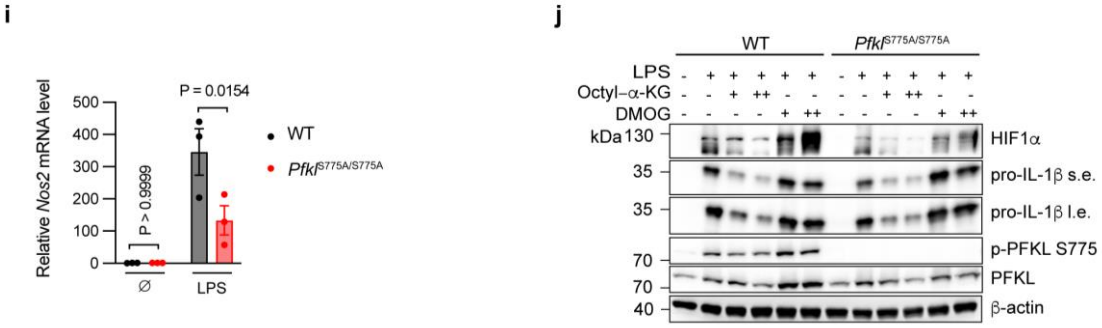

Figure 4.14 PFKL Ser775 phosphorylation is required for LPS-induced HIF1α and IL-1β production in primary macrophages. **a**, mBMDM from WT and *Pfkl*$^{S775A/S775A}$ mice were stimulated with LPS (200 ng/ml) for the indicated time periods. Indicated genes were analyzed by western blot. β-actin was used as a loading control. **b-e**, LPS-induced *Hif1a* (**b**), *Il1b* (**c**), *Il6* (**d**), and *Tnf* (**e**) mRNA levels in WT and *Pfkl*$^{S775A/S775A}$ mBMDM were measured by qPCR and normalized to β-actin mRNA levels. Data are presented as mean ± SEM (*n* = 3), statistics indicate unpaired two-tailed student's *t*-test. **f**, mBMDM from WT and *Pfkl*$^{S775A/S775A}$ mice were stimulated with LPS for the indicated time periods. Indicated genes were analyzed by western blot (top panel). LPS-induced pro-IL-1β were quantified by normalization to β-actin at indicated time points (bottom panel). Data are presented as mean ± SEM (*n* = 3), statistics indicate unpaired two-tailed student's *t*-test. **g** and **h**, LPS-induced IL6 (**g**) and TNF (**h**) production in WT and *Pfkl*$^{S775A/S775A}$ mBMDM was measured by ELISA. Data are presented as mean ± SEM (4 h, *n* = 3; 8 h, *n* = 5), statistics indicate two-way ANOVA with Šidák's correction for multiple comparisons test. **i**, mBMDM from WT and *Pfkl*$^{S775A/S775A}$ mice were stimulated with LPS for 24 h and *Nos2* mRNA levels were measured by qPCR and normalized to β-actin mRNA levels. Data are presented as mean ± SEM (*n* = 3), statistics indicate two-way ANOVA with Šidák's correction for multiple comparisons test. **j**, mBMDM from WT and *Pfkl*$^{S775A/S775A}$ mice were pretreated with octyl-α-KG (+, 0.5 mM; ++, 1 mM) or DMOG (+, 0.25 mM; ++, 0.5 mM) for 2 h and then stimulated with LPS for 24 h. Indicated genes were analyzed by western blot. β-actin was used as a loading control. Octyl-α-KG, octyl-α-ketoglutarate; DMOG, dimethyloxalyl glycine; s.e., short exposure; l.e., long exposure. **a** and **j** are representative of three independent experiments.

octyl-α-KG, which can be converted into α-KG in cells, reversing the inhibitory effects of succinate on PHDs (MacKenzie et al., 2007). Our result showed that activated WT cells required more octyl-α-KG to reduce levels of HIF1α and pro-IL-1β to those observed in *Pfkl*$^{S775A/S775A}$ cells (Figure 4.14j), suggesting higher succinate levels in activated WT cells. We further treated cells with DMOG, a PHD inhibitor to stabilize HIF1α. Pretreatment with DMOG caused the disappearance of the lower bands and an increase in the top band of HIF1α, indicating that the lower bands represent degradation products of HIF1α (Figure 4.14j). Notably, when the same amount of DMOG was applied, WT cells produced more HIF1α than *Pfkl*$^{S775A/S775A}$ cells in response to LPS (Figure 4.14j), again suggesting higher succinate levels in WT cells.

Overall, these results support the critical role of PFKL Ser775 phosphorylation in HIF1α stabilization and the regulation of pro-inflammatory gene expression, particularly *Il1b* and *Nos2*, which is likely mediated by succinate-dependent stabilization of HIF1α.

5 Discussion

5.1 PFKL Ser775 phosphorylation connects TLR signaling to the glycolytic pathway in primary macrophages

The interplay between innate immune responses and central metabolic pathways is well established. A well-studied model of this relationship is macrophages stimulated by PAMPs, such as LPS. In response to LPS, macrophages undergo a metabolic shift toward aerobic glycolysis. This shift has been shown to be mediated by two main mechanisms: increased expression of glycolytic enzymes and dysregulated mitochondria, as discussed in Section 1.4. However, these mechanisms do not account for the metabolic changes that occur in the early stages of macrophage activation. Seahorse assays showed that glycolysis is upregulated within 10-20 min of injection with TLR agonists (Figure 4.1a and 4.1b). Furthermore, our results indicate that macrophages retain a functional mitochondrial OXPHOS system during the early stages of activation, as evidenced by increased basal and maximal OCR following 1 or 2 h of LPS treatment (Figure 4.1c), which is consistent with previous studies (Langston et al., 2019; Lauterbach et al., 2019).

Despite the established role of TBK1/IKKε in modulating early glycolysis in LPS-treated macrophages and DCs (Everts et al., 2014; Tan and Kagan, 2019), it remains unclear whether TAK1 and the IKK complex are also involved in this process. TAK1 and the IKK complex are components of the NF-κB signaling pathway, which is the major pathway downstream of TLR signaling. Our study showed that TAK1 and IKKβ inhibitors almost completely blocked R848-induced glycolysis in primary macrophages (Figure 4.2a-4.2d), indicating that they are necessary for the early glycolytic burst. The PI3K-AKT axis has been suggested to play a critical role in driving the glycolytic response in DCs (Krawczyk et al., 2010). This signaling pathway facilitates glycolysis by promoting the expression of glycolytic enzymes such as glucose transporter 1 on the cell surface, which leads to an increase in cytoplasmic glucose concentration, thereby promoting glycolysis (Frauwirth et al., 2002). In contrast, it has been described that only AKT is downstream of TBK1/IKKε in regulating early glycolysis in DCs, whereas inhibition of PI3K had no effect on this process (Everts et al., 2014). Of note, this study used triciribine, a DNA synthesis inhibitor, to inhibit AKT. The observed inhibitory effect of triciribine on LPS-induced early glycolysis is most likely due to its off-target effects rather than its intended role as an AKT inhibitor. In our study, we used a highly selective inhibitor of AKT and found that this inhibitor had little effect on R848-induced glycolysis in macrophages (Figure 4.2e and 4.2f). Furthermore, inhibition of its upstream kinase PI3K only inhibited glycolysis within 1 h of stimulation (Figure 4.2g and 4.2h). To some extent, these results are consistent with previous studies that have indicated the absence of AKT and PI3K involvement

in TBK-1-mediated glycolysis in macrophages (Balic et al., 2020; Tan and Kagan, 2019). Our observation of the modest effect of PI3K-AKT inhibition on R848-induced early glycolysis in macrophages could be attributed to its function in regulating glucose transporter translocation (Ramachandran and Saravanan, 2015; Sommermann et al., 2011). These inhibitors may slow down this process, but ultimately an adequate amount of glucose transporters may still translocate to the cell membrane over time.

Glycolysis is tightly controlled by 3 rate-limiting enzymes: HK, PFK1, and PK. To achieve rapid modulation of glycolysis, it is necessary to carefully regulate the activity of these enzymes. One potential mechanism for enhancing enzyme activity is through allosteric regulation, which involves changes in their subcellular localization or post-translational modifications. For example, in DCs, HK-II has been observed to undergo phosphorylation in response to LPS, which promotes its association with mitochondria. This association is believed to increase ATP supply, thereby increasing the activity of HK-II (Everts et al., 2014). However, in mBMDM, only HK-II mRNA was detected, while the protein remained undetectable (Cheng et al., 2014; De Jesus et al., 2022). In contrast, the major isoform in mBMDM is HK-I (Cheng et al., 2014). To investigate potential downstream targets of TLR signaling in macrophages, we analyzed phosphoproteome data generated from macrophages treated with TLR agonists (Sjoelund et al., 2014; Weintz et al., 2010). Interestingly, HK-I phosphorylation was not observed in activated macrophages. Instead, PFKL, another rate-limiting enzyme, showed increased phosphorylation at Ser775 after 30 min of LPS stimulation and ranked among the top ten genes (Sjoelund et al., 2014) (Figure 4.3a). PFKL is an isoform of PFK1, which catalyzes the committed step of glycolysis and is predominantly expressed in macrophages (Figure 4.3c). We further confirmed the significant upregulation of PFKL phosphorylation at Ser775 in primary macrophages in response to TLR stimuli by producing a PFKL antibody that specifically detects this phosphorylation (Figure 4.3d-4.3f).

Our investigation further revealed that TAK1 and the IKK complex act as upstream kinases for TLR-induced PFKL Ser775 phosphorylation (Figure 4.4a-4.4d). Although PFKL has a phosphorylation motif similar to that of AKT substrates (Figure 5.1), suggesting that it may be a substrate of AKT, and TLR ligands rapidly activated AKT in an IKK-PI3K-dependent manner (Figure 4.4a-4.4d), our study showed that the Ser775 phosphorylation of PFKL induced by TLR activation was not affected by PI3K and AKT signaling pathways (Figure 4.5). In addition, we found that PKC activation could also induce PFKL Ser775 phosphorylation (Figure 4.4f and 4.4j). LPS and other TLR ligands have been shown to activate most PKC isoforms in DCs, monocytes and macrophages. These isoforms sit at different nodes in the signaling network that are important for cytokine production (Loegering and Lennartz, 2011). Under the conditions tested in this study, PKC inhibition did not affect the activation of the IKK complex.

More specifically, p65 phosphorylation induced by various TLR ligands was unaffected by PKC inhibition (Figure 4.4g). Similarly, PKC inhibition had no effect on TLR-induced PFKL Ser775 phosphorylation (Figure 4.4g). While PKC inhibition effectively suppressed zymosan-induced PFKL Ser775 phosphorylation (Figure 4.4f), this effect appeared to be independent of the IKK complex, as PKC inhibition did not reduce p65 phosphorylation (Figure 4.4f). These results suggest that macrophages use different mechanisms to regulate different pathways following TLR activation. Both PFKL and PKC are downstream targets of the IKK complex. PFKL may be activated for metabolic purposes, while PKC may be activated to regulate cytokine production. Notably, treatment with a PKC inhibitor slightly increased zymosan-induced p65 phosphorylation, suggesting the possible presence of feedback mechanisms in this context (Li et al., 2016). Future studies are necessary to identify whether other kinases are involved in TLR-induced phosphorylation of PFKL at Ser775.

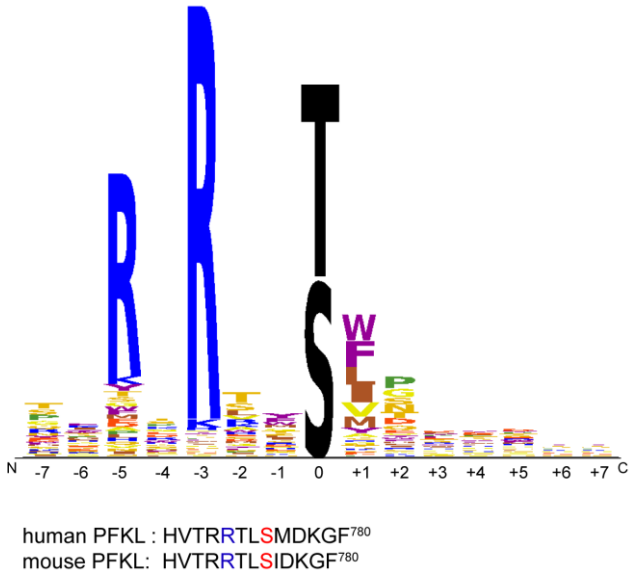

Figure 5.1 Analysis of AKT phosphorylation motif. Scansite (https://scansite4.mit.edu) predicts that the Ser775 residues of both human and mouse PFKL are possibly modified by AKT.

5.2 PFKL Ser775 phosphorylation upregulates its catalytic activity, thus contributing to TLR-induced glycolysis

All three PFK1 isozymes share significant sequence similarity in their core catalytic domains, while their regulatory domains differ, allowing modulation of their catalytic activities based on metabolic demands (Fernandes et al., 2020). Allosteric regulation is the primary means of modulation, and several small molecule metabolites that reflect the metabolic state of the cell

are important allosteric regulators. AMP and ADP, which are indicators of low energy levels in cells, increase PFK1 enzymatic activity. Conversely, lactate, the end product of glycolysis, decreases PFK1 enzymatic activity and provides negative feedback to decrease glycolytic rate (Costa Leite et al., 2007). While less is known about the post-translational modifications that regulate their activity, GlcNAcylation has been shown to decrease the enzymatic activity of PFK1 (Yi et al., 2012b). PFK1 enzymes function as a tetramer composed of different isoenzymes (Dunaway et al., 1988). Their activity is allosterically regulated by conformational changes between the active R and inactive T states (Schirmer and Evans, 1990). Allosteric activators, such as AMP, bind to the allosteric site to facilitate the formation of the R state by inducing structural changes within the enzyme. PFKL has the unique property of forming filamentous structures, with its C-terminal regulatory domain being critical for filament formation (Webb et al., 2017). The fact that PFKL filament assembly is dependent on its substrate, and that tetramers within the filaments are aligned with an exposed catalytic site, suggests that the enzyme is in an active state when assembled into polymers. Our in vitro biochemical assays suggest that phosphorylation of PFKL Ser775 enhances the catalytic activity of PFKL (Figure 4.6i), although the exact mechanism remains unclear. Phosphorylation may affect the conformational equilibrium of the tetramer between the active R-state and the inactive T-state or influence filament formation.

PFKL was identified as a key regulatory protein in the insulin-dependent enhancement of glycolytic flux using a systems biology approach based on time-course phosphoproteomic and metabolomic data (Yugi et al., 2014). Increased PFK1 activity was found to coincide with PFKL Ser775 phosphorylation, and phosphormimetic PFKL mutants were shown to exhibit enhanced kinase activity compared to WT PFKL. These results suggest that the enhancement of PFKL activity by Ser775 phosphorylation is not limited to innate immune cells, but may have a broader role in the regulation of glucose metabolism. The catalytic activity of PFKL increased upon phosphorylation at Ser775 (Figure 4.6i). This phosphorylation process was dependent on the upstream kinases TAK1 and the IKK complex (Figure 4.4a-4.4e), which were shown to be necessary for TLR-induced glycolysis in primary macrophages (Figure 4.2a-4.4d). These findings suggest that PFKL phosphorylation may act as a crucial link that connects TLR signaling to early glycolysis in primary macrophages. To explore whether PFKL Ser775 phosphorylation is a mechanism through which macrophages upregulate early glycolysis in response to TLR stimuli, we generated *Pfkl*$^{S775A/S775A}$ mice, in which PFKL cannot be phosphorylated at Ser775. We also verified that PFKL expression in mBMDM from these mice is not affected (Figure 4.7d). This mouse model enabled us to specifically study the role of PFKL Ser775 phosphorylation in TLR-induced early glycolysis in primary macrophages, allowing us to reduce confounding factors and gain a clearer understanding of the genuine

influence of the targeted pathways on macrophage function and immune responses, ultimately providing more reliable insights into the underlying biology. Seahorse and isotopic tracing assays demonstrated that LPS and zymosan-induced early glycolysis was decreased in *Pfkl*$^{S775A/S775A}$ macrophages (Figure 4.12), suggesting a role of PFKL Ser775 phosphorylation in TLR-induced glycolysis. However, *Pfkl*$^{S775A/S775A}$ macrophages still showed an increase in glycolysis that was approximately two-thirds that of WT cells (Figure 4.12b). Studying the role of a single posttranslational modification in a complex metabolic pathway carries the risk of redundancy, as multiple modulatory steps may impact glycolysis. Considering this, we believe that the moderate but significant quantitative differences observed as a function of PFKL being phosphorylatable or not are plausible and represent a conceivable biological correlate of enhanced glycolysis. To our knowledge, our study provides the first unambiguous molecular link between PRR signaling and a shift towards Warburg metabolism. At the same time, our experiments also suggest that additional mechanisms must exist that drive the glycolytic switch upon innate immune stimulation. In this regard, increased HK-recruitment to mitochondria observed in DCs (Everts et al., 2014), increased glucose uptake through enhanced externalization of glucose transporters (Sommermann et al., 2011), and other allosteric modulations on other enzymes may also play a role in addition to PFKL Ser775 phosphorylation in macrophages.

5.3 The role of PFKL Ser775 phosphorylation at steady state

In macrophages, PFKL showed stimulation-dependent phosphorylation at Ser775, which upregulates its kinase activity and consequently increases glycolysis. *Pfkl*$^{S775A/S775A}$ mice did not show any evident developmental defects. To investigate the impact of PFKL Ser775 phosphorylation on the immune cell population, we designed a flow cytometry analysis panel that enables the examination of major lymphoid and myeloid cell types in mice. Surprisingly, PFKL phosphorylation seemed to moderately affect the composition of the immune cell population at steady state. Specifically, CD4$^+$ T cells (Figure 4.9a), NK cells (Figure 4.9b), and CD19$^+$ B cells (Figure 4.9d) were decreased in the bone marrow of *Pfkl*$^{S775A/S775A}$ mice. More interestingly, an increase in neutrophil numbers was observed in both the bone marrow and spleen of *Pfkl*$^{S775A/S775A}$ mice (Figure 4.9e and 4.10f). Neutrophils serve as the initial line of defense against invading pathogens, and a deficiency in neutrophils, known as neutropenia, increases the susceptibility to infections (Crawford et al., 2004). However, excessive numbers of neutrophils can also lead to significant inflammatory damage (Butterfield et al., 2006; Segel et al., 2011). As a result, the quantity of neutrophils is closely regulated. Neutrophils are produced in the bone marrow from hematopoietic stem cells (HSCs). The bone marrow is a sophisticated network of microenvironments or niches that form the backbone for the efficient operation of both immune cells and HSCs (Mercier et al., 2011). These niches dynamically

process and convey information, enabling the hematopoietic and immune systems to rapidly respond and adapt to the demands of the organism. Granulopoiesis is a remarkable example of the bone marrow's adaptive capacity, which is regulated by intrinsic and extrinsic factors. In response to inflammatory mediators produced during infection or injury, the *de novo* production of neutrophils increases, a process known as emergency granulopoiesis (Manz and Boettcher, 2014). This process provides a rapid supply of neutrophils to sites of infection or injury to help combat the pathogen or heal the injury. The serum of *Pfkl*$^{S775A/S775A}$ mice exhibited normal levels of several important inflammatory cytokines (Figure 4.11), suggesting that the increased number of neutrophils observed in these mice may not be the result of emergency granulopoiesis. However, the precise mechanism by which the downregulation of PFKL activity affects steady-state granulopoiesis in mice remains elusive. It could potentially be attributed to the metabolic stress induced by the downregulation of PFKL activity. Further research is needed to confirm this hypothesis and gain a deeper understanding of the complex biological processes involved.

5.4 The role of PFKL Ser775 phosphorylation in innate immune response

Several studies have convincingly demonstrated that macrophage activation by innate immune stimulation has a significant impact on fundamental metabolic processes. A notable example of this is the glycolytic switch investigated in this study, which is evident in numerous activated immune cells such as T cells, DCs, NK cells, and macrophages (O'Brien and Finlay, 2019; Pearce and Pearce, 2013; Slack et al., 2015). The transition to aerobic glycolysis is well documented by various measures, such as the production of specific metabolites like lactate, ECAR, or even an entire metabolome. However, the critical issue is to determine how these metabolic changes can be linked to functional outcomes. 2DG is widely used to study the role of glycolysis in macrophage function. It acts as an inhibitor of HK, the first enzyme in the glycolytic pathway. As expected, treatment of macrophages with 2DG significantly reduces the glycolytic flux and lactate production induced by innate stimulation (Tan and Kagan, 2019; Wang et al., 2018a). This treatment results in significant destabilization of HIF1α in LPS-stimulated macrophages, leading to modulation of HIF1α target genes, particularly IL-1β (Tannahill et al., 2013). This relationship suggests a role for glycolysis in promoting inflammation. Importantly, the fact that treatment with 2DG does not affect the production of TNF and IL-6 implies that 2DG has no effect on the activation of critical pro-inflammatory signaling components such as NF-κB (Tannahill et al., 2013), suggesting that its specific inhibitory effect is limited to glycolysis rather than being a general inhibitor of inflammation. However, it is important to note that 2DG has several off-target effects beyond its inhibition of

glycolysis. One of the most relevant off-target effects is its ability to decrease intracellular ATP levels (Michl et al., 1976; Wang et al., 2018a; Wang et al., 2018b), which can affect multiple enzymatic reactions. This raises questions about the specificity of 2DG as a tool to study the role of glycolysis in innate immune responses. Indeed, studies have shown that culturing cells in glucose-free medium or replacing glucose with galactose, which also blunts the glycolytic switch response, has only a moderate effect on pro-inflammatory readouts such as IL-1β production (Wang et al., 2018b). Similarly, gene knockout may lead to compensatory mechanisms that may obscure the true effects of the targeted gene on metabolism and immune response. Therefore, more specific approaches may be needed to better understand the precise role of metabolism in the innate immune response. In our research, we used a targeted and specific approach to study the function of a specific rate-limiting step in glycolysis without disrupting it, allowing for a comprehensive and precise understanding of this crucial molecular link. Previous research has highlighted the importance of glycolysis in regulating immune responses to stimulation (Ganeshan and Chawla, 2014). We observed that *Pfkl*$^{S775A/S775A}$ macrophages exhibited reduced glycolysis, which was linked to a decrease in IL-1β production in response to LPS treatment (Figure 4.14c and 4.14f). However, the production of IL-6 and TNF remained unaffected (Figure 4.14d-4.14e and 4.14g-4.14h). These findings align with earlier studies that have demonstrated that LPS-induced glycolysis mainly influences the production of IL-1β, rather than pro-inflammatory cytokines in general (Tannahill et al., 2013). This has been attributed to the unique role of HIF1α in IL-1β expression. We also observed higher protein levels of HIF1α in WT mBMDM compared to *Pfkl*$^{S775A/S775A}$ mBMDM in response to LPS (Figure 4.14a), while its mRNA levels remained similar between these two types of cells (Figure 4.14b). Notably, in the western blot analysis of HIF1α, two prominent bands were observed (Figure 4.14a and 4.14j). Given that HIF1α has an incredibly short half-life of less than 5 min when exposed to oxygen (Huang et al., 1996), it is plausible that the lower band observed is a degradation product of HIF1α. This hypothesis is supported by the reduction of the lower band upon pretreatment of cells with the PHDs inhibitor DMOG (Figure 4.14j). Mechanistically, it has been demonstrated that the increase in glycolysis leads to an accumulation of succinate, which stabilizes HIF1α and consequently enhances the transcription of HIF1α target genes (Tannahill et al., 2013). The stabilization of HIF1α by succinate occurs through a product inhibition mechanism, where PHDs hydrolyze HIF1α while using α-KG as a substrate and producing succinate (Selak et al., 2005). In activated WT cells, a greater amount of octyl-α-KG was required to reverse the inhibitory effect on HIF1α caused by cellular succinate (Figure 4.14j), indicating that WT cells possess higher levels of cellular succinate.

A previous study has shown that an early increase in glycolytic flux induced by LPS is also required for the expression of pro-inflammatory genes at a later stage. This study demonstrated that TLR signaling modifies the flow of glycolysis and the TCA cycle, leading to the production of more acetyl-CoA, which enhances histone acetylation of specific regulatory regions of LPS-inducible gene sets. One of the prominent genes that is affected by this mechanism is IL-6 (Lauterbach et al., 2019). However, our study did not find any differences in IL-6 levels between WT and *Pfkl*$^{S775A/S775A}$ macrophages after LPS treatment, suggesting that changes in PFKL activity may not affect citrate and acetyl-CoA production. This indicates that while glycolysis fuels the TCA cycle for the production of citrate and succinate, distinct mechanisms may specifically regulate their accumulation. In fact, the accumulation of citrate has been linked to LPS-induced downregulation of isocitrate dehydrogenase (IDH) (Jha et al., 2015), while succinate accumulation is believed to be controlled by immunoresponsive gene 1 (IRG1). IRG1 produces itaconate, which subsequently inhibits SDH activity (Lampropoulou et al., 2016).

Alongside glycolysis, the PPP is also activated by innate stimulation in macrophages (Nagy and Haschemi, 2015). The oxidative phase uses the energy from G6P conversion into ribulose-5-phosphate for the reduction of $NADP^+$ into NADPH. Several enzymes, including the NADPH oxidase, use NADPH, which generates ROS. This is crucial for macrophage responses and aids in the killing of pathogens (Jackson et al., 1995; Yi et al., 2012a). Ribulose-5-phosphate can enter the non-oxidative phase of PPP to produce ribose-5-phosphate, which serves as a precursor for the synthesis of nucleotides and amino acids. According to our study, *Pfkl*$^{S775A/S775A}$ macrophages displayed greater ROS production and improved bacterial elimination in comparison to WT cells (Figure 4.13a-4.13c). Our study also revealed that PFKL is phosphorylated at Ser775 during neutrophil activation (Figure 4.13d), which downregulates ROS production and bacterial killing efficiency (Figure 4.13e-4.13g). These results are consistent with prior research that indicates a negative correlation between PFKL activity and ROS production (Amara et al., 2021; Graham et al., 2015). ROS can be generated through various cellular processes and can be produced excessively in response to diverse stimuli (Canton et al., 2021). Excessive ROS is able to oxidize and subsequently damage DNA, proteins, and (membrane) lipids, which is detrimental to host (Görlach et al., 2015). To maintain oxidative homeostasis, healthy cells possess several antioxidant systems. One important mechanism that protects cells against oxidative stress is the Nrf2/ARE (the nuclear factor erythroid 2–related factor 2/antioxidant response element) signaling pathway. This pathway plays a pivotal role in preserving cellular and tissue homeostasis by regulating the expression of genes associated with detoxification and antioxidation in response to oxidative stress (Saha et al., 2020). Our study revealed a novel mechanism employed by macrophages

and neutrophils to regulate redox homeostasis, specifically by inducing the phosphorylation of PFKL at Ser775. As shown in previous studies, the activity of PFKL determines whether glycolysis or the PPP is preferred for cells to metabolize glucose (Amara et al., 2021; Graham et al., 2015). The lack of PFKL phosphorylation at Ser775 may lead to a higher flux of glucose through the PPP, resulting in an increase in NADPH production and subsequently, an elevation in ROS levels.

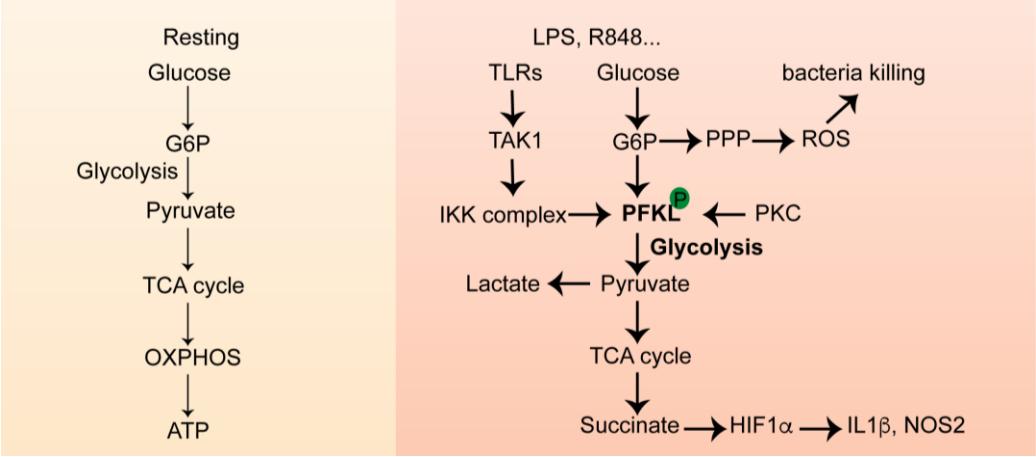

Figure 5.2 The mechanism and role of TLR-induced early glycolysis in primary macrophages. Macrophages show increased glycolysis during early stages of activation, but the underlying mechanism and role of this early glycolysis are unknown. We revealed that PFKL Ser775 phosphorylation, which is induced by innate immune stimulation, increases its catalytic activity, consequently contributing to the early glycolytic burst. This early glycolytic burst is critical for the accumulation of succinate, which stabilizes HIF1α and upregulates proinflammatory genes targeted by HIF1α.

6 Summary

The immune system safeguards the organism against pathogens and maintains tissue homeostasis over the course of its lifetime. There is a close interconnection between these functions and cellular metabolic pathways such as glycolysis, OXPHOS, and the PPP (Ganeshan and Chawla, 2014). These metabolic pathways not only provide energy but also influence associated biosynthetic pathways, which are necessary for proper immune functions (Pearce and Pearce, 2013). Additionally, altering these metabolic pathways enables the production of specific metabolites that possess distinct non-metabolic functions to support immediate effector functions or regulate gene expression (Kelly and O'Neill, 2015; O'Neill and Artyomov, 2019). It is well documented that macrophages exhibit elevated glycolysis upon treatment with TLR agonists. This upregulation can be detected within as little as 10 min following R848 treatment by measuring ECAR in primary macrophages. However, the underlying mechanism and function of this early glycolysis in macrophages remain poorly understood. We postulated that a phosphorylation event could be accountable for this response, and therefore examined the phosphoproteomic dataset of TLR-stimulated macrophages. We identified PFKL as a possible candidate for modification in response to stimulation (Sjoelund et al., 2014). PFKL, a gatekeeper of glycolysis that is mainly expressed in macrophages, exhibited stimulation-induced phosphorylation at Ser775. The IKK complex was responsible for this phosphorylation, whereas it was independent of PI3K and AKT. Enzymatic assays revealed that Ser775 phosphorylation increased PFKL kinase activity. To explore whether the stimulation-induced phosphorylation of PFKL Ser775 is a mechanism for primary macrophages to rapidly increase glycolysis during activation, we generated a genetically engineered mouse model incapable of undergoing PFKL S775 phosphorylation (*Pfkl*$^{S775A/S775A}$). Using this model, we observed that LPS-treated WT showed higher glycolysis compared to *Pfkl*$^{S775A/S775A}$ mBMDM. As glycolysis was inefficient in *Pfkl*$^{S775A/S775A}$ macrophages, it appeared that more glucose was metabolized through the PPP, which resulted in increased ROS production and bacterial killing in these cells. Comparing WT and *Pfkl*$^{S775A/S775A}$ macrophages in response to LPS, we discovered that the increase in early glycolysis was vital for the expression of pro-inflammatory genes such as IL-1β and NOS2. Intriguingly, *Pfkl*$^{S775A/S775A}$ mice displayed an increase in neutrophils in both bone marrow and spleen, indicating that PFKL Ser775 phosphorylation may also moderate the immune system's composition at a steady state in addition to controlling the inflammatory response to TLR stimuli. Overall, these findings demonstrate a role for PFKL Ser775 phosphorylation in controlling glycolytic flux in innate immune cells. Importantly, by employing a targeted perturbation rather than small molecule inhibitors that are susceptible to off-target effects, this study presents unique insights into the impact of innate-dependent enhancement of glycolysis.

7 References

Akinbi, H.T., Epaud, R., Bhatt, H., and Weaver, T.E. (2000). Bacterial Killing Is Enhanced by Expression of Lysozyme in the Lungs of Transgenic Mice. The Journal of Immunology *165*, 5760-5766.

Amara, N., Cooper, M.P., Voronkova, M.A., Webb, B.A., Lynch, E.M., Kollman, J.M., Ma, T., Yu, K., Lai, Z., Sangaraju, D.*, et al.* (2021). Selective activation of PFKL suppresses the phagocytic oxidative burst. Cell *184*, 4480-4494.e4415.

Bailey, J.D., Diotallevi, M., Nicol, T., McNeill, E., Shaw, A., Chuaiphichai, S., Hale, A., Starr, A., Nandi, M., Stylianou, E.*, et al.* (2019). Nitric Oxide Modulates Metabolic Remodeling in Inflammatory Macrophages through TCA Cycle Regulation and Itaconate Accumulation. Cell Reports *28*, 218-230.e217.

Balic, J.J., Albargy, H., Luu, K., Kirby, F.J., Jayasekara, W.S.N., Mansell, F., Garama, D.J., De Nardo, D., Baschuk, N., Louis, C.*, et al.* (2020). STAT3 serine phosphorylation is required for TLR4 metabolic reprogramming and IL-1β expression. Nature Communications *11*.

Bateman, A., Martin, M.-J., Orchard, S., Magrane, M., Agivetova, R., Ahmad, S., Alpi, E., Bowler-Barnett, E.H., Britto, R., Bursteinas, B.*, et al.* (2021). UniProt: the universal protein knowledgebase in 2021. Nucleic Acids Research *49*, D480-D489.

Bey, E.A., Xu, B., Bhattacharjee, A., Oldfield, C.M., Zhao, X., Li, Q., Subbulakshmi, V., Feldman, G.M., Wientjes, F.B., and Cathcart, M.K. (2004). Protein Kinase Cδ Is Required for p47phoxPhosphorylation and Translocation in Activated Human Monocytes. The Journal of Immunology *173*, 5730-5738.

Blouin, C.C., Pagé, E.L., Soucy, G.M., and Richard, D.E. (2004). Hypoxic gene activation by lipopolysaccharide in macrophages: implication of hypoxia-inducible factor 1α. Blood *103*, 1124-1130.

Boller, T., and He, S.Y. (2009). Innate Immunity in Plants: An Arms Race Between Pattern Recognition Receptors in Plants and Effectors in Microbial Pathogens. Science *324*, 742-744.

Brinkmann, V., Reichard, U., Goosmann, C., Fauler, B., Uhlemann, Y., Weiss, D.S., Weinrauch, Y., and Zychlinsky, A. (2004). Neutrophil extracellular traps kill bacteria. Science *303*, 1532-1535.

Brown, G., and Gordon, S. (2001). Immune recognition: a new receptor for β-glucans. Nature *413*, 36-37.

Brown, G.D. (2005). Dectin-1: a signalling non-TLR pattern-recognition receptor. Nature Reviews Immunology *6*, 33-43.

Brown, G.D., Willment, J.A., and Whitehead, L. (2018). C-type lectins in immunity and homeostasis. Nature Reviews Immunology *18*, 374-389.

Butterfield, T.A., Best, T.M., and A., M.M. (2006). The Dual Roles of Neutrophils and Macrophages in Inflammation- A Critical Balance Between Tissue Damage and Repair. Journal of Athletic Training *41*, 457-465.

Byles, V., Covarrubias, A.J., Ben-Sahra, I., Lamming, D.W., Sabatini, D.M., Manning, B.D., and Horng, T. (2013). The TSC-mTOR pathway regulates macrophage polarization. Nature Communications *4*.

Canton, M., Sánchez-Rodríguez, R., Spera, I., Venegas, F.C., Favia, M., Viola, A., and Castegna, A. (2021). Reactive Oxygen Species in Macrophages: Sources and Targets. Frontiers in Immunology *12*.

Chan, M.P., Onji, M., Fukui, R., Kawane, K., Shibata, T., Saitoh, S.-i., Ohto, U., Shimizu, T., Barber, G.N., and Miyake, K. (2015). DNase II-dependent DNA digestion is required for DNA sensing by TLR9. Nature Communications *6*.

Chaplin, D.D. (2010). Overview of the immune response. Journal of Allergy and Clinical Immunology *125*, S3-S23.

Cheng, S.-C., Quintin, J., Cramer, R.A., Shepardson, K.M., Saeed, S., Kumar, V., Giamarellos-Bourboulis, E.J., Martens, J.H.A., Rao, N.A., Aghajanirefah, A.*, et al.* (2014). mTOR- and HIF-1α–mediated aerobic glycolysis as metabolic basis for trained immunity. Science *345*.

Clark, R., and Kupper, T. (2005). Old Meets New: The interaction between innate and adaptive immunity. J Invest Dermatol 125, 629-637.

Cleeter, M.W., Cooper, J.M., Darley-Usmar, V.M., Moncada, S., and AH, S. (1994). Reversible inhibition of cytochrome c oxidase, the terminal enzyme of the mitochondrial respiratory chain, by nitric oxide. Implications for neurodegenerative diseases. FEBS Lett *345*, 50-54.

Clementi, E., Brown, GC., Feelisch, M., and S, M. (1998). Persistent inhibition of cell respiration by nitric oxide: Crucial role of S-nitrosylation of mitochondrial complex I and protective action of glutathione. Proc Natl Acad Sci USA *95*, 7631-7636.

Concordet, J.-P., and Haeussler, M. (2018). CRISPOR: intuitive guide selection for CRISPR/Cas9 genome editing experiments and screens. Nucleic Acids Research *46*, W242-W245.

Costa Leite, T., Da Silva, D., Guimarães Coelho, R., Zancan, P., and Sola-Penna, M. (2007). Lactate favours the dissociation of skeletal muscle 6-phosphofructo-1-kinase tetramers down-regulating the enzyme and muscle glycolysis. Biochemical Journal *408*, 123-130.

Cramer, T., Yamanishi, Y., Clausen, B.E., Förster, I., Pawlinski, R., Mackman, N., Haase, V.H., Jaenisch, R., Corr, M., Nizet, V.*, et al.* (2003). HIF-1alpha is essential for myeloid cell-mediated inflammation. Cell *112(5)*, 645-657.

Crawford, J., Dale, D.C., and Lyman, G.H. (2004). Chemotherapy-induced neutropenia. Cancer *100*, 228-237.

Dambuza, I.M., and Brown, G.D. (2015). C-type lectins in immunity: recent developments. Current Opinion in Immunology *32*, 21-27.

De Jesus, A., Keyhani-Nejad, F., Pusec, C.M., Goodman, L., Geier, J.A., Stoolman, J.S., Stanczyk, P.J., Nguyen, T., Xu, K., Suresh, K.V.*, et al.* (2022). Hexokinase 1 cellular localization regulates the metabolic fate of glucose. Molecular Cell *82*, 1261-1277.e1269.

Dodd, K.M., Yang, J., Shen, M.H., Sampson, J.R., and Tee, A.R. (2014). mTORC1 drives HIF-1α and VEGF-A signalling via multiple mechanisms involving 4E-BP1, S6K1 and STAT3. Oncogene *34*, 2239-2250.

Dunaway, G.A., Kasten, T.P., Sebo, T., and Trapp, R. (1988). Analysis of the phosphofructokinase subunits and isoenzymes in human tissues. Biochem J *251*, 677-683.

Dunkelberger, J.R., and Song, W.-C. (2009). Complement and its role in innate and adaptive immune responses. Cell Research *20*, 34-50.

Elsori, D.H., Yakubenko, V.P., Roome, T., Thiagarajan, P.S., Bhattacharjee, A., Yadav, S.P., and Cathcart, M.K. (2011). Protein kinase Cδ is a critical component of Dectin-1 signaling in primary human monocytes. Journal of Leukocyte Biology *90*, 599-611.

Everts, B., Amiel, E., Huang, S.C.-C., Smith, A.M., Chang, C.-H., Lam, W.Y., Redmann, V., Freitas, T.C., Blagih, J., van der Windt, G.J.W.*, et al.* (2014). TLR-driven early glycolytic reprogramming via the kinases TBK1-IKKε supports the anabolic demands of dendritic cell activation. Nature Immunology *15*, 323-332.

Ewald, S.E., Engel, A., Lee, J., Wang, M., Bogyo, M., and Barton, G.M. (2011). Nucleic acid recognition by Toll-like receptors is coupled to stepwise processing by cathepsins and asparagine endopeptidase. Journal of Experimental Medicine *208*, 643-651.

Fan, K., Lin, L., Ai, Q., Wan, J., Dai, J., Liu, G., Tang, L., Yang, Y., Ge, P., Jiang, R.*, et al.* (2018). Lipopolysaccharide-Induced Dephosphorylation of AMPK-Activated Protein Kinase Potentiates Inflammatory Injury via Repression of ULK1-Dependent Autophagy. Frontiers in Immunology *9*.

Fang, F.C. (2004). Antimicrobial reactive oxygen and nitrogen species: concepts and controversies. Nature Reviews Microbiology *2*, 820-832.

Fantin, V.R., St-Pierre, J., and Leder, P. (2006). Attenuation of LDH-A expression uncovers a link between glycolysis, mitochondrial physiology, and tumor maintenance. Cancer Cell 9, 425-434.

Fernandes, P.M., Kinkead, J., McNae, I., Michels, P.A.M., and Walkinshaw, M.D. (2020). Biochemical and transcript level differences between the three human phosphofructokinases show optimisation of each isoform for specific metabolic niches. Biochemical Journal *477*, 4425-4441.

Fitzgerald, K.A., and Kagan, J.C. (2020). Toll-like Receptors and the Control of Immunity. Cell *180*, 1044-1066.

Flajnik, M.F., and Kasahara, M. (2009). Origin and evolution of the adaptive immune system: genetic events and selective pressures. Nature Reviews Genetics *11*, 47-59.

Frauwirth, K.A., Riley, J.L., Harris, M.H., Parry, R.V., Rathmell, J.C., Plas, D.R., Elstrom, R.L., June, C.H., and Thompson, C.B. (2002). The CD28 Signaling Pathway Regulates Glucose Metabolism. Immunity *16*, 769-777.

Ganeshan, K., and Chawla, A. (2014). Metabolic Regulation of Immune Responses. Annual Review of Immunology *32*, 609-634.

Gantner, B.N., Simmons, R.M., Canavera, S.J., Akira, S., and Underhill, D.M. (2003). Collaborative Induction of Inflammatory Responses by Dectin-1 and Toll-like Receptor 2. Journal of Experimental Medicine *197*, 1107-1117.

Gerdin, A.K. (2010). The Sanger Mouse Genetics Programme: high throughput characterisation of knockout mice. Acta Ophthalmologica *88*, 925-927.

Görlach, A., Dimova, E.Y., Petry, A., Martínez-Ruiz, A., Hernansanz-Agustín, P., Rolo, A.P., Palmeira, C.M., and Kietzmann, T. (2015). Reactive oxygen species, nutrition, hypoxia and diseases: Problems solved? Redox Biology *6*, 372-385.

Gough, D.J., Corlett, A., Schlessinger, K., Wegrzyn, J., Larner, A.C., and Levy, D.E. (2009). Mitochondrial STAT3 Supports Ras-Dependent Oncogenic Transformation. Science *324*, 1713-1716.

Graham, D.B., Becker, C.E., Doan, A., Goel, G., Villablanca, E.J., Knights, D., Mok, A., Ng, A.C.Y., Doench, J.G., Root, D.E.*, et al.* (2015). Functional genomics identifies negative regulatory nodes controlling phagocyte oxidative burst. Nature Communications *6*.

Greulich, W., Wagner, M., Gaidt, M.M., Stafford, C., Cheng, Y., Linder, A., Carell, T., and Hornung, V. (2019). TLR8 Is a Sensor of RNase T2 Degradation Products. Cell *179*, 1264-1275.e1213.

Gross, O., Gewies, A., Finger, K., Schäfer, M., Sparwasser, T., Peschel, C., Förster, I., and Ruland, J. (2006). Card9 controls a non-TLR signalling pathway for innate anti-fungal immunity. Nature *442*, 651-656.

Hard, G. (1970). Some biochemical aspects of the immune macrophage. Br J Exp Pathol *51*, 97-105.

Herre, J. (2004). Dectin-1 uses novel mechanisms for yeast phagocytosis in macrophages. Blood *104*, 4038-4045.

Hitosugi, T., Kang, S., Vander Heiden, M.G., Chung, T.-W., Elf, S., Lythgoe, K., Dong, S., Lonial, S., Wang, X., Chen, G.Z.*, et al.* (2009). Tyrosine Phosphorylation Inhibits PKM2 to Promote the Warburg Effect and Tumor Growth. Science Signaling *2*.

Hopfner, K.-P., and Hornung, V. (2020). Molecular mechanisms and cellular functions of cGAS–STING signalling. Nature Reviews Molecular Cell Biology 21, 501-521.

Hornung, V., Ellegast, J., Kim, S., Brzózka, K., Jung, A., Kato, H., Poeck, H., Akira, S., Conzelmann, K.-K., Schlee, M.*, et al.* (2006). 5'-Triphosphate RNA Is the Ligand for RIG-I. Science *314*, 994-997.

Horwitz, M.S., García, M., Pujol, A., Ruzo, A., Riu, E., Ruberte, J., Arbós, A., Serafín, A., Albella, B., Felíu, J.E.*, et al.* (2009). Phosphofructo-1-Kinase Deficiency Leads to a Severe Cardiac and Hematological Disorder in Addition to Skeletal Muscle Glycogenosis. PLoS Genetics *5*, e1000615.

Huang, L.E., Arany, Z., Livingston, D.M., and Bunn, H.F. (1996). Activation of Hypoxia-inducible Transcription Factor Depends Primarily upon Redox-sensitive Stabilization of Its α Subunit. Journal of Biological Chemistry *271*, 32253-32259.

Huo, Y., Iadevaia, V., Yao, Z., Kelly, I., Cosulich, S., Guichard, S., Foster, Leonard J., and Proud, Christopher G. (2012). Stable isotope-labelling analysis of the impact of inhibition of the mammalian target of rapamycin on protein synthesis. Biochemical Journal *444*, 141-151.

Infantino, V., Convertini, P., Cucci, L., Panaro, Maria A., Di Noia, Maria A., Calvello, R., Palmieri, F., and Iacobazzi, V. (2011). The mitochondrial citrate carrier: a new player in inflammation. Biochemical Journal *438*, 433-436.

Jackson, S.H., Gallin, J.I., and M., H.S. (1995). The p47phox mouse knock-out model of chronic granulomatous disease. The Journal of Experimental Medicine *182*, 751-758.

Jeon, J.-H., Hong, C.-W., Kim, E.Y., and Lee, J.M. (2020). Current Understanding on the Metabolism of Neutrophils. Immune Network *20*.

Jha, Abhishek K., Huang, Stanley C.-C., Sergushichev, A., Lampropoulou, V., Ivanova, Y., Loginicheva, E., Chmielewski, K., Stewart, Kelly M., Ashall, J., Everts, B.*, et al.* (2015). Network Integration of Parallel Metabolic and Transcriptional Data Reveals Metabolic Modules that Regulate Macrophage Polarization. Immunity *42*, 419-430.

Judge, A., and Dodd, Michael S. (2020). Metabolism. Essays in Biochemistry *64*, 607-647.

Kawai, T., and Akira, S. (2010). The role of pattern-recognition receptors in innate immunity: update on Toll-like receptors. Nature Immunology *11*, 373-384.

Kayagaki, N., Warming, S., Lamkanfi, M., Walle, L.V., Louie, S., Dong, J., Newton, K., Qu, Y., Liu, J., Heldens, S.*, et al.* (2011). Non-canonical inflammasome activation targets caspase-11. Nature *479*, 117-121.

Kelly, B., and O'Neill, L.A.J. (2015). Metabolic reprogramming in macrophages and dendrictic cells in innate immunity. Cell Research *25*, 771-784.

Kim, Y.-M., Brinkmann, M.M., Paquet, M.-E., and Ploegh, H.L. (2008). UNC93B1 delivers nucleotide-sensing toll-like receptors to endolysosomes. Nature *452*, 234-238.

Koppenol, W.H., Bounds, P.L., and Dang, C.V. (2011). Otto Warburg's contributions to current concepts of cancer metabolism. Nature Reviews Cancer *11*, 325-337.

Krautz, R., Arefin, B., and Theopold, U. (2014). Damage signals in the insect immune response. Frontiers in Plant Science *5*.

Krawczyk, C.M., Holowka, T., Sun, J., Blagih, J., Amiel, E., DeBerardinis, R.J., Cross, J.R., Jung, E., Thompson, C.B., Jones, R.G.*, et al.* (2010). Toll-like receptor–induced changes in glycolytic metabolism regulate dendritic cell activation. Blood *115*, 4742-4749.

Lam, G.Y., Huang, J., and Brumell, J.H. (2010). The many roles of NOX2 NADPH oxidase-derived ROS in immunity. Seminars in Immunopathology *32*, 415-430.

Lampropoulou, V., Sergushichev, A., Bambouskova, M., Nair, S., Vincent, Emma E., Loginicheva, E., Cervantes-Barragan, L., Ma, X., Huang, Stanley C.-C., Griss, T.*, et al.* (2016). Itaconate Links Inhibition of Succinate Dehydrogenase with Macrophage Metabolic Remodeling and Regulation of Inflammation. Cell Metabolism *24*, 158-166.

Land, S.C., and Tee, A.R. (2007). Hypoxia-inducible Factor 1α Is Regulated by the Mammalian Target of Rapamycin (mTOR) via an mTOR Signaling Motif. Journal of Biological Chemistry *282*, 20534-20543.

Langston, P.K., Nambu, A., Jung, J., Shibata, M., Aksoylar, H.I., Lei, J., Xu, P., Doan, M.T., Jiang, H., MacArthur, M.R.*, et al.* (2019). Glycerol phosphate shuttle enzyme GPD2 regulates macrophage inflammatory responses. Nature Immunology *20*, 1186-1195.

Latz, E., Verma, A., Visintin, A., Gong, M., Sirois, C.M., Klein, D.C.G., Monks, B.G., McKnight, C.J., Lamphier, M.S., Duprex, W.P.*, et al.* (2007). Ligand-induced conformational changes allosterically activate Toll-like receptor 9. Nature Immunology *8*, 772-779.

Lauterbach, M.A., Hanke, J.E., Serefidou, M., Mangan, M.S.J., Kolbe, C.-C., Hess, T., Rothe, M., Kaiser, R., Hoss, F., Gehlen, J.*, et al.* (2019). Toll-like Receptor Signaling Rewires Macrophage Metabolism and Promotes Histone Acetylation via ATP-Citrate Lyase. Immunity *51*, 997-1011.e1017.

Lee, J.-H., Liu, R., Li, J., Zhang, C., Wang, Y., Cai, Q., Qian, X., Xia, Y., Zheng, Y., Piao, Y.*, et al.* (2017). Stabilization of phosphofructokinase 1 platelet isoform by AKT promotes tumorigenesis. Nature Communications *8*.

Lee, S.-H., and Griffiths, J.R. (2020). How and Why Are Cancers Acidic? Carbonic Anhydrase IX and the Homeostatic Control of Tumour Extracellular pH. Cancers *12*, 1616.

Li, X., Cullere, X., Nishi, H., Saggu, G., Durand, E., Mansour, M.K., Tam, J.M., Song, X.-y., Lin, X., Vyas, J.M.*, et al.* (2016). PKC-δ activation in neutrophils promotes fungal clearance. Journal of Leukocyte Biology *100*, 581-588.

Liu, X., Zhang, Z., Ruan, J., Pan, Y., Magupalli, V.G., Wu, H., and Lieberman, J. (2016). Inflammasome-activated gasdermin D causes pyroptosis by forming membrane pores. Nature *535*, 153-158.

Loegering, D.J., and Lennartz, M.R. (2011). Protein Kinase C and Toll-Like Receptor Signaling. Enzyme Research *2011*, 1-7.

Lorsbach, R.B., Murphy, W.J., Lowenstein, C.J., Snyder, S.H., and Russell, S.W. (1993). Expression of the nitric oxide synthase gene in mouse macrophages activated for tumor cell killing. Molecular basis for the synergy between interferon-gamma and lipopolysaccharide. Journal of Biological Chemistry *268*, 1908-1913.

Lzzo, L.T., and Wellen, K.E. (2019). Histone lactylation links metabolism and gene regulation. Nature *574*, 492-493.

MacKenzie, E.D., Selak, M.A., Tennant, D.A., Payne, L.J., Crosby, S., Frederiksen, C.M., Watson, D.G., and Gottlieb, E. (2007). Cell-Permeating α-Ketoglutarate Derivatives Alleviate Pseudohypoxia in Succinate Dehydrogenase-Deficient Cells. Molecular and Cellular Biology *27*, 3282-3289.

Man, S.M., Karki, R., and Kanneganti, T.-D. (2017). Molecular mechanisms and functions of pyroptosis, inflammatory caspases and inflammasomes in infectious diseases. Immunological Reviews *277*, 61-75.

Manning, B.D., and Toker, A. (2017). AKT/PKB Signaling: Navigating the Network. Cell *169*, 381-405.

Manz, M.G., and Boettcher, S. (2014). Emergency granulopoiesis. Nature Reviews Immunology *14*, 302-314.

Marsin, A.-S., Bouzin, C., Bertrand, L., and Hue, L. (2002). The Stimulation of Glycolysis by Hypoxia in Activated Monocytes Is Mediated by AMP-activated Protein Kinase and Inducible 6-Phosphofructo-2-kinase. Journal of Biological Chemistry *277*, 30778-30783.

Melillo, G., Musso, T., Sica, A., Taylor, L.S., Cox, G.W., and Varesio, L. (1995). A hypoxia-responsive element mediates a novel pathway of activation of the inducible nitric oxide synthase promoter. Journal of Experimental Medicine *182*, 1683-1698.

Mercier, F.E., Ragu, C., and Scadden, D.T. (2011). The bone marrow at the crossroads of blood and immunity. Nature Reviews Immunology *12*, 49-60.

Michl, J., Ohlbaum, D.J., and Silverstein, S.C. (1976). 2-Deoxyglucose selectively inhibits Fc and complement receptor-mediated phagocytosis in mouse peritoneal macrophages II. Dissociation of the inhibitory effects of 2-deoxyglucose on phagocytosis and ATP generation. Journal of Experimental Medicine *144*, 1484-1493.

Millet, P., Vachharajani, V., McPhail, L., Yoza, B., and McCall, C.E. (2016). GAPDH Binding to TNF-α mRNA Contributes to Posttranscriptional Repression in Monocytes: A Novel Mechanism of Communication between Inflammation and Metabolism. The Journal of Immunology *196*, 2541-2551.

Mills, E.L., Kelly, B., Logan, A., Costa, A.S.H., Varma, M., Bryant, C.E., Tourlomousis, P., Däbritz, J.H.M., Gottlieb, E., Latorre, I.*, et al.* (2016). Succinate Dehydrogenase Supports Metabolic Repurposing of Mitochondria to Drive Inflammatory Macrophages. Cell *167*, 457-470.e413.

Murphy, K., Weaver, C., Mowat, A., Berg, L., & Chaplin, D. (2016). Janeway's immunobiology. Garland Science/Taylor & Francis Group, LLC

Muschter, S., Berthold, T., Bhardwaj, G., Hammer, E., Dhople, V.M., Wesche, J., Reil, A., Bux, J., Bakchoul, T., Steil, L.*, et al.* (2015). Mass spectrometric phosphoproteome analysis of small-sized samples of human neutrophils. Clinica Chimica Acta *451*, 199-207.

Nagy, C., and Haschemi, A. (2015). Time and Demand are Two Critical Dimensions of Immunometabolism: The Process of Macrophage Activation and the Pentose Phosphate Pathway. Frontiers in Immunology *6*.

Nainu, F., Shiratsuchi, A., and Nakanishi, Y. (2017). Induction of Apoptosis and Subsequent Phagocytosis of Virus-Infected Cells As an Antiviral Mechanism. Frontiers in Immunology *8*.

Newsholme, P., Gordon, S., and Newsholme, E. (1987). Rates of utilization and fates of glucose, glutamine, pyruvate, fatty acids and ketone bodies by mouse macrophages. Biochem J *242*, 631-636.

O'Neill, L.A.J., Golenbock, D., and Bowie, A.G. (2013). The history of Toll-like receptors — redefining innate immunity. Nature Reviews Immunology *13*, 453-460.

O'Brien, K.L., and Finlay, D.K. (2019). Immunometabolism and natural killer cell responses. Nature Reviews Immunology *19*, 282-290.

O'Neill, L.A.J., and Artyomov, M.N. (2019). Itaconate: the poster child of metabolic reprogramming in macrophage function. Nature Reviews Immunology *19*, 273-281.

Obach, M., Navarro-Sabaté, À., Caro, J., Kong, X., Duran, J., Gómez, M., Perales, J.C., Ventura, F., Rosa, J.L., and Bartrons, R. (2004). 6-Phosphofructo-2-kinase (pfkfb3) Gene Promoter Contains Hypoxia-inducible Factor-1 Binding Sites Necessary for Transactivation in Response to Hypoxia. Journal of Biological Chemistry *279*, 53562-53570.

Ohto, U., Ishida, H., Shibata, T., Sato, R., Miyake, K., and Shimizu, T. (2018). Toll-like Receptor 9 Contains Two DNA Binding Sites that Function Cooperatively to Promote Receptor Dimerization and Activation. Immunity *48*, 649-658.e644.

Palmieri, E.M., Gonzalez-Cotto, M., Baseler, W.A., Davies, L.C., Ghesquière, B., Maio, N., Rice, C.M., Rouault, T.A., Cassel, T., Higashi, R.M.*, et al.* (2020). Nitric oxide orchestrates metabolic rewiring in M1 macrophages by targeting aconitase 2 and pyruvate dehydrogenase. Nature Communications *11*.

Palsson-McDermott, Eva M., Curtis, Anne M., Goel, G., Lauterbach, Mario A.R., Sheedy, Frederick J., Gleeson, Laura E., van den Bosch, Mirjam W.M., Quinn, Susan R., Domingo-Fernandez, R., Johnston, Daniel G.W.*, et al.* (2015). Pyruvate Kinase M2 Regulates Hif-1α Activity and IL-1β Induction and Is a Critical Determinant of the Warburg Effect in LPS-Activated Macrophages. Cell Metabolism *21*, 65-80.

Park, J.S., Burckhardt, C.J., Lazcano, R., Solis, L.M., Isogai, T., Li, L., Chen, C.S., Gao, B., Minna, J.D., Bachoo, R.*, et al.* (2020). Mechanical regulation of glycolysis via cytoskeleton architecture. Nature *578*, 621-626.

Patra, Krushna C., Wang, Q., Bhaskar, Prashanth T., Miller, L., Wang, Z., Wheaton, W., Chandel, N., Laakso, M., Muller, William J., Allen, Eric L., et al. (2013). Hexokinase 2 Is Required for Tumor Initiation and Maintenance and Its Systemic Deletion Is Therapeutic in Mouse Models of Cancer. Cancer Cell 24, 213-228.

Pearce, Erika L., and Pearce, Edward J. (2013). Metabolic Pathways in Immune Cell Activation and Quiescence. Immunity *38*, 633-643.

Pegram, H.J., Andrews, D.M., Smyth, M.J., Darcy, P.K., and Kershaw, M.H. (2010). Activating and inhibitory receptors of natural killer cells. Immunology & Cell Biology *89*, 216-224.

Peyssonnaux, C., Datta, V., Cramer, T., Doedens, A., Theodorakis, E.A., Gallo, R.L., Hurtado-Ziola, N., Nizet, V., and Johnson, R.S. (2005). HIF-1α expression regulates the bactericidal capacity of phagocytes. Journal of Clinical Investigation *115*, 1806-1815.

Pichlmair, A., Schulz, O., Pan, C.P., Näslund, T.I., Liljeström, P., Weber, F., and Sousa, C.R.e. (2006). RIG-I–Mediated AntiviralResponses to Single-StrandedRNA Bearing 5'-Phosphates. Science *314*, 997-1001.

Quintin, J., Saeed, S., Martens, Joost H.A., Giamarellos-Bourboulis, Evangelos J., Ifrim, Daniela C., Logie, C., Jacobs, L., Jansen, T., Kullberg, B.-J., Wijmenga, C.*, et al.* (2012). Candida albicans Infection Affords Protection against Reinfection via Functional Reprogramming of Monocytes. Cell Host & Microbe *12*, 223-232.

Ramachandran, V., and Saravanan, R. (2015). Glucose uptake through translocation and activation of GLUT4 in PI3K/Akt signaling pathway by asiatic acid in diabetic rats. Human & Experimental Toxicology *34*, 884-893.

Raulet, D.H., and Vance, R.E. (2006). Self-tolerance of natural killer cells. Nature Reviews Immunology *6*, 520-531.

Real-Hohn, A., Zancan, P., Da Silva, D., Martins, E.R., Salgado, L.T., Mermelstein, C.S., Gomes, A.M.O., and Sola-Penna, M. (2010). Filamentous actin and its associated binding proteins are the stimulatory site for 6-phosphofructo-1-kinase association within the membrane of human erythrocytes. Biochimie *92*, 538-544.

Rius, J., Guma, M., Schachtrup, C., Akassoglou, K., Zinkernagel, A.S., Nizet, V., Johnson, R.S., Haddad, G.G., and Karin, M. (2008). NF-κB links innate immunity to the hypoxic response through transcriptional regulation of HIF-1α. Nature *453*, 807-811.

Rodríguez-Espinosa, O., Rojas-Espinosa, O., Moreno-Altamirano, M.M.B., López-Villegas, E.O., and Sánchez-García, F.J. (2015). Metabolic requirements for neutrophil extracellular traps formation. Immunology *145*, 213-224.

Rodríguez-Prados, J.-C., Través, P.G., Cuenca, J., Rico, D., Aragonés, J., Martín-Sanz, P., Cascante, M., and Boscá, L. (2010). Substrate Fate in Activated Macrophages: A Comparison between Innate, Classic, and Alternative Activation. The Journal of Immunology *185*, 605-614.

Ruiz-García, A., Monsalve, E., Novellasdemunt, L., Navarro-Sabaté, À., Manzano, A., Rivero, S., Castrillo, A., Casado, M., Laborda, J., Bartrons, R*., et al.* (2011). Cooperation of Adenosine with Macrophage Toll-4 Receptor Agonists Leads to Increased Glycolytic Flux through the Enhanced Expression of PFKFB3 Gene. Journal of Biological Chemistry *286*, 19247-19258.

Saeed, S., Quintin, J., Kerstens, H.H.D., Rao, N.A., Aghajanirefah, A., Matarese, F., Cheng, S.-C., Ratter, J., Berentsen, K., van der Ent, M.A*., et al.* (2014). Epigenetic programming of monocyte-to-macrophage differentiation and trained innate immunity. Science *345*.

Sag, D., Carling, D., Stout, R.D., and Stuttles, J. (2008). AMP-activated protein kinase promotes macrophage polarization to an anti-inflammatory functional phenotype. Journal of Immunology *181(12)*, 8633-8641.

Saha, S., Buttari, B., Panieri, E., Profumo, E., and Saso, L. (2020). An Overview of Nrf2 Signaling Pathway and Its Role in Inflammation. Molecules *25*, 5474.

Sbarra, A.J., and Karnovsky, M.L. (1959). The Biochemical Basis of Phagocytosis. Journal of Biological Chemistry *234*, 1355-1362.

Schindelin, J., Arganda-Carreras, I., Frise, E., Kaynig, V., Longair, M., Pietzsch, T., Preibisch, S., Rueden, C., Saalfeld, S., Schmid, B*., et al.* (2012). Fiji: an open-source platform for biological-image analysis. Nature Methods *9*, 676-682.

Schirmer, T., and Evans, P.R. (1990). Structural basis of the allosteric behaviour of phosphofructokinase. Nature *343*, 140-145.

Schmid-Burgk, J.L., Schmidt, T., Gaidt, M.M., Pelka, K., Latz, E., Ebert, T.S., and Hornung, V. (2014). OutKnocker: a web tool for rapid and simple genotyping of designer nuclease edited cell lines. Genome Research *24*, 1719-1723.

Schroder, K., and Tschopp, J. (2010). The Inflammasomes. Cell *140*, 821-832.

Segel, G.B., Halterman, M.W., and Lichtman, M.A. (2011). The paradox of the neutrophilʹs role in tissue injury. Journal of Leukocyte Biology *89*, 359-372.

Selak, M.A., Armour, S.M., MacKenzie, E.D., Boulahbel, H., Watson, D.G., Mansfield, K.D., Pan, Y., Simon, M.C., Thompson, C.B., and Gottlieb, E. (2005). Succinate links TCA cycle dysfunction to oncogenesis by inhibiting HIF-α prolyl hydroxylase. Cancer Cell *7*, 77-85.

Semenza GL, Jiang BH, Leung SW, Passantino R, Concordet JP, Maire P, and A., G. (1996). Hypoxia response elements in the aldolase A, enolase 1, and lactate dehydrogenase A gene promoters contain essential binding sites for hypoxia-inducible factor 1. J Biol Chem *271 (51)*, 32529-32537.

Semenza GL, Roth PH, Fang HM, and GL, W. (1994). Transcriptional regulation of genes encoding glycolytic enzymes by hypoxia-inducible factor 1. J Biol Chem *269 (38)*, 23757-23763.

Shi, H., and Chi, H. (2019). Metabolic Control of Treg Cell Stability, Plasticity, and Tissue-Specific Heterogeneity. Frontiers in Immunology *10*.

Shi, J., Zhao, Y., Wang, K., Shi, X., Wang, Y., Huang, H., Zhuang, Y., Cai, T., Wang, F., and Shao, F. (2015). Cleavage of GSDMD by inflammatory caspases determines pyroptotic cell death. Nature *526*, 660-665.

Sjoelund, V., Smelkinson, M., and Nita-Lazar, A. (2014). Phosphoproteome Profiling of the Macrophage Response to Different Toll-Like Receptor Ligands Identifies Differences in Global Phosphorylation Dynamics. Journal of Proteome Research *13*, 5185-5197.

Slack, M., Wang, T., and Wang, R. (2015). T cell metabolic reprogramming and plasticity. Molecular Immunology *68*, 507-512.

Sommermann, T.G., O'Neill, K., Plas, D.R., and Cahir-McFarland, E. (2011). IKKβ and NF-κB Transcription Govern Lymphoma Cell Survival through AKT-Induced Plasma Membrane Trafficking of GLUT1. Cancer Research *71*, 7291-7300.

Steinberg, S.F. (2008). Structural Basis of Protein Kinase C Isoform Function. Physiological Reviews *88*, 1341-1378.

Takeuchi, O., and Akira, S. (2010). Pattern Recognition Receptors and Inflammation. Cell *140*, 805-820.

Tan, Y., and Kagan, J.C. (2019). Innate Immune Signaling Organelles Display Natural and Programmable Signaling Flexibility. Cell *177*, 384-398.e311.

Tanji, H., Ohto, U., Motoi, Y., Shibata, T., Miyake, K., and Shimizu, T. (2016). Autoinhibition and relief mechanism by the proteolytic processing of Toll-like receptor 8. Proceedings of the National Academy of Sciences *113*, 3012-3017.

Tannahill, G.M., Curtis, A.M., Adamik, J., Palsson-McDermott, E.M., McGettrick, A.F., Goel, G., Frezza, C., Bernard, N.J., Kelly, B., Foley, N.H.*, et al.* (2013). Succinate is an inflammatory signal that induces IL-1β through HIF-1α. Nature *496*, 238-242.

Tanner, L.B., Goglia, A.G., Wei, M.H., Sehgal, T., Parsons, L.R., Park, J.O., White, E., Toettcher, J.E., and Rabinowitz, J.D. (2018). Four Key Steps Control Glycolytic Flux in Mammalian Cells. Cell Systems *7*, 49-62.e48.

Toscano, A., and Musumeci, O. (2007). Tarui disease and distal glycogenoses: clinical and genetic update. Acta Myologica, 105-107.

Turner, S.J., Doherty, P.C., McCluskey, J., and Rossjohn J. (2006). Structural determinants of T-cell recepor bias in immunity. Nature Reviews Immunology 6, 883-894.

Underhill, D.M., Ozinsky, A., Hajjar, A.M., Stevens, A., Wilson, C.B., Bassetti, M., and Aderem, A. (1999). The Toll-like receptor 2 is recruited to macrophage phagosomes and discriminates between pathogens. Nature *401*, 811-815.

Underhill, D.M., Rossnagle, E., Lowell, C.A., and Simmons, R.M. (2005). Dectin-1 activates Syk tyrosine kinase in a dynamic subset of macrophages for reactive oxygen production. Blood *106*, 2543-2550.

Untergasser, A., Nijveen, H., Rao, X., Bisseling, T., Geurts, R., and Leunissen, J.A.M. (2007). Primer3Plus, an enhanced web interface to Primer3. Nucleic Acids Research *35*, W71-W74.

Vabret, N., and Blander, J.M. (2013). Sensing Microbial RNA in the Cytosol. Frontiers in Immunology *4*.

Van den Bossche, J., O'Neill, L.A., and Menon, D. (2017). Macrophage Immunometabolism: Where Are We (Going)? Trends in Immunology *38*, 395-406.

van Uden, P., Kenneth, Niall S., and Rocha, S. (2008). Regulation of hypoxia-inducible factor-1α by NF-κB. Biochemical Journal *412*, 477-484.

Vandenabeele, P., Galluzzi, L., Vanden Berghe, T., and Kroemer, G. (2010). Molecular mechanisms of necroptosis: an ordered cellular explosion. Nature Reviews Molecular Cell Biology *11*, 700-714.

Vazquez, A., Liu, J., Zhou, Y., and Oltvai, Z.N. (2010). Catabolic efficiency of aerobic glycolysis: The Warburg effect revisited. BMC Systems Biology *4*.

Viola, A., Munari, F., Sánchez-Rodríguez, R., Scolaro, T., and Castegna, A. (2019). The Metabolic Signature of Macrophage Responses. Frontiers in Immunology *10*.

Vora, S., Seaman, C., Durham, S., and Piomelli, S. (1980). Isozymes of human phosphofructokinase- Identification and subunit structural characterization of a new system. Proc Natl Acad Sci USA *77*, 62-66.

Wang, F., Zhang, S., Jeon, R., Vuckovic, I., Jiang, X., Lerman, A., Folmes, C.D., Dzeja, P.D., and Herrmann, J. (2018a). Interferon Gamma Induces Reversible Metabolic Reprogramming of M1 Macrophages to Sustain Cell Viability and Pro-Inflammatory Activity. EBioMedicine *30*, 303-316.

Wang, F., Zhang, S., Vuckovic, I., Jeon, R., Lerman, A., Folmes, C.D., Dzeja, P.P., and Herrmann, J. (2018b). Glycolytic Stimulation Is Not a Requirement for M2 Macrophage Differentiation. Cell Metabolism *28*, 463-475.e464.

Watson, M.J., Vignali, P.D.A., Mullett, S.J., Overacre-Delgoffe, A.E., Peralta, R.M., Grebinoski, S., Menk, A.V., Rittenhouse, N.L., DePeaux, K., Whetstone, R.D.*, et al.* (2021). Metabolic support of tumour-infiltrating regulatory T cells by lactic acid. Nature *591*, 645-651.

Webb, B.A., Dosey, A.M., Wittmann, T., Kollman, J.M., and Barber, D.L. (2017). The glycolytic enzyme phosphofructokinase-1 assembles into filaments. Journal of Cell Biology *216*, 2305-2313.

Webb, B.A., Forouhar, F., Szu, F.-E., Seetharaman, J., Tong, L., and Barber, D.L. (2015). Structures of human phosphofructokinase-1 and atomic basis of cancer-associated mutations. Nature *523*, 111-114.

Wefers, B., Bashir, S., Rossius, J., Wurst, W., and Kühn, R. (2017). Gene editing in mouse zygotes using the CRISPR/Cas9 system. Methods *121-122*, 55-67.

Wegrzyn, J., Potla, R., Chwae, Y.-J., Sepuri, N.B.V., Zhang, Q., Koeck, T., Derecka, M., Szczepanek, K., Szelag, M., Gornicka, A.*, et al.* (2009). Function of Mitochondrial Stat3 inCellular Respiration. Science *323*, 793-797.

Weichhart, T., Costantino, G., Poglitsch, M., Rosner, M., Zeyda, M., Stuhlmeier, K.M., Kolbe, T., Stulnig, T.M., Hörl, W.H., Hengstschläger, M.*, et al.* (2008). The TSC-mTOR Signaling Pathway Regulates the Innate Inflammatory Response. Immunity *29*, 565-577.

Weintz, G., Olsen, J.V., Frühauf, K., Niedzielska, M., Amit, I., Jantsch, J., Mages, J., Frech, C., Dölken, L., Mann, M.*, et al.* (2010). The phosphoproteome of toll-like receptor-activated macrophages. Molecular Systems Biology *6*, 371.

Wellen, K.E., Hatzivassiliou, G., Sachdeva, U.M., Bui, T.V., Cross, J.R., and Thompson, C.B. (2009). ATP-Citrate Lyase Links Cellular Metabolism to Histone Acetylation. Science *324*, 1076-1080.

West, A.P., Brodsky, I.E., Rahner, C., Woo, D.K., Erdjument-Bromage, H., Tempst, P., Walsh, M.C., Choi, Y., Shadel, G.S., and Ghosh, S. (2011). TLR signalling augments macrophage bactericidal activity through mitochondrial ROS. Nature *472*, 476-480.

Xia, S., Zhang, Z., Magupalli, V.G., Pablo, J.L., Dong, Y., Vora, S.M., Wang, L., Fu, T.-M., Jacobson, M.P., Greka, A.*, et al.* (2021). Gasdermin D pore structure reveals preferential release of mature interleukin-1. Nature *593*, 607-611.

Yalcin, A., Telang, S., Clem, B., and Chesney, J. (2009). Regulation of glucose metabolism by 6-phosphofructo-2-kinase/fructose-2,6-bisphosphatases in cancer. Experimental and Molecular Pathology *86*, 174-179.

Yang, Y., Ishak Gabra, M.B., Hanse, E.A., Lowman, X.H., Tran, T.Q., Li, H., Milman, N., Liu, J., Reid, M.A., Locasale, J.W.*, et al.* (2019). MiR-135 suppresses glycolysis and promotes pancreatic cancer cell adaptation to metabolic stress by targeting phosphofructokinase-1. Nature Communications *10*.

Yi, L., Liu, Q., Orandle, M.S., Sadiq-Ali, S., Koontz, S.M., Choi, U., Torres-Velez, F.J., and Jackson, S.H. (2012a). p47phox Directs Murine Macrophage Cell Fate Decisions. The American Journal of Pathology *180*, 1049-1058.

Yi, W., Clark, P.M., Mason, D.E., Keenan, M.C., Hill, C., Goddard, W.A., Peters, E.C., Driggers, E.M., and Hsieh-Wilson, L.C. (2012b). Phosphofructokinase 1 Glycosylation Regulates Cell Growth and Metabolism. Science *337*, 975-980.

Yu, P., Zhang, X., Liu, N., Tang, L., Peng, C., and Chen, X. (2021). Pyroptosis: mechanisms and diseases. Signal Transduction and Targeted Therapy *6*.

Yuan, M., Breitkopf, S.B., Yang, X., and Asara, J.M. (2012). A positive/negative ion–switching, targeted mass spectrometry–based metabolomics platform for bodily fluids, cells, and fresh and fixed tissue. Nature Protocols *7*, 872-881.

Yuan, M., Kremer, D.M., Huang, H., Breitkopf, S.B., Ben-Sahra, I., Manning, B.D., Lyssiotis, C.A., and Asara, J.M. (2019). Ex vivo and in vivo stable isotope labelling of central carbon metabolism and related pathways with analysis by LC–MS/MS. Nature Protocols *14*, 313-330.

Yugi, K., Kubota, H., Toyoshima, Y., Noguchi, R., Kawata, K., Komori, Y., Uda, S., Kunida, K., Tomizawa, Y., Funato, Y.*, et al.* (2014). Reconstruction of Insulin Signal Flow from Phosphoproteome and Metabolome Data. Cell Reports *8*, 1171-1183.

Yunna, C., Mengru, H., Lei, W., and Weidong, C. (2020). Macrophage M1/M2 polarization. European Journal of Pharmacology *877*, 173090.

Zancan, P., Marinho-Carvalho, M.M., Faber-Barata, J., Dellias, J.M.M., and Sola-Penna, M. (2008). ATP and fructose-2,6-bisphosphate regulate skeletal muscle 6-phosphofructo-1-kinase by altering its quaternary structure. IUBMB Life *60*, 526-533.

Zhang, D., Tang, Z., Huang, H., Zhou, G., Cui, C., Weng, Y., Liu, W., Kim, S., Lee, S., Perez-Neut, M.*, et al.* (2019). Metabolic regulation of gene expression by histone lactylation. Nature *574*, 575-580.

8 List of abbreviation

1,3BGP	1,3-Bisphosphoglyceric acid
2-DG	2-Deoxy-d-glucose
2PG	2-Phosphoglycerate
3PG	3-Phosphoglycerate
5'-TOP	5'-Terminal oligopyrimidine motif
Acetyl-CoA	Acetyl coenzyme A
ACC	Acetyl-CoA carboxylase
ACLY	ATP citrate synthase
ADP	Adenosine diphosphate
α-KG	α-ketoglutarate
ALDA	Aldolase A
AMP	Adenosine monophosphate
AMPK	AMP-activated protein kinase
AP-1	Activator protein 1
Arg1	Arginase 1
ATP	Adenosine triphosphate
ARE	Antioxidant response element
BCA	Bicinchoninic acid assay
BM	Bone marrow
BMDM	Bone marrow derived macrophages
bp	base pair
BSA	Bovine serum albumin
cGAS	Cyclic GMP-AMP synthase
CLRs	C-type lectin receptors
CMV	Cytomegalovirus
CO_2	Carbon dioxide
CTLDs	C-type lectin-like domains
DAMPs	Damage associated molecular patters
DCs	Dendritic cells
DD	Death domain

DHAP	Dihydroxyacetone phosphate
DMOG	Dimethyloxalyl glycine
DNA	Deoxyribonucleic acid
dNTPs	Deoxynucleoside triphosphate
ds	Double stranded
ECAR	Extracellular acidification rate
ECM	Extracellular matrix
EGFR	Epidermal growth factor receptor
ELISA	Enzyme-linked immunosorbent assay
ENO1	Enolase 1
ER	Endoplasmic reticulum
Erks	Extracellular signal-regulated kinases
ETC	Electoral transport chain
F6P	Fructose 6 phosphate
F1,6BP	Fructose 1,6 bisphosphate
F2,6BP	Fructose 2,6 bisphosphate
$FADH_2$	Flavin adenine dinucleotide
FBS	Fetal bovine serum
FCCP	Carbonyl cyanide-p-trifluoromethoxyphenylhydrazone
fMLP	N-Formylmethionyl-leucyl-phenylalanine
FMO	Fluorescence Minus One
GA3P	Glyceraldehyde 3-phosphate
GAPDH	Glyceraldehyde-3-Phosphate Dehydrogenase
G6P	Glucose 6 phosphate
G6PD	Glucose-6-phosphate dehydrogenase
GPI	Glucose-6-phosphate isomerase
GSDMD	Gasdermin D
HCC	Hepatocellular carcinoma
HIF1α	Hypoxia inducible factor 1
HK	Hexokinase
h	hour
HREs	Hypoxia response elements

HSCs	Hematopoietic stem cells
IDH	Isocitrate dehydrogenase
IFNs	Interferons
IKK	Inhibitor of nuclear factor kappa-B kinase
IL-1	Interleukin-1
iNOS	Inducible nitric oxide synthase
IRAKs	Interleukin-1 receptor-associated kinase
IRF7	Interferon regulatory factor
IRG1	Immunoresponsive gene 1
ITAM	Immunoreceptor tyrosine based activation-like motif
JAK	Janus kinase
JNK	c-Jun N-terminal kinases
LC-MS	Liquid chromatography–mass spectrometry
LDHA	Lactate dehydrogenase A
LGP2	Laboratory of Genetics and Physiology 2
LPS	Lipopolysaccharide
LIC	Ligation independent cloning
LRR	Leucine-rich repeat
MAC	Membrane attack complex
MAL	MyD88 adaptor like protein
MAPK	Mitogen- activated protein kinase
M-CSF	Macrophage colony-stimulating factor
MDA5	Melanoma differentiation-associated protein 5
MHC	Major histocompatibility complex
min	minutes
MOI	Multiplicity of infection
mTOR	Mammalian target of rapamycin
MyD88	Myeloid differentiation primary response 88
NADH	Nicotinamide adenine dinucleotide
NADPH	Nicotinamide adenine dinucleotide phosphate
NETs	Neutrophil extracellular traps
NF-KB	Nuclear factor kappa-light-chain-enhancer of activated B cells

NK cells	Natural killer cells
NLRs	Nucleotide-binding and oligomerization domain (NOD)-like
NO	Nitric oxide
Nrf2	Nuclear factor erythroid 2–related factor 2
OCR	Oxygen consumption rate
OXPHOS	Oxidative phosphorylation
PAMPs	Pathogen-associated molecular pattern molecules
PBMCs	Peripheral blood mononuclear cells
PCR	Polymerase chain reaction
PDAC	Pancreatic ductal adenocarcinoma
PDH	Pyruvate dehydrogenase
PFK1	Phosphofructokinase 1
PFKFB3	6-phosphofructo-2-kinase/fructose-2,6-biphosphatase 3
PGK1	Phosphoglycerate kinase 1
PGM	Phosphoglycerate mutase
PHD	Prolyl hydroxylase domain enzymes
PI3K	Phosphoinositide 3-kinases
PK	Pyruvate kinase
PKC	Protein kinase C
PKM2	pyruvate kinase muscle isozyme M2
PMA	Phorbol 12,13-myristate acetate
PPP	Pentose phosphate pathway
PRRs	Pattern Recognition Receptors
R5P	Ribose 5 phosphate
RET	Reverse electoral transfer
RIG-I	Retinoic acid-inducible gene I
RIPK1	Receptor Interacting Serine/Threonine Kinase 1
RLRs	Retinoic acid-inducible gene-I-like receptors
RNA	Ribonucleic acid
ROS	Reactive oxygen species
s	Second
SDH	Succinate dehydrogenase

Slc25a1	Solute carrier family 25 member 1
ss	Single stranded
STING	Stimulator of interferon genes
Syk	Spleen associated tyrosine kinase
TAK1	Transforming growth factor-β (TGF-β)-activated kinase 1
TBK1	TANK-binding kinase 1
TCA cycle	Tricarboxylic acid cycle
TIR domain	Toll/interleukin-1 receptor domain
TIRAP	TIR Domain Containing Adaptor Protein
TLRs	Toll-like receptors
TME	Tumor microenvironment
TNF	Tumor necrosis factor
TPI	Triosephosphate isomerase
TRAF6	TNF receptor associated factor 6
TRAM	TRIF-related adaptor molecule
TRIF	TIR-domain-containing adapter-inducing interferon-β
WT	Wide type

9 Acknowledgments

First of all, I would like to thank Prof. Veit Hornung for giving me the opportunity to do my PhD thesis in your lab. Many thanks for all of your assistance and guidance during my PhD. When I was having problems, you could come up with really helpful suggestions and ideas.

Next, I want to thank all my collaborators: Dr. Heinrich Flaswinkel, who generated PFKL antibodies. Dr. Thomas Fröhlich, who measured my in vitro enzymatic samples by MS. Dr. Benedikt Wefers, who generated *Pfkl*$^{S775A/S775A}$ mice. Prof. Sebastian Theurich, who allowed me to use the Seahorse XFe96 Analyzer in his lab. Abhinav Joshi from Prof. Jürgen Ruland's lab and Alexander Heinz from Prof. Karsten Hiller's lab, who measured and helped with the analysis of metabolic samples. Thanks to all of you, I could not complete my PhD without your help.

Thanks to Dr. Dhruv Chauhan who supervised me in the first 6 months of my PhD. I really appreciate your help and teaching.

I also want to thank all my colleagues: Dr. Francesca Pinci, Dr. Stefan Bauernfried, Stefan Benkert, Marleen Berouti, Annika Büscher, Dr. Ciana Diskin, Rebekka Endres, Hannah Fischer, Dr. Carlos Gomez Diaz, Janina Graf, Larissa Hansbauer, Julia Kamper, Kristin Leike, Dr. Andreas Linder, Dr. Lin Liu, Claudia Ludwig, Dr. Mohamed Antar Aziz Mohamed, Dr. Ignazio Piseddu, Jochen Rech, Dr. Ulrike Schillinger, Niklas Schmacke, Dr. Che Stafford, Dr. Zhiqi Sun, Inga Szymanska, and Varvara Varlamova. Thanks for all your kind help whenever I have questions. I really enjoy working with you everyone.

Special thanks to my bench partner Marleen Berouti and Julia Kamper. I am really lucky to meet and know you. Thank you for making my crow's feet deeper. The memories we have created together will remain etched in my mind forever!

In the end, I want to thank my family and my husband Xiang. Thanks for your huge support and encouragement during my stressful times. Love you forever!